The Influences of Pollution and Climate on the Trends and Variability of Radiation Fog Frequency

By

Ellyn Gray

A dissertation submitted in partial satisfaction of the

requirements for the degree of

Doctor of Philosophy

in

Environmental Science, Policy, and Management

in the

Graduate Division

of the

University of California, Berkeley

Committee in charge:

Professor Allen H. Goldstein, Chair
Professor Dennis D. Baldocchi
Professor Todd Dawson

Fall 2019

The Influences of Pollution and Climate on the Trends and Variability of Radiation Fog Frequency

by

Ellyn Gray

Abstract

The Influences of Pollution and Climate on the Trends and Variability of Radiation Fog Frequency

by

Ellyn Gray

Doctor of Philosophy in Environmental Science, Policy, and Management

University of California, Berkeley

Professor Allen H. Goldstein, Chair

Abstract: Fog has broad impacts on transportation safety, agricultural production, drought resilience, and climate. The frequency of wintertime radiation fog in valleys throughout the world has been changing over the past century. This dissertation focuses on understanding the drivers of fog trends observed in California's Central Valley and Italy's Po Valley, specifically investigating the competing effects of warming climate versus air pollution controls in the twentieth and early twenty-first century.

Beginning in the Central Valley, this dissertation finds that dense fog frequency (visibility < 400 meters) increased 85% from 1930-1970, then declined 76% in the last 36 winters. Throughout these changes, fog frequency exhibited a consistent north-south trend, with maxima in southern latitudes. I analyzed seven decades of meteorological data and five decades of air pollution data to determine the most likely drivers changing fog, including temperature, dew point depression, precipitation, wind speed, and NO_x (oxides of nitrogen) concentration. Climate variables, most critically dew point depression (DPD), strongly influence the short-term (daily to annual) variability in fog frequency; however, the frequency of optimal conditions for fog formation show no observable long-term trend from 1980 to 2016. NO_x concentration, which is a limiting precursor to the ammonium nitrate aerosol that dominates wintertime particulate matter in the valley, has an increasing north-south concentration gradient, consistent with the gradient in fog frequency. NO_x declined continuously over this period, also consistent with the long-term temporal and spatial trends in fog. As development in the Central Valley increased direct particle and other pollutant emissions from 1930-1970, fog frequency increased. Following the Clean Air Act, particle emissions quickly declined, and NO_x emissions declined steadily, reducing the cloud condensation nuclei (CCN) available for fog formation. I conclude that while the short-term fog variability is dominantly driven by climate fluctuations, the longer-term temporal and spatial changes in fog have been driven by changes in air pollution. For conditions close to the dew point, a decrease in fog of 5 days per year per 10 ppb NO_x decrease occurred across the Central Valley.

To further understand the multivariate, nonlinear contributors to fog formation, this dissertation used generalized additive models to identify the relative significance of climate and air pollution variables affecting visibility, an indicator of dense fog, and compare the drivers changing fog in the Central Valley to Italy's Po Valley, which saw a 50% decline in fog frequency since 1980.

Effective regulatory strategies in the Po Valley have also resulted in stark reductions in inorganic pollution emissions, thus reducing the CCN available for fog formation. Over 56-65% of the variance in visibility is consistently explained by variability in DPD, pollution concentration, wind speed, and precipitation. Variability in DPD, which incorporates both water availability and temperature, has the most pronounced influence on daily time scales, but shows no substantial long-term trends in time over the observation period. The variability in NO_x concentration explains 33-70% of the variance in visibility (depending on the site) when investigating days with average DPD < 3.5℃. This suggests that fog frequency is specifically sensitive to fluctuations in CCN number concentration when meteorological conditions are favorable to fog formation (e.g. when DPD is low). While DPD is a primary driver of daily variability, the significant influence of NO_x concentration on the visibility response suggests that rapid pollution declines in both valleys have had an important impact on the diminished fog season since 1980. This demonstrates that the regulatory measures that mitigate pollution concentration have valuable benefits, not only on the health outcomes of those potentially exposed, but also in reducing the dangerous dense fog frequency that was anthropogenically enhanced with industrialization.

To further understand the safety implications of reductions in air pollution and fog events, I analyzed a 20-year record of fog-related accidents in the Central Valley (1996-2016). Decades of multicar pile-ups along its highways made the region widely-known for the frequency and severity of its fog-related accidents. Yet, the Central Valley saw a 65% decline in fog-related accidents over 20 winters, the variance of which is best explained by the sharply declining trend in seasonal fog hours over the same period. Annual frequency of fog hours as summarized for each fog season explain an average of ~80% of the annual variability in fog-related accidents in the counties of highest roadway volume, showing that the declining trend in fog is a strong determinant in the declining trend in accidents. The subsequent improvement in visibility results in annual fog-related injuries falling by 72%, with the valley seeing an average of 550 fewer injuries from fog accidents in 2015-2016 than in 1996-1997.

The human safety and commercial benefits to a reduction in fog-accidents and the resulting roadway delays is well documented. The declining trend in dense fog in this region has had a pronounced impact on the declining frequency of fog-related accidents. This dissertation implicates regional air pollution concentration as a critical driver in the long-term trend of fog frequency. The strong link between the historical number of Central Valley fog events and trends in pollution concentration provides a measure of how regulations that led to decreases in aerosol concentration, and thereby wintertime fog frequency, also influenced the declining trend in fog-related accidents.

Table of Contents

Acknowledgements:

I'd like to first express my sincerest gratitude to my advisor, Allen Goldstein. My experience in graduate school is incomparable to many, because I was led by a mentor with boundless enthusiasm for science who never ceased to encourage me to make important (somewhat scary) next steps. This helped me grow significantly in my confidence as a scientist and as a person. Allen never lost site of the big picture and the impact our work could have, and because of that, we were able to share it with a lot of people. With his support, my graduate degree was full of big adventures, like working abroad with collaborators in Italy, presenting at international conferences, and speaking live on the evening news. I couldn't be more grateful for his mentorship.

I also benefited from significant mentorship from other Berkeley professors and collaborators. I would like to thank Professor Dennis Baldocchi for consistently greeting me with a friendly face and inquisitive question every week as I brought yet another paper to discuss before my qualifying exam, always excited to chat about micrometeorology and thermodynamics no matter how busy his day. He has essentially been a co-advisor and graciously contributed feedback every step along the way. I'd also like to thank Professor Todd Dawson for being another inquisitive fog ear on campus. I'm very appreciative for all the time he made for me to talk about results and fog papers with such enthusiasm.

I may have been lost in this project long ago without the help of Stefania Gilardoni from the CNR-Bologna. She got excited about our inquiry from the beginning, and I immediately benefited greatly from her background in fog chemistry. Thank you so much for years of Skype calls! With her support, I was a visiting graduate student researcher in Bologna for two visits, both of which were highlights of my life and made profound impacts on my dissertation. Not only did Stefania become deeply involved in the brainstorming and methodology of my project, she also took me under her wing when approaching some of the challenges of living abroad. Having someone to translate important websites or show me where to buy cold medicine was at times just as important as having an incredible mentor and ally to slog through the menial details of statistical modeling.

I also owe a huge debt of gratitude to the Goldstein lab, past and present. After so many hours together, they became my second family, especially the baseball crew, Caleb Arata and Jeremy Nowak. I'm so grateful for all the late night work parties, with baseball as our companion. Dodger game broadcasts may forever feel synonymous with MATLAB error noises, but I wouldn't change a thing. In particular, Jeremy was the best officemate I could ask for. He's been an amazing confidant, cheerleader, comedian, and friend. Our late night pep talks about the future helped put so many personal and career goals into perspective, for which I'm forever grateful.

Words cannot express how important my cohort (Spiderhort 2014) has been to me and will continue to be to me. I lucked out in starting graduate school with people who became my best friends, and these have been the happiest years of my life. In particular, I'd like to acknowledge Ignacio Escalante, Brian Klein, Matt Libassi, Liam Maier, and Jon Proctor for their friendship and for helping put the stressful times in perspective (WILSG?!). I am also very grateful to the ESPM department, administration, and graduate student association for funding, guidance, seminars, and social events.

I would also like to acknowledge the incredible women I met as a part of SoSF. Aside from being a huge part of my community and support system during my graduate degree, the career-driven women and intense leadership experiences I was exposed to became a critical part of my professional development. Their influence inadvertently broadened my horizons to the impact I wanted to have in my career. Through all of this, I have made incredible friends who supported me even when I disappeared behind a computer for months at a time. In particular, I'm so grateful to my roommates Joanna Burlison and Amy Constable, as well as my close friends Cyn Haueter and Jamie Young. Thank you for celebrating even the smallest wins, listening to me vent, constantly uplifting me, and being great dog moms to James during late nights and conferences.

To my friends, especially those outside of academia, who let me talk their ear off about fog and climate change and bought me a beer or found a +1 concert ticket when I was too broke to attend (looking at you Adrian Spinelli, Sean Swaby, and Kayla Ghassemi), thank you for making another 5 years of school and scraping pennies feel easy. I can't wait to extend the favor. The next ∞ rounds are on me.

Most importantly, I want to thank my parents and siblings for their support throughout all my education. My wonderful parents, Raul & Nan Alvarez-Gray and Fred & Christy Gray, who were incredible cheerleaders and proofreaders. They supported every next step I took with full confidence in me, never questioning each big leap no matter how audacious it seemed. The older I get, the more special I realize that was. It built me into who I am today, and I am so grateful. I also want to acknowledge my brother, Frederic Gray, and his wife and my dear friend, Joan. Freddie consistently had my back even in the darkest days of coursework when I was barely known to lift my head away from a book to look across the dinner table. I owe you a lifetime of Michelle's. Fred and Joan let me crash on their floor more times than I can count, always with a smile and a stocked fridge. Thank you for being such good friends to me. Included in my family, I also want to acknowledge my Berkeley family, the Bains, who were my home away from home. And finally, my dog, James, for being the best family a human could ask for. To my family of all locations, shapes, and sizes: thank you for all the love, hugs, and guidance.

I owe a debt of gratitude to many people in the scientific community who mentored, tutored, and fixed broken code without asking anything in return. Thank you to Willie Horn for all the free tutoring and convincing me to become a scientist. Thank you to all the online message boards that taught me programming and statistics, and all the YouTube videos that taught me physics and Calculus. Thank you to all the scientists at CARB and the EPA who sent me so much data and answered my endless follow up questions. Thank you to Berkeley Connect for funding my dissertation year and infusing my last year of graduate school with so much purpose. And thank you to the NSF for believing in this project and awarding me a Graduate Research Fellowship, which ultimately gave me the freedom to take it in very independent directions.

Finally, I want to thank the person who got me through the last months of my dissertation, Stephen Johnson. Thank you for being as patient and understanding about the demands of finishing as you were excited about every result along the way. Stephen went so far above and beyond to make everything else in my life go as smoothly as possible so I could just focus on this. Words can't express my gratitude. And of course, thank you for beautifully compiling all that elevation data, and I promise I'll learn my computer shortcuts.

Chapter 1:

Introduction

1. Motivation for radiation fog research

Fog occurs in multiples seasons in regions throughout the world. The most common types of fog impacting humans and land ecology are radiation, advection, and orographic fog. While these have differing formation mechanisms and seasonal maxima, all occur when atmospheric water vapor cools and condenses on hygroscopic, micron-size particles at low elevation (Gultepe, 2007).

Under high relative humidity (RH), radiation fog forms after sunset when the thermal emission of the surface is not balanced by incoming solar radiation, causing surface conditions to radiative cool (Sierbert et al., 1992). Radiation fog formation is most common on long winter nights with clear skies, which maximizes surface heat loss, and strong inversion layers, which minimizes turbulence (Roach & Brown, 1976). Radiation fog often exhibits high spatial heterogeneity since it is very sensitive to fluxes in temperature and moisture (Gultepe, 2007). Evaporation commonly begins at the edges due to dry entrainment or at the center of an urban region, yet even events at the same site can display vastly different patterns of dissipation (Underwood et al., 2004). Significant effort has been made to develop numerical models for fog prediction, which reveal the complexity of parameterizing the surface-atmosphere exchanges (Bergot & Guedalia, 1994; Sierbert et al., 1992). Variations in surface roughness, soil moisture, and vegetative coverage influence surface turbulence, radiative cooling, and fog liquid water content, allowing for a profound impact on fog development.

Researchers have identified many regions globally in which the frequency and intensity of fog events have changed over time (Klemm & Lin, 2015). This dissertation focuses on trends in radiation fog frequency, though there exist notable changes in advection and advection-radiation fog, as well. Two of the most heavily researched valley fogs in the world – California's Central Valley and Italy's Po Valley – saw a significant change in the frequency of events during the twentieth century. Episodes of dense fog in the Central Valley increased from 1930-1970 followed by a 46-50% decline since 1980 (Baldocchi & Waller, 2014; Herckes et al., 2015), during which time rural and urban stations in the Po Valley observed a 47% reduction in hours of dense fog (Giulianelli et al., 2014; Mariani, 2009). Similar reductions in dense fog (visibility < 200 m) were also recorded in research throughout Northern and Eastern Europe, with most stations reporting half the number of low visibility days when compared to the mid-1970s (van Oldenborg et al., 2009). Declining trends continue to be identified, such as those in South Korea over a 25-year period (Belorid et al., 2014).

Conversely, many developing regions with conditions for radiation fog are experiencing an increase in fog frequency in recent decades. For instance, in New Delhi, fog episodes (visibility < 200 m and 500 m) increased from just 6.4% of the season in the early 1950s to 58% in the late 1990s (Tiwari et al., 2011). These results were confirmed by Syed et al., 2012 which found that fog was three times as frequent post-1998 as pre-1988 in India, Pakistan, and Bangladesh. Rapidly developing regions throughout East-Central China also report increasing numbers of fog events at

many sites, as well as notable increases in fog duration, over recent decades (Fu et al., 2014; Niu et al., 2010; Quan et al., 2011; Shi et al., 2008); while the period of steepest increase differs by province, most saw the largest increases in the 1980s.

As fluctuating trends in radiation fog frequency continue to be identified, this dissertation presents an explanation for those observed in California's Central Valley and Italy's Po Valley in order to develop a conceptual framework for the trends seen in other regions. These valleys are of great interest not only for their unusual trends, but also their long history of observations. The length and spatial coverage of the Central Valley's meteorological and air quality record is ideal for robust trend analysis, and the temporal resolution of the Po Valley's pollution observations allows for a deeper understanding of the high frequency variability in the study. Comparing and contrasting the results creates more confidence in the conclusions drawn.

While many studies have identified trends in radiation fog frequency, most have only postulated, but not tested, possible causes. Past works have suggested the following drivers for decreases in fog frequency:

1. Greenhouse gas-induced climate change causing an increase in minimum temperatures and reduced diurnal temperature range (Dai et al., 1999), thus hindering condensation.
2. Expanding coverage of concrete and asphalt surfaces from rapid urbanization increases the thermal conductivity of the ground relative to natural vegetation, thus increasing nighttime temperatures and reducing RH (Oke, 1973), limiting fog formation.
3. Agricultural expansion enlarging the coverage of irrigated land, which increases surface albedo, and thereby increases thermal conductivity, decreases radiative cooling, and decreases the diurnal temperature range (LaDochy et al., 2007; Christy et al., 2004; Christy et al., 2006; Bonfils et al., 2007), thus limiting fog formation.
4. A change in abundance of hygroscopic aerosols that serve as cloud condensation nuclei causing supersaturation to occur at less favorable conditions (RH ≥ 100), (Gultepe, 2007; Hudson et al., 1980; Frank et al., 1998; Laaksonen et al., 1998; Roach and Brown, 1976), thereby reducing fog formation.

I approach hypotheses 1-3 with skepticism, most notably because they only address drivers for the decreasing trend, yet increases in fog frequency have clearly been observed in recent years in South Asia and East-Central China, as well as historically in California. Specifically for the Central Valley, trends in hypotheses 1-3 were largely positive over the twentieth century, which conflicts with the observed upward (1930 to 1970) then downward (1980 to present) trends in fog frequency. In California, Cordero et al., 2011 reports an increase in minimum temperature from 1918-2006, which presumably would have a diminishing impact on fog frequency contrary to the increasing trend mid-century; further, evidence of the warming signal is least prominent during the winter season, making climate change-induced fog changes even less likely in this region (Bonfils et al., 2007; Christy et al., 2004; LaDochy et al., 2007). Instead, the Central Valley shows increased warming during seasons of artificial irrigation, of which there is almost none in the winter (Christy et al., 2006; Bonfils et al., 2007; Salas et al., 2006). Land use changes such as increasing urbanization and agricultural expansion, while offering potential explanations for the recent declining trend, also conflict with the upward trend from 1930 to 1970, because rates of both population and farm coverage grew positively (CRS, 2005). Additionally, the fog decline is apparent in both urban and rural locations when investigated from satellite imagery (Baldocchi &

Waller, 2014), suggesting a common driver throughout the valley, rather than just the urban sites.

Instead, changes in radiation fog frequency in the Central Valley have been most temporally consistent with hypothesis 4, which would suggest that unregulated increases in anthropogenic aerosols enhanced fog formation, only to weaken with recent pollution mitigation strategies. A dependence on air pollution aligns with the fog patterns of the majority of radiation fog observations seen globally, with many more regulated, developed regions seeing a decrease in fog frequency and developing regions with less regulated pollution seeing a rapid increase.

Significant research has investigated how the number concentration and composition of particles impact fog frequency, density, and duration (Gultepe, 2007; Roach and Brown, 1976). In order for a cloud droplet to form, two effects are in competition: the Raoult effect, in which vapor pressure decreases based on the dissolved substance, and the Kelvin effect, in which vapor pressure increases with decreasing radius due to droplet curvature. There exists a critical size, as described by Köhler Theory, where the Raoult effect is in balance with the Kelvin effect, and anything above this size is considered an activated droplet, which then grows exponentially under supersaturated conditions (Köhler, 1936). Exceeding this critical value is only achievable through heterogeneous nucleation where a soluble aerosol, known as cloud condensation nuclei (CCN), lowers the equilibrium water vapor pressure, thus allowing activation at lower supersaturation than a pure water droplet. It is now understood that the presence of soluble gases, such as nitric acid (HNO_3), or surfactants, which reduce surface tension, also lower the vapor pressure, enhancing the likelihood of activation. While aerosol size has a dominating effect on CCN efficiency, composition plays a more significant role in lowering vapor pressure at very low supersaturations ($S < 0.25\%$), which are nearly always found in fog, as opposed to clouds (Hudson et al., 1980; Dusek et al., 2006)

Fog CCN sources vary based on the type of fog. In contrast to advection fog, which forms over the ocean on naturally occurring sodium chloride aerosols, radiation fog forms over land and is typically more polluted (Gultepe, 2007). Local pollution can have a critical impact on the formation and number concentration of both activated and unactivated droplets (Eldridge, 1966; Neirburger & Wurtele, 1948; Hudson et al., 1980). Research on radiation fog microstructure suggests that unlike clouds, fog is mainly composed of unactivated droplets, which, by way of soluble gas dissolution, can theoretically swell up to 10 microns and are primarily responsible for fog vision impairment (Hudson et al., 1980; Frank et al., 1998; Laaksonen et al., 1998). In conditions where supersaturation is below one, the addition of hygroscopic (HNO_3) and ammonia (NH_3) gases to the water droplet can yield the impression of an activated cloud droplet, such that it is impossible to distinguish unactivated haze aerosols from truly activated droplets without sophisticated methods (Kulmala et al., 1997). Thus, pollution enhances the formation of low-visibility unactivated fog and was likely a catalyst for historical instances of dangerous urban fogs, such as during the deadly London Smog of 1952 and the ‘pea-soupers’ of the nineteenth century (Kokkola et al., 2002; Roach and Brown, 1976; Wilkins, 1954). Regulation enacted with London’s Clean Air Act of 1956 was then credited for a subsequent reduction in dense fog episodes (Brimblecombe, 1977). Hence, our focus on air pollution as a primary driver of radiation fog trends is rooted in the reductions driven by historically successful emission regulations.

Twentieth century industrialization throughout Western countries caused air pollution to rapidly

increase with intensifying urbanization, spurred by unregulated fuel consumption and inefficient home heating. Severe pollution episodes were recorded in California as early as 1903 due to dense photochemical smog, even though its formation chemistry was unknown at the time (Senn, 1948). Both the Po and Central Valley are characterized as highly polluted regions (American Lung Association, 2016; European Environment Agency, 2014), owing to emissions from their large populations and intensive agricultural, livestock, and industrial activities, combined with regularly occurring episodes of stagnant valley air. Reactions of primary pollutants sulfur dioxide (SO_2), oxides of nitrogen ($NO_x = NO + NO_2$), and ammonia (NH_3) result in the formation of ammonium nitrate (NH_4NO_3) and ammonium sulfates ($(NH_4)_2SO_4$ and NH_4HSO_4) which are important contributors to fine wintertime particulate matter, causing frequent regulatory exceedances. Historically, the Central Valley has had low SO_2 emissions relative to both the Po Valley and other Western sites due its limited coal production and use of alternative fossil fuel sources (Kirchstetter et al., 2017). Both valleys also executed effective SO_2 control measures prior to those of NO_x, causing NO_x to be an increasingly large percentage of the inorganic pollution burden (Chow et al., 2008). Since the mid-1990s, emissions of SO_2 from anthropogenic sources have been negligible in the Central Valley, making NH_4NO_3 the dominant component of aerosols during the winter (Chow et al., 2006). As such, this dissertation primarily focuses on the role of NO_x – as an indicator of air pollution leading to fog CCN – for comparability, length of record, and modern relevancy to the pollution mix.

In the Central Valley, wintertime NO_x processing to form NH_4NO_3 – which is a product of NH_3 and HNO_3 – has been well characterized by modeling and field studies. While emissions of NH_3 from animal agriculture and vehicles peak during the summer, the abundance of valley sources, as well as the uniquely low wintertime planetary boundary layer, make NH_4NO_3 formation HNO_3-limited (Battye et al., 2003; Schiferl et al., 2014). HNO_3 is formed through both daytime and nighttime mechanisms involving nitrogen dioxide (NO_2). Combustion provides the dominant source of NO_x which undergoes daytime oxidation by the hydroxyl radical (OH) to form HNO_3 (equation 1).

$$NO_2 + OH \rightarrow HNO_3 \qquad \text{(eq. 1)}$$

Nighttime formation is the result of heterogeneous chemistry where NO_2 titrates ozone, forming a nitrate radical (NO_3). NO_3 then reacts with NO_2 to produce dinitrogen pentoxide (N_2O_5). Finally, N_2O_5 reacts with water, forming HNO_3 (equations 2-4).

$$NO_2 + O_3 \rightarrow NO_3 + O_2 \qquad \text{(eq. 2)}$$
$$NO_3 + NO_2 \rightarrow N_2O_5 \qquad \text{(eq. 3)}$$
$$N_2O_5 + H_2O \rightarrow 2HNO_3 \qquad \text{(eq. 4)}$$

The HNO_3, whether produced through daytime photochemistry or nighttime heterogeneous chemistry, reacts with the available ammonia, making NH_4NO_3 (equation 5).

$$NH_3 + HNO_3 \leftrightharpoons NH_4NO_3 \qquad \text{(eq. 5)}$$

Model simulations suggest that 80% of the HNO_3 produced under Central Valley wintertime conditions can be converted to particulate nitrate (NO^-_3) (Stockwell, 1999). NO^-_3 production is then very sensitive to changes in NO_x concentration, with trends that scale proportionally (Pusede

et al., 2016). Additionally, NH_4NO_3 is very hygroscopic, making it an ideal CCN for potential cloud and fog formation at low supersaturation (Petters and Kreidenweis, 2007).

HNO_3 and NH_3, the precursors to NH_4NO_3 formation, also have an impact on vapor pressure when dissolved in liquid droplets. In gas phase, HNO_3 and NH_3 can condense onto aqueous particles, dramatically increasing hygroscopicity and, in turn, the number of activated CCN (Kulmala et. al., 1998; Andreae et al., 2008). Also, a reduced vapor pressure allows activation to take place at smaller sizes; thus, polluted cloud and fog consist of a higher number concentration of small cloud droplets (Kulmala et al., 1995). This is known to increase cloudiness and prolong the lifetime of the clouds, both of which would have a significant impact on surface radiation fog.

Air pollution in the Central Valley and Po Valley has declined at a similar rate and over a similar period as fog frequency due to regulatory intervention. In the Po Valley, substantial reductions in primary pollutant emissions since the 1980s contributed to declining trends in particulate matter with aerodynamic diameter 2.5 micrometers or less ($PM_{2.5}$), most significantly in the winter (Cusack et al., 2012; Putaud et al., 2014). Bigi & Ghermandi, 2016 determined this trend was largely attributable to a regulatory-initiated renewal of vehicles with more advanced emission controls and efficient engines – an impact which is also seen in decreasing fuel sales. Additionally, a decline in emissions from industrial combustion due to technological improvements influenced the trend (Bigi & Ghermandi, 2016).

Similarly, the Central Valley has experienced concurrent reductions in primary emissions and secondary inorganic aerosols (Pusede et al., 2016) due mainly to transportation emission controls. These have made rapid advancements by focusing on fuel reformulation, improved combustion control, and increased automotive inspection. Most noteworthy was the implementation of the three-way catalytic converter in the early 1980s which began a stark trend of emission improvements, as seen in a 50% reduction in gasoline-NO_x emission from 1990-2010 in the San Joaquin Valley despite pronounced population growth (McDonald et. al., 2012). Progress in emission reductions from diesel trucks has lagged behind gasoline-powered vehicles, making diesel trucks the largest current on-road source of NO_x in the San Joaquin Valley (McDonald et. al., 2012). However, significant progress in NO_x emission factors is being reached with the enforced implementation of selective catalytic reduction (SCR), decreasing NO_x emissions by 76% on average (Preble et al., 2015). NH_4NO_3 concentration has fallen proportionally with measurements of NO_2 over the last 12 years, with Central Valley $PM_{2.5}$ declining at a rate of 2% a year (Pusede, 2016). This suggests that changes in NO_x concentration directly impact the availability of NH_4NO_3 as potential wintertime CCN. As such, this tremendous success in air quality regulation has possible unexpected outcomes on the fate of atmospheric moisture.

Understanding the drivers of radiation fog trends has important health, safety, and ecological implications on both regions. The hazards of radiation fog, particularly in urban environments, are often underestimated. Past works have identified dense radiation fog as the leading cause of weather-related traffic accidents in California, within which the Central Valley is a national hotspot for fatalities from vision-obscured accidents (Ashley et al., 2015; United States Department of Transportation, 2017). Further, the economic costs associated with fog episodes are estimated to be comparable to those of tornadoes, and in some instances, even hurricanes and winter storms (Gultepe et al., 2007). Much of the economic losses come from unpredicted delays

in aviation, as well as the halting of ground transportation. This postpones the delivery of goods, as well as causes the temporary closure of schools and businesses. Thus, a regional decrease in fog events has considerable safety and economic advantages.

Radiation fog also has important impacts on the boundary level radiation budget by reducing radiative cooling, moderating surface temperatures, and blocking incoming solar radiation. In the Central Valley, the rapid agricultural development throughout the twentieth century relied on the increased occurrence of wintertime radiation fog. Prolonged periods of dense fog are ideal for meeting the required dormancy period of fruit and nut trees in an otherwise warm and arid climate. This dormancy period, known as "winter chill," consists of the accumulated cold-season hours below 7°C that each plant is required to meet in order to avoid poor fruit set (Baldocchi et al., 2006; Baldocchi and Wong, 2008). As fog events continue to decrease, amplified surface energy on clear days increases bud temperatures by 4°C, thereby reducing the number of crops that meet the dormancy threshold. In addition to growing concern for California's water availability, the agricultural region currently experiences an estimated 400 fewer hours of winter chill per year (Baldocchi and Waller, 2014). As such, understanding the future of radiation fog trends holds agricultural value.

Here I present an investigation of the response of radiation fog frequency to trends in meteorology and air pollution in order to better understand the mechanistic drivers of fog formation and the relevancy of pollution mitigation on its long-term trends in California's Central Valley and Italy's Po Valley. I then investigate the roadway safety implications of this decline for the Central Valley.

2. Description of Chapters

2.1. Summary of Chapter 2
Impact of air pollution controls on radiation fog frequency in the Central Valley of California

In Chapter 2, I present a Central Valley fog climatology of 15 sites throughout the region spanning 75 winters. I use the climatology to investigate historical trends of both fog and key drivers of its formation in order to determine a cause for the increase in fog frequency from 1930-1970, followed by the rapidly declining trend since 1980. The investigation includes historical trends (1963-2014) in NO_x concentration, which are used as a proxy for nitrate aerosol loading to estimate the role of CCN on fog formation. I use the fog climatology to analyze the spatial, temporal, and interannual correlation between meteorology, air pollution, and fog frequency. Central Valley meteorology shows no trend in the occurrence of favorable conditions for fog formation since 1980, yet the fog continues to decline. Instead, the historical observations of the climate variables show rapid interannual variability. As such, the short-term variance in dew point depression and wind speed demonstrate much better correlation with the high frequency trend of annual fog events.

When investigating the driver of the historical upward-then-downward trend, I conclude that the coherence of both the temporal trend and spatial gradient of fog events is unique to fog frequency and air pollution. As inorganic aerosol number concentration fell, so did the hygroscopicity of CCN sources and the amount of soluble gases dissolved into the water droplets – both of which previously aided fog formation occurring at nontraditional activation conditions (RH < 100%). Without the effect of pollution, Central Valley fog frequency has become more sensitive to

temperature and water availability, with nearly all fog days occurring during the most favorable meteorological conditions, unlike 35-years ago. I estimate that for conditions close to the dew point, a decrease in fog of 5 days per year per 10 ppb NO_x decrease occurred across the Central Valley over the past four decades.

2.2. Summary of Chapter 3

Unraveling the influence of pollution and climate variability on radiation fog frequency in California's Central Valley and Italy's Po Valley

In Chapter 3, I investigate daily wintertime visibility observations in the Po Valley and Central Valley as an indicator of dense fog. The goal of the study is to analyze known and suspected drivers of fog formation with a multivariate model to identify each predictor variable's relative contribution to daily visibility with the ultimate goal of elucidating causes to the diminishing radiation fog season. I find that a 50% decline in Po Valley fog and 76% decline in Central Valley fog occurred since 1980, concurrent with reductions in NO_x, SO_2, and particulate concentration. Meanwhile, changing climate and continued urbanization present possible obstacles to fog formation. Using generalized additive models, I find that low visibility conditions are most strongly impacted by DPD < 4℃, high NO_x concentration, low wind speed, and days with precipitation.

Chapter 3 then compares each predictor variable's relative impact on the visibility response to further elucidate which has a controlling influence on the trend in visibility. I analyze pollution in conditions of high dew point depression and low dew point depression, as Chapter 2 clarifies that pollution correlations are highest when looking at the response segmented by conditions with the moisture and temperature profile to possibly support fog formation. While DPD is a primary driver of daily variability, trends show no substantial change in the 1980s and 1990s, when fog frequency began rapidly declining. Instead, the large impact of air pollution on the visibility response suggests that the declines in NO_x concentration in the Central and Po Valley (61-65%) has had a critical impact on the diminished fog season since 1980.

2.3. Summary of Chapter 4

Trends in frequency, rate, and severity of Central Valley fog-related traffic accidents

In Chapter 4, I focused on the impact of declining Central Valley fog events on the annual frequency, rate, and severity of resulting fog-related accidents. This chapter analyzes descriptive statistics and trends in fog-related accidents from 1996-1997 to 2015-2016 fog seasons, finding a 65% decline in fog-related accidents over 20 winters. I present summary statistics and trends for the counties of highest population and frequency of accidents. This study finds that the annual number of dense fog events, identified by visibility at local airports, is the strongest determinant in the declining trend in fog-related accidents, describing a majority of the interannual variability. Since there has also been significant increases in total roadway volume over the study period, I also investigate this trend by normalizing by total distance driven in each county investigated, which is available for 2002-2015. This results in up to a 16% increase in the declining trend in fog-related accidents over the period. The subsequent improvement in visibility results in annual fog-related injuries falling by 72%, with the valley seeing an average of 550 fewer injuries from fog accidents in 2015-2016 than in 1996-1997. The strong link between the historical number of

Central Valley fog events and trends in pollution concentration suggest that regulatory measures that led to decreases in aerosol concentration, and thereby wintertime fog frequency, also influenced the declining trend in fog-related accidents.

I also investigate the rate of fog-related accidents per fog hour identified at local airports. At least two counties indicate there have been statistically significant declining trends in the rate of fog accidents during fog events, which suggests that improvements to vehicle safety, roadway notifications, and traffic diversion may make notable impacts. Additionally, there is evidence that fog-related accidents grew less severe over the 20-year study when investigating the frequency of accidents in five collision severity categories relative to the total fog accidents each season. In most counties, trends in less serious accidents are increasing at the expense of more dangerous collisions, which are decreasing. However, the number of collisions per fog-related accident and the frequency of fatal accidents show no trend, suggesting there continue to be important opportunities for roadway and vehicle safety improvements.

2.4. Conclusion

In Chapter 5, I summarize the conclusions contained herein and recommend possible directions for future work.

Chapter 2:

Impact of air pollution controls on radiation fog frequency in the Central Valley of California

Adapted from:

Gray, E., Gilardoni, S., Baldocchi, D., McDonald, B.C., Facchini, M.C., & Goldstein, A.H. (2019). Impact of air pollution controls on radiation fog frequency in the Central Valley of California. *Journal of Geophysical Research: Atmospheres, 124*(11), 5889-5905. https://doi.org/10.1029/2018JD029419

Abstract: In California's Central Valley, tule fog frequency increased 85% from 1930-1970, then declined 76% in the last 36 winters. Throughout these changes, fog frequency exhibited a consistent north-south trend, with maxima in southern latitudes. Chapter 1 analyzes seven decades of meteorological data and five decades of air pollution data to determine the most likely drivers changing fog, including temperature, dew point depression, precipitation, wind speed, and NO_x (oxides of nitrogen) concentration. Climate variables, most critically dew point depression, strongly influence the short-term (annual) variability in fog frequency; however, the frequency of optimal conditions for fog formation show no observable trend from 1980 to 2016. NO_x concentration, which has a decreasing north-south concentration gradient, declined continuously over this period, consistent with the long-term temporal and spatial trends in fog. As development in the Central Valley increased direct particle and other pollutant emissions from 1930-1970, fog frequency increased. Following the Clean Air Act, particle emissions quickly declined, and NO_x emissions declined steadily, reducing the cloud condensation nuclei (CCN) available for fog formation. As a precursor of ammonium nitrate aerosols, which are efficient CCN, this chapter uses NO_x measurements and emission trends as a proxy for the CCN trend. I conclude that while the short-term fog variability is dominantly driven by climate fluctuations, the longer-term temporal and spatial changes in fog have been driven by changes in air pollution. For conditions close to the dew point, a decrease in fog of 5 days per year per 10 ppb NO_x decrease occurred across the Central Valley.

1. Introduction

Understanding the drivers of dense radiation fog, known as tule fog, in California's Central Valley is important for the safety, economic development, and agricultural viability of the region. Central Valley fog events are the primary cause of California's weather-related accidents, making this region a national leader in vision-impaired vehicle collisions (Ashley et al., 2015). Radiation fog also inflicts an economic toll due to delayed aviation and temporary closure of businesses and schools. Thus, a regional decrease in fog events has considerable safety and economic advantages for the valley's 6.5 million residents.

However, the rapid agricultural development in the valley throughout the twentieth-century relied on the increased occurrence of wintertime radiation fog. Prolonged periods of dense fog were ideal for meeting the required cold season dormancy period of fruit and nut trees, known as "winter chill," to avoid poor fruit set (Baldocchi & Wong, 2008; Luedeling et al., 2009). The region experienced up to 400 fewer hours of winter chill per year in 2012 when compared to 1982 due to a reduction in dense fog (Baldocchi & Waller, 2014). Fog also influences surface conditions by nearly eliminating the vapor pressure deficit that drives evapotranspiration; hence, declining fog can enhance evaporation in an already drought stressed region (Fischer et al., 2009; Williams et al., 2018). As such, understanding the drivers of the tule fog trend holds agricultural value for the valley, which exceeded ~~$47~~ billion in revenue in 2015 (CFDA, 2016).

Throughout the twentieth-century, trends in tule fog frequency have changed dramatically. While fog frequency increased steadily from 1930-1970, with cities such as Fresno seeing an 85% increase in dense fog episodes, analysis from both ground and remote sensing measurements found a 46-50% reduction in fog beginning in 1980 (Baldocchi & Waller, 2014; Herckes et al., 2015). Despite significant research on the thermodynamic contributors to tule fog (Bergot & Guedala, 1994; Roach et al, 1976), no explanation consistent with the upward-then-downward trend in its frequency over the last century has been identified. This study seeks to elucidate both the long-term contributors to fog enhancement and decline, as well as better understand what influences the large interannual variability.

Central Valley meteorological trends may be important, as there are a number of anthropogenic changes that could inhibit maximum radiative cooling, making it more difficult to reach dew point and for condensation to form fog. Notable changes include rising temperatures associated with climate change and/or the urban heat island effect. However, temperature alone as the dominant variable driving the tule fog trend cannot explain the observations, as the rising temperatures associated with both climate change and urban expansion would be largely positive over the past century, unlike the upward-then-downward signal seen in fog frequency. The role of urbanization has also been investigated due to the occurrence of urban clear islands in highly populated Central Valley cities (Lee, 1987; Suckling & Mitchel, 1988), such as in Fresno where dense fog episodes detected via satellite imagery begin dissipating from the center of the urban footprint (Underwood & Hansen, 2008). However, fog decline is apparent in both urban and rural locations when investigated from satellite imagery (Baldocchi & Waller, 2014), suggesting a common driver throughout the valley, rather than just the urban sites. Changes in water availability due to agricultural expansion may also have notable climate effects; however, wintertime irrigation is much less common during California's rainy season, making it a less likely driver (Salas et al.,

2006).

The upward-then-downward trend may be better correlated with Central Valley air pollution trends. The number concentration and composition of aerosols can play a significant role in fog's frequency, density, and persistence, with fog being more likely to occur in regions with high aerosol concentration and low supersaturation (Gultepe et al., 2007). Increased air pollution has been identified as a catalyst for enhanced radiation fog in the past, such as during the deadly London Smog of 1952 (Wilkins, 1954). Subsequent reductions in dense fog episodes in London have been attributed to regulation of emissions through the Clean Air Act of 1956 (Brimblecombe, 1977). Hence, our interest in air pollution as an important variable changing fog frequency and persistence is rooted in the observed effect from past regulation.

The Central Valley is consistently out of compliance with air quality standards for particulate matter, with air quality assessments ranking it among the worst areas in the nation (American Lung Association, 2016).
During the cool, winter months, conditions are ideal for the formation of ammonium nitrate (NH_4NO_3), which is the dominant (30-80%) inorganic particulate matter with aerodynamic diameter 2.5 micrometers or less ($PM_{2.5}$); the remaining PM is dominated by organic species (Chow et al., 2006). While NH_4NO_3 is a product of ammonia (NH_3) and nitric acid (HNO_3), the high abundance of primary NH_3 from agricultural sources make Central Valley NH_4NO_3 formation HNO_3-limited (Battye et al., 2003; Schiferl et al., 2014). HNO_3 is formed from oxides of nitrogen (NO_x = NO + NO_2) through both daytime oxidation by the hydroxyl radical and nighttime oxidation by ozone. Central Valley NH_4NO_3 production is thus very sensitive to changes in NO_x concentration, and reductions in NO_x have been shown to cause corresponding reductions in NH_4NO_3 in $PM_{2.5}$ (Pusede et al., 2016).

NH_4NO_3 is very hygroscopic, making it an ideal cloud condensation nuclei (CCN) for cloud and fog formation at low supersaturation (Petters & Kreidenweis, 2007). Scavenging measurements indicate that ammonium nitrate is effectively removed by fog for nucleation scavenging, confirming its ability to act as CCN at low supersaturation typical of fog (Gilardoni et al., 2014). Additionally, HNO_3 and NH_3, the precursors to NH_4NO_3 formation, reduce vapor pressure, increasing hygroscopicity and allowing activation at smaller sizes (Kulmala et. al., 1998; Andreae et al., 2008). Polluted fog consists of a higher number concentration of small droplets, which in turn increases cloudiness and prolongs the lifetime of clouds and fog (Kulmala et al., 1995). Klemm et al. (2016) modeled fog formation in regimes with relative humidity (RH) < 100% finding equivalent reductions in fog with increases in temperature and reductions in aerosol concentration, likely tied to changes in hygroscopic gases such as SO_2 and NO_x.

Further, the presence of HNO_3 and NH_3 in water droplets can also alter the hygroscopicity and size of unactivated droplets – droplets that do not reach the supersaturated conditions critical for growth – but can nonetheless yield the impression of dense fog (Kulmala et al., 1997; Laaksonen et al., 1998; Charlson et al., 2001; Kokkola et al., 2002). The hygroscopicity of the NH_3 and HNO_3 allow cloud-droplet-sized particles to form in RH of less than 100%, causing low-visibility, fog-like conditions.

As the primary precursor to ammonium nitrate PM in the Central Valley, this chapter focuses on

trends in NO_x as an indicator of the impact of changing air pollution on fog frequency.

Here I developed and compare historical records of temporal and spatial patterns for fog events, climatic variables, and air pollution to investigate the dominant drivers for fog frequency and persistence.

2. Study region

The Sierra Nevada to the east and Coastal Range to the west create ideal valley geography for persistent radiation fog episodes. Tule fog season spans November to March, during which weather conditions are characteristically binary: dry, cloudless days permeated by occasional wet winter storms. Clear conditions favor rapid radiative surface cooling following sunset, and if relative humidity is high and temperature and wind speeds are low, atmospheric moisture can condense to form ground fog. The wintertime inversion causes fog to linger close to the surface, typically below 300 meters, constrained horizontally by the perimeter mountain ranges (Underwood et al., 2004; Bianco et al., 2011). The stagnant conditions and low wind speed usually associated with the Great Basin High cause fog events with visibility often below 200 meters to persist for as long as 12 to 18 hours, usually dissipating mid-morning (Herckes et al., 2015).

The Central Valley has distinct differences in a variety of attributes as a function of latitude including fog occurrence, climate variables, urbanization, and air pollution. For the purposes of analyses in this paper, I divide the study region by latitude and aggregate data for specific representative areas, as shown in *Figure 1*. To emphasize the spatial gradients of different variables, each degree of descending latitude, beginning at 40°N, is represented by a different color in the spectral color scheme, with cooler colors representing the northernmost locations and warmer colors representing the southernmost.

3. Methods

The longest record of fog frequency available was obtained from the National Oceanic and Atmospheric Administration (NOAA) archive for Fresno dense fog days beginning in 1909. This record wholly encapsulates the upward-then-downward trend in fog frequency observed in the 20th century that cannot be fully observed in modern records from the National Climatic Data Center (NCDC) which are shorter (1940-2016), but more temporally and spatially complete. However, when compared, both data sets show excellent agreement, thus providing greater confidence for the NOAA data, as analysis will show.

I developed a detailed fog climatology using up to 75 years of visibility measurements from the NCDC spanning 15 sites typically located at airports (https://www7.ncdc.noaa.gov/CDO/cdoselect.cmd). Dense fog was defined as visibility below 400 meters (one quarter-mile). The climatology is derived from hourly data wherever possible, rather than daily, to account for the highly episodic nature of dense fog. Any day with at least one hour of dense fog is considered a fog day, all of which are summed over each fog season (November-March), representing annual fog days per year. In order to calculate annual fog days, each month needed > 90% hourly coverage. If all five months of the fog season had > 90% (with most years included having > 98% coverage), annual fog days were summarized. Average duration was

determined by dividing the total number of dense fog hours in a winter season by the total fog days.

Visibility was initially measured by the Surface Aviation Observation (SAO) guidelines prior to 1996, whereby visibility was manually recorded by meteorologists using visible markers. Post-1996, the Automated Surface Observation System (ASOS) was standardized, where visibility was automatically recorded using a forward scatter visibility sensor that measures the attenuation of light at 20 second intervals. There are differences in the maximum visibility recorded between the SAO and ASOS guidelines, thus I limited all visibility measurements to 16 kilometers for consistency. No other inconsistencies as a result of the instrumentation change were found in the record.

Historical records of temperature, dew point, and wind speed from airports throughout the valley were accessed through the NCDC. Daily averages were calculated by extracting measurements taken every three hours, (eight measurements per day) with a minimum of seven measurements per day to calculate a daily average with even temporal coverage. Data for maximum/minimum temperature and precipitation were pulled from daily measurements calculated by the NCDC at the same airports (https://www.ncdc.noaa.gov/cdo-web/datatools/lcd). I set a 65% minimum reporting threshold to calculate monthly averages from daily values for the fog season months of November-March; however, most months had either very low reporting or above 95%. I determined 65% as the necessary threshold through random sampling t-tests of large iterations and requiring deviation from the mean be less than 5%. Annual wintertime (Nov-March) averages were then calculated by averaging over the fog season, with all five months required per season to ensure comparability year over year. Records were inspected for station location continuity whenever possible and reviewed for instrument malfunction.

Trends in particulate matter (PM_{10}) and NO_x emissions were first obtained through the Environmental Protection Agency (EPA) NO_x Emission Inventory from 1940-1998 (EPA, 2000). More modern trends for NO_x emissions from 1970-2017 were obtained from the EPA's website (https://www.epa.gov/air-emissions-inventories/air-pollutant-emissions-trends-data). A localized fuel-based emission inventory of NO_x for the San Joaquin Valley and the Central Valley (San Joaquin + Sacramento Valley) was developed using the methods described in McDonald, B.C. et al., 2012. Briefly, mobile source emissions are estimated using a fuel-based approach, including on-road engines (e.g., passenger vehicles, heavy-duty trucks), off-road diesel engines (e.g., tractors, construction equipment), and small two- and four-stroke off-road gasoline engines. Mobile source engine activity is estimated using state-level fuel sales reports for on-road and off-road engines and allocated to the San Joaquin and Sacramento Valley air basins using California's 2009 Emissions Almanac (CARB, 2009). Long-term trends in mobile source NO_x emission factors have been characterized from the 1960s to the present day by Hassler et al., 2016. All other anthropogenic sources of emissions are from California's Emissions Almanac, which reports emissions from 1975 to the present day for stationary and area sources of emissions. Prior to 1975, I extrapolate stationary and area sources of NO_x emissions to 1960 based on annual fuel activity data from the State Energy Database System (EIA, 2017).

I also obtained historical trends in NO_x concentration using data from the California Air Resources Board (ARB) archive (https://www.arb.ca.gov/adam/). Each city has multiple monitoring stations

where NO_x is measured by chemiluminescence and averaged over 24-hours. The length of data recorded at each monitoring station can vary significantly, ranging from a few years to multiple decades. In order to develop a historical record with a similar latitude distribution as the meteorological variables, I selected stations within the urban plume of the local airport meteorological stations, with the largest distribution perimeter being those of Fresno and Bakersfield (14.5 x 13 kilometers). I compared the monitoring stations within each urban plume to confirm consistency of station reporting. After removing severe station outliers, I calculated monthly averages for November – March of all stations in the city over the course of the record, requiring 65% of daily measurements per month, followed by calculating an annual winter average. The representativeness of ground-based measurements for the valley has been confirmed by NO_2 retrievals using the earth-observing satellite Ozone Monitoring Instrument (OMI) in past studies (Russell et. al., 2010). I acknowledge that some NO_x data for this study are averaged for a city plume originating as much as 8-15 kilometers from the visibility measurements, which are typically observed at airports. While NO_x does exhibit distinct urban plumes when observed by OMI, past work characterized Central Valley boundary layer pollution as well-mixed within latitude bands, especially during frequent multiday pollution episodes and wintertime stagnation (Pusede & Cohen, 2012). Further, Chow et al., 2006 found San Joaquin Valley wintertime NH_4NO_3 $PM_{2.5}$ much more uniformly distributed outside urban plumes than carbonaceous PM, with the zone of representativeness for monitoring sites being between 10-20 kilometers, increasing even further when observations were annually averaged. This suggests that the urban monitoring sites are sufficiently representative for this study.

Trends in predictor variables were analyzed using the non-parametric two-tailed Mann-Kendall trend test and the Theil-Sen estimator (http://www.mathworks.com/matlabcentral/fileexchange/authors/23983). The Mann-Kendall trend test assesses the null hypothesis (H_0), which assumes there is no trend in the data, against the alternative (H_1) without requiring linearity (Mann, 1945; Kendall, 1955). The Mann-Kendall test outputs H = 0 when the null hypothesis passes and H = 1 when it fails, meaning that there is a statistically significant trend at the $\propto = 0.01$ significance level. The Theil-Sen estimator is a non-parametric technique for robustly fitting data to a line while minimizing the influence of outliers (Theil, 1950; Sen, 1968). The Sen's slope (Q_i) is determined by finding the median of all the slopes between pairs of points over the designated period:

$$Q_i = \frac{(x_j - x_k)}{(j - k)} \; for \; i = 1, \ldots n$$

where x_j and x_k are data at times j and k, and n is the number of data points. The average of these n values for Q_i is Sen's slope. A best fit line is calculated using the slope and y-intercept. The Theil-Sen estimator was used to determine the average change in each variable per year over the course of the period of inquiry.

In order to separate the high frequency, shorter-term signal from the long-term trend, I first ran a Lomb-Scargle periodogram on daily averages to identify significant periods in the data, despite its uneven sampling (Lomb, 1976; Scargle, 1982). Dew point depression, temperature, NO_x concentration, wind speed, precipitation, and visibility (as a continuous variable highly correlated with fog days) were analyzed. The input data was processed by normalizing by its 1-norm and

detrending before analyzing the output frequencies of highest spectral significance ($p < 0.01$). The frequencies were compared between variables to identify common periods of variability. These periods were used as windows for a low pass filter, calculated by a moving mean, in order to isolate the long-term trend from the high frequency variability, calculated as the residuals of the moving mean. The decomposed trends for dew point depression, wind speed, and NO_x were then tested for correlation with daily visibility.

Correlation between annual fog days and predictor variables was found using orthogonal linear regression, in which errors in both the dependent and independent variables were determined for the linear fit (https://www.mathworks.com/matlabcentral/fileexchange/16800-orthogonal-linear-regression). The linear correlation was calculated using the Pearson correlation coefficient and was then squared to find the coefficient of determination, which estimates the fraction of variance in fog days explained by the predictor variable. When analyzing the correlation between fog days and air pollution, meteorology of sufficient time resolution for calculating Sen's slopes was not available for Chico, Yuba City, or Modesto. In these instances, data from adjacent meteorological stations were substituted with reporting from Red Bluff, Beale Air Force Base, and Castle Air Force Base, respectively. Meteorology data at the paired sites were highly correlated, with R^2 ranging from 0.81-0.88 (*Table 1*). Air pollution data were available for a smaller window of 1980-2014. An exception was made for Chico – where observations concluded in 2008 – because it is the northernmost site with available NO_x measurements, making these data of great interest.

Table 2 provides a description of the observational sites, including location, length of high-resolution operation, and completeness of record from 1963-2016 for meteorology and 1963-2014 for NO_x concentration.

4. Results and discussion

4.1. Radiation fog trend

4.1.1. Temporal variability

The number of dense fog days in Fresno, the longest record available, increased 2% per year on average from 1930 to 1970, demonstrating a statistically significant 85% growth ($p < 0.01$). A distinct decrease in fog days began for all locations around 1980, with sites in the north exhibiting the most rapid decline at 2.5% fewer fog days per year (*Table 3*). Fog decline is most apparent when the trend is averaged over all sites using the hourly NCDC record, demonstrating a valley-wide decrease in both occurrence and duration of fog (black lines in *Figure 2*). From 1980 to 2016, fog days have declined on average by 76% ($p < 0.01$), with average fog episode per day declining by 56% from a valley-wide average of 6.2 hours per day to 2.7.

Historically, dense fog episodes were characterized by late night low visibility events – particularly in the foggiest locations such as Fresno (*Figure 3c*) – when the surface radiatively cools. As the cooler conditions continue to favor condensation throughout the night, denser fog develops into the early morning hours, reaching its peak after 5 am. However, the diurnal pattern of wintertime visibility has gradually transitioned since ~1980, with low visibility events now forming in the early morning (fewer blue colors from 20-24 hours) and dissipating more quickly the following day (*Figure 3*). The reduction in dense fog events demonstrated in *Figure 2* has a substantial

impact on conditions later in the day, with average afternoon visibility increasing since 1990 at all locations. The impact is seen most strongly in Red Bluff (*Figure 3a*) where the fog season has nearly ceased to occur.

4.1.2. Spatial variability

Central Valley fog frequency exhibits a pronounced north-south gradient, with fog consistently more frequent in southern latitudes than northern over the course of the NCDC record (*Figure 4*). This pattern is represented throughout the analysis by the spectral color scheme, in which cooler colors represent northern latitudes and warmer colors represent southern latitudes. Sites throughout the 700-kilometer-long region have strong year-to-year variability that is coincident, suggesting that large scale mechanisms control this variability. A deviation from the observed north-south fog gradient is seen in the southernmost city, Bakersfield, which I will explore further in the meteorological analysis.

The chapter uses the spatial gradient, in conjunction with the long-term upward-then-downward temporal trend in *Figure 2a*, to identify drivers of changing fog formation by their correspondence to the unique spatiotemporal features of the fog record.

4.2. Climate trends

Here this chapter presents available trends of the key climatic drivers likely to be associated with fog formation: minimum temperature, dew point depression, precipitation, and wind speed. Each variable is considered, when possible, for its relationship to the spatial (distinct north-south gradient) and temporal (upward-then-downward signal), and regression statistics were calculated to compare their explanatory significance. Figures are included for all statistically significant findings.

4.2.1. Minimum temperature

This study focuses on minimum temperature (T_{min}), because radiation fog most commonly forms after sunset (*Figure 3*) due to rapid surface radiative cooling. I would expect colder temperatures to be associated with frequent fog and low visibility, as it is easier for atmospheric moisture to reach saturation and condense. However, if the fog formation trend was heavily dependent on temperature, fog frequency would instead be highest in the northern valley where it is colder on average, rather than the southern where it is warmer on average. When comparing the spatial gradient of fog days (*Figure 4*) and T_{min} (*Figure 5a*), temperature demonstrates significantly less N-S latitude consistency, with regions in the north, such as Redding and Red Bluff, occasionally reaching yearly-averaged T_{min} higher than locations hundreds of kilometers south, such as between 1950-70, only to return to being the colder cities. However, more recent fog seasons – particularly in the last decade – show increased latitudinal consistency, with wintertime T_{min} throughout the valley both rising and becoming more homogenous.

With respect to historical trends, the valley experienced much less wintertime T_{min} warming than in other seasons. The T_{min} trend from 1980-2016 is not statistically significant (*Figure 6a*) and thus its direction cannot be determined (*Table 3*). A distinct warming signal is not evident until the last decade, suggesting that T_{min} did not influence the initial decline in fog days. These results then

imply that T_{min} alone is not a dominate variable in fog frequency.

4.2.2. Dew point depression

When the temperature is at or near the dew point, condensation of atmospheric moisture into fog droplets can occur, thus the variable dew point depression (DPD), calculated by subtracting dew point from ambient temperature, is expected to be related to fog formation. DPD must be at or near zero for fog droplet formation, so substantially foggy periods have low average DPD. A time series of DPD trends (*Figure 7a*) reveals that the northernmost sites Red Bluff and Redding have the highest DPD, and thus largest average temperature decline needed during nighttime radiative cooling to reach condensation and fog formation. Meanwhile, Bakersfield, the most southern site, also has a relatively high seasonal DPD. This explains why its fog trend does not as consistently adhere to the north-south gradient of fog frequency (*Figure 4*) – the location is much dryer than sites at a proportional latitude, creating a larger threshold of DPD that must be surmounted in order to form fog. However, DPD alone cannot explain fog formation, because Bakersfield is one of the more frequently foggy sites. Thus, DPD can be an explanatory predictor, but clearly works in concert with other variables. This is further demonstrated by the lack of latitude consistency shown in *Figure 7a,* in which sites with the lowest DPD (shown in the yellow and green colors of Travis, Sacramento, and Beale) occur in central and northern locations of the valley that do not have the most fog.

Temporal trends of DPD reveal a valley-wide average increase of 39.5% from 1980-2016 ($p < 0.01$), suggesting that a decrease in fog days could be the result of concurrent changes in water availability and temperature (*Table 3*). However, when comparing Mann-Kendall trend test results for each decade from 1980-2016, results indicate that DPD began increasing at least 10 years after the decline in fog frequency; further, DPD decreased from 1990-2000, suggesting that it would enhance fog, but fog days continued declining. The high confidence intervals for the slope of DPD from 1980-2016 reflect the uncertainty in the strength and consistency of the trend (*Table 3*). Thus, while the overarching positive trend from 1980-2016 is statistically significant and likely impacting fog by inhibiting condensation, its initial increase does not agree with fog trends suggesting DPD alone is not responsible for the loss in fog days.

However, years of low DPD are well correlated with years of high fog frequency, with explanatory value for 24% of the annual variability (*Figure5b*). This suggests that much can be understood about the stark interannual variability in fog events by looking at trends of water availability and temperature concurrently.

4.2.3. Precipitation

In contrast to temperature and DPD, precipitation displays a pronounced north-south gradient, with regions in the north consistently receiving more rain than those in the south (*Figure 5b*). While yearly precipitation exhibits strong interannual variability, the majority of the precipitation trend, aside from the droughts experienced from 2006-2010 and, most severely, 2012-2017, remains neutral with studies showing Northern and Central California getting wetter over the 20th century and winter precipitation stable for the entire state (Killam, 2014). Only trends in Red Bluff were statistically significant ($p < 0.01$), demonstrating a 36.4% decline in precipitation, though with

very wide confidence intervals (*Table 3*). The remaining sites exhibited no significant trend from 1980-2016.

Fog's sensitivity to precipitation remains an ongoing research question. While years of high rainfall are associated with an increase in fog events, many heavy fog years appear inversely correlated with precipitation when historical trends are compared (*Figure 9*). Additionally, I found that fog frequency has no correlation with the El Nino Southern Oscillation index, similar to the results of Herckes et al., 2015. The data suggests that there is some ideal precipitation amount for enhancing fog, and beyond that level fog is suppressed. This threshold likely exists because intense winter storms are associated with turbulent conditions unfavorable to fog formation. Similarly, frequent radiation fog can occur in years of low precipitation, because a significant rain event followed by high pressure and clear conditions is ideal for formation. Additionally, annual winter time precipitation demonstrates no statistically significant correlation with annual fog days, further highlighting the ambiguity (*Figure 6b*). Here the results show that when holding a given annual precipitation constant, such as 300 mm, a site could predictively expect a large range of potential fog days, from as low as 0 to as high as 50.

4.2.4. Wind speed

Wind speed can play a significant role in radiation fog formation, with fog typically occurring in periods of atmospheric stability and wind speeds below < 1 m/s (Herckes et al., 2015). Higher wind speeds increase surface mixing and inhibit radiative cooling after sunset. Thus, I would spatially expect northern regions with less frequent fog to have higher wind speeds than southern regions of more frequent fog, as well as historically expect wind trends to be increasing since ~1980. However, the analyzed record from 1940-2016 demonstrates little latitude consistency, with no clear pattern from north to south regarding magnitude of wind speed (*Figure 7c*).
While the valley-wide ~27% decrease in wind ($p < 0.01$) correlates well with decreased fog events, it should have the opposite result (*Table 3*). Instead, I would expect this trend to enhance fog formation through more stable atmospheric conditions and more rapid radiative cooling at night. This puzzling trend is consistent with recent evidence for a 5-15% midlatitude atmospheric stilling (Vautard et al., 2010), and suggests that had average wind speed not declined during this period, fog events would have been further diminished.
Wind speed demonstrated a low, but statistically significant predictive impact on fog frequency, explaining 9% of the variance (*Figure 7d*). Here the results show that lower wind speeds are associated with higher fog frequency – a relationship likely made more complicated by trends in atmospheric stilling.

4.2.5. Segmenting trends with meteorologically favorable fog conditions

This chapter further investigates the tule fog trend by segmenting by times when conditions were optimal for fog formation, defined as average daily dew point depression < 4.2 °C and wind speed < 2 meters per second (m/s). The goal was to determine whether tule fog is more sensitive to the frequency of these meteorological conditions or some other potential driver when looking at daily data, rather than seasonal. The thresholds were determined by comparing the summary statistics for meteorology on foggy versus clear days. The frequency of optimal fog condition occurrence has no statistically significant trend during the period from 1980-2016, with a Mann-Kendall result

of H=0 at a 99% confidence interval (*Figure 10*). The frequency of favorable fog formation conditions remained consistent during this period despite increases in average dew point depression since 2000.

While there is no trend in the number of days with optimal fog conditions, the fraction of days where radiation fog actually occurred under these conditions declined significantly over this period ($p < 0.01$). In 1980, dense radiation fog occurred ~55% of the time when optimal fog conditions were met, but since 2010 fog only occurred ~35% of the time under these same conditions (*Figure 8a*). The observations suggest a mechanism unrelated to these meteorological variables is necessary to explain the observed decline in fog days.

This is further confirmed by analyzing the meteorology on the days when dense radiation fog forms (*Figure 8b*). The frequency of fog occurring under optimal conditions, relative to the total annual fog days, has increased significantly ($p < 0.01$), from ~50% (50% occurred outside optimal meteorological conditions) in the early 1980s, to ~80% since 2010 (20% occurred outside optimal meteorological conditions). This suggests that radiation fog occurred much more frequently at higher dew point depressions and higher wind speeds in the 1980s than in later years, which would be consistent with a reduction in the number of hygroscopic particles available for water to condense on. This effect is well documented in modeling studies which show that an increase in air pollutant concentration can allow for fog droplet growth under untraditional activation conditions where relative humidity is below 100% (Charlson et al., 2001).

4.3. Air pollution trend

Air pollution throughout the United States rapidly increased with intensifying urbanization in the twentieth century, spurred by unregulated fuel consumption and inefficient home heating. Severe pollution episodes were recorded in California as early as 1903 due to dense photochemical smog, which formation chemistry at the time was unknown (Senn, 1948). Valley population grew rapidly beginning in the early 20th century, with cities such as Fresno seeing a 103% growth from 1920-1950 and the Central Valley population growing by 52% from 1940-1950 alone (U.S. Census; Gregor, 1963). This population growth was associated with industrial and agricultural development, resulting in significant air pollution increases. Expansive oil fields and refineries, rail freights, and increased vehicle use contributed to early pollution challenges. Similarly, the increasing use of agricultural burning and off-road equipment were unregulated.

While there are few observations of Central Valley NO_x prior to the mid-1960s, national EPA emission inventories for NO_x and PM_{10} give a picture of historical pollution trends (*Figure 11*), thus providing an estimate for increasing emissions in the mid-20th century and the potential CCN availability. The magnitude of the national PM_{10} trend is consistent with California archival records from 1960-2005 for coefficient of haze, a retired measurement of particulate matter, found in Kirchstetter et al., 2017. Earlier PM_{10} inventory data are estimated based on total suspended particle (TSP) measurements and are less reliable. Nationally, derived PM_{10} emissions were greater than NO_x by mass prior to 1960 (*Figure 11*), but saw initial declines due to the effective mitigation of industrial sources (EPA, 2000). Sulfur dioxide (SO_2) in the San Joaquin Valley was likely an important contributor to CCN in the earlier record, because the southern valley had considerable sulfate concentrations from local oil extraction (Jacob & Shair, 1986). However, due to its greater dominance as an air pollutant in much of the country, using a national inventory would not be representative of local trends in California where the use of coal for in-state electricity

generation is less prevalent. Local San Joaquin Valley SO_2 archives beginning in 1975 demonstrate that concentrations had already greatly increased by the 1970s and began rapidly falling decades prior to effective NO_x controls (*Figure 11*).

Instead, since the 1970s, NO_x has been the predominant inorganic pollutant – and most likely limiting wintertime CCN precursor – in the Central Valley. National NO_x emission inventories for 1940-1998 and 1970-2017 demonstrate the rise in NO_x sources with increasing fossil fuel use, followed by its subsequent decline beginning in the early 1980s, which is consistent with the locally developed fuel-based inventory for San Joaquin Valley. Implementation of California's vehicle tailpipe standards for hydrocarbons and carbon monoxide (1966), oxides of nitrogen (1971), and particulate matter from diesel-fueled vehicles (1982) began a substantial reduction in valley air pollution (California Air Resources Board, 2012). Transportation emission controls have made rapid advancements through engine modifications and exhaust after-treatment devices. Most noteworthy was the implementation of the three-way catalytic converter on passenger vehicles in the early 1980s which began a stark trend of emission improvements, as seen in a 50% reduction in gasoline-NO_x emission from 1990-2010 in the San Joaquin Valley despite a 43% population growth (McDonald et al., 2012). Power plant emissions of NO_x also decreased from implementation of stack controls (Frost et al., 2006). Our SJV inventory suggests that in 1960, around half of the NO_x emissions are from stationary sources and the other half from mobile sources. By 2014, I estimate that mobile sources dominate (> 80% of the NO_x total) in the San Joaquin Valley.

NH_4NO_3 concentration fell proportionally with measurements of NO_x, the limiting precursor, from 2000-2015, as Central Valley $PM_{2.5}$ declined at a rate of 2% a year (Pusede et al., 2016). This suggests that reductions in NO_x concentration directly reduced the availability of NH_4NO_3 as potential wintertime CCN. Trends in Fresno fog frequency and trends in San Joaquin Valley NO_x emissions have declined in concert (*Figure 11),* though fog frequency has significantly more variability. While the length of local records limits our understanding of California pollutants prior to 1960s, I can infer from the slope of the local SO_2 (1975-2015) and national PM (1940-2017) inventories that other sources dominated and influenced the number of CCN available for fog formation.

These emissions trends are confirmed by local annual NO_x concentration measurements for seven cities throughout the valley (*Figure 12*). The trend shows an initial rapid increase, followed by a ~50% decline from 1980-2014 ($p < 0.01$), though the completeness of each record varies. Air pollution is the only fog contributor analyzed that began declining in the same decade as fog frequency and consistently continued declining from 1980-2016. Additionally, NO_x concentration exhibits a similar north-south gradient as seen with fog frequency, with concentration consistently highest in the south which is more populated and polluted (*Figure 12*). The north-south gradient remains persistent throughout the 50-year record despite the declining trend and interannual variability. Thus, NO_x decline has both a temporal and spatial signature consistent with that of fog frequency.

Annual fog days and NO_x concentration are significantly correlated ($p < 0.01$) with NO_x explaining an estimated 24% of the variance in fog frequency when examining all sites across all years (*Figure 13a*). This influence is further demonstrated when segmenting by the most impactful climate

variable, DPD, in three quantiles by high, average, and low (*Figure 13b*). When DPD is high, representing high temperature and low water availability, fog frequency is less sensitive to additional CCN, explaining 29% of fog variance, because meteorological conditions are less sufficient for condensation. In this high DPD scenario, the regression slope is only 0.2, suggesting 2 additional fog days for every 10 parts per billion (ppb) increase of NO_x concentration. However, as DPD decreases and physical conditions get closer to causing condensation, the slope increases, representing fog frequency's increasing sensitivity to changes in air pollution. The coefficient of determination also increases, as NO_x has more explanatory significance. At low DPD conditions, with an average of 3.6°C, NO_x concentration explains an estimated 46% of annual fog frequency. Thus, when average DPD is above 5°C, sites are much less impacted by trends in NO_x, but given sufficiently low dew point depression, air pollution trends have a pronounced influence, with an estimated 5 additional fog days for every 10 ppb increase.

4.4. Separating drivers of short-term and long-term variability

Despite the strong influence of NO_x found in the fog frequency record, there remains considerable high frequency (short-term) variability in the record that is not observed in NO_x concentration. By decomposing the fog trends into high frequency and low frequency (long-term) components, this chapter quantifies the impact of meteorology on high frequency variability.

Analysis using a Lomb-Scargle periodogram identified the full 151 days included to represent each annual fog season ($p < 0.001$) as having the highest and most consistent spectral significance of any period in the data set, meaning that annual seasonal changes dominate the periodicity. The trend was therefore decomposed by applying a low pass filter with a period of 151 days on daily averages of fog season visibility, dew point depression, NO_x concentration, and wind speed for 1973-2014, the most complete time window for all variables. The high frequency data, determined as the residuals of the low pass filter, show that meteorology explains much more of the short-term variance than NO_x concentration. When testing the correlation of predictor variables with the daily visibility residuals and then calculating a coefficient of determination, dew point depression explains 29% and wind speed explains 22% of the variance in day-to-day average visibility (*Table 4*). By contrast, NO_x concentration captures only 10% of the variance. This indicates short-term variability in wintertime visibility is driven more by water availability, temperature, and wind speed than by processes associated with NO_x concentrations.

The low pass filter reveals long-term trends with the high frequency (short-term) variability removed. The trend component of each predictor variable was tested for correlation with the visibility trend, revealing that the NO_x concentration trend has the highest correlation with visibility, explaining 38% of the trend (*Table 4*), far more than the dew point depression, which explains 16%, or the wind speed, which explains 11%. The separation of long-term and short-term components clarifies that the NO_x trend better accounts for reductions in fog formation from 1980-2016, while meteorology better explains the short-term variability throughout the record.

5. Summary and conclusions

The short-term variability in meteorology correlates with the strong variability of fog events, but cannot explain the observed longer-term trends in fog frequency. Dew point depression has the

strongest explanatory robustness of the meteorological variables, as potential to form fog is clearly a function of both water availability and sufficiently low temperature to allow condensation. Additionally, until recently, low wind speed had a strong correlation with years of frequent fog events. The recent "atmospheric stilling" observed in the wind speed record favors fog frequency, thus masking the even more complete collapse of the fog season that would have likely occurred otherwise.

The coherence of *both* the spatial (north-south) gradient and historical (upward-then-downward) trend is unique to fog frequency and air pollution. Despite some changes to climate in recent decades, the frequency of optimal fog conditions remains stable, yet fog continues to decline relative to the number of low dew point depression and low wind speed days occurring each year. Additionally, nearly all tule fog events in recent years occur during the most favorable fog conditions, whereas 35 years ago fog occurred on warmer days with higher wind speeds and less water availability much more frequently. This is consistent with the impact of higher air pollution historically causing a higher number concentration of hygroscopic particles for condensation, as well as pollution causing nontraditional activation of droplets when RH < 100%.

Controlling for the large interannual variability in DPD further elucidates the statistically robust relationship between fog frequency and air pollution, particularly under conditions of low DPD. When annual average conditions have sufficient atmospheric moisture and low temperatures necessary to support condensation, fog frequency is significantly more sensitive to the resulting increases in condensation nuclei from high pollution concentrations. This relationship is weakest in fog seasons where DPD is high, but it is still significant. Our findings demonstrate that in low DPD conditions, a decrease of 5 fog days per year occurred for every 10 ppb NO_x decrease over the past 36 years. The upward trend in fog frequency from 1930-1970 was likely driven by increases in emissions of other air pollutants including primary particles and possibly SO_2, but no observational data are available to further constrain the specific pollutants involved prior to the initiation of the long-term air pollution measurement network in California.

Changes in fog frequency have broad impacts on transportation safety, agricultural production, drought resilience, and climate. While the interannual influence of meteorology is key to understanding its year-to-year signal, our analysis demonstrates that changes in air pollution emissions are the main driver of the observed long-term trend of radiation fog frequency, and that reducing air pollution has had the added benefit of reducing tule fog in California's Central Valley. The impacts of reductions in air pollution emissions on fog frequency, and resulting changes for the agricultural economy, transportation safety, and climate, should be analyzed in future assessments of the co-benefits of air pollution controls.

6. Figures and tables

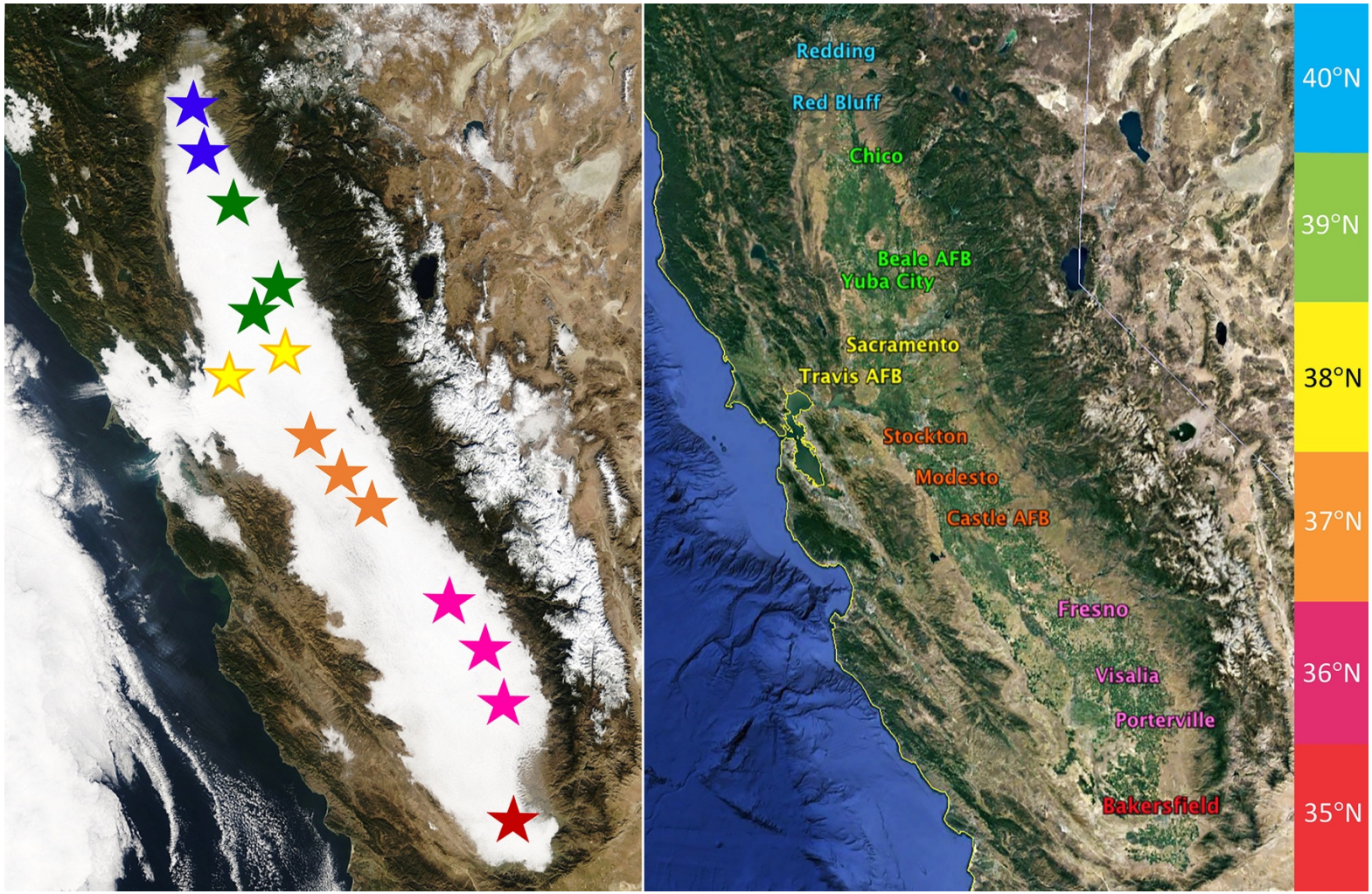

Figure 1. Map of Central Valley sites color coded by latitude from Terra MODIS. Color coding represents change in 1° of latitude, beginning at 40° N. Sacramento contains two sites: Sacramento Executive Airport and Mather Field Airport in Rancho Cordova.

Table 1. Stations where air pollution from an adjacent observation station was used by substitution.

Location	Distance (km)	Meteorology R^2
Red Bluff	50	0.81
Chico		
Beale Air Force Base	30	0.85
Yuba City		
Castle Air Force Base	45	0.88
Modesto		

Table 2. Meteorological and NO_x stations with high resolution data

Location	Met Years	NO_x Years	Lat (◦)	Lon (◦)	Population	Elevation (m)	Met %[a] (1963-2016)	NO_x %[b] (1963-2014)
Redding Municipal Airport 24257	1986-2016	1986-1989	40.52	-122.30	91,794	153	56	6
Red Bluff Municipal Airport 24216	1948-2016	-	40.15	-122.25	14,158	107.6	73	4
Chico Municipal Airport 93203	2009-2014	1965-2008	39.80	-121.85	91,567	82.9	10	80
Beale Air Force Base 93216	1959-2016	-	39.13	-121.43	1,319	34.4	77	-
Yuba City/Country Airport 93205	1973-2016	1971-2014	39.10	-121.57	66,845	18.9	46	52
Sacramento Executive Airport 23232	1947-2016	1964-2014	38.51	-121.50	495,234	4.6	81	86
Sacramento International Airport 93225	1972-2016	1964-2014	38.70	-121.59	495,234	7	61	86
Sacramento McClellan AFB 23208	1942-2016	1964-2014	38.67	-121.40	495,234	23.5	67	86
Travis Air Force Base 23202	1943-2016	-	38.27	-121.93	15,280	18.9	83	-
Stockton Metropolitan Airport 23237	1941-2016	-	37.89	-121.23	310,496	7.9	75	-
Modesto City Co Airport 23258	1998-2016	1964-2014	37.62	-120.95	212,175	22.3	33	92
Castle Air Force Base 23203	1942-2016	-	37.38	-120.57	-	58.2	64	-
Fresno International Airport 93193	1942-2016	1963-2014	36.78	-119.72	522,053	101.5	85	100
Visalia Municipal Airport 93144	1992-2014	1970-2014	36.32	-119.40	133,010	89.9	31	84
Porterville Municipal Airport 99999	1992-2014	-	36.03	-119.07	59,145	132	35	-
Bakersfield Meadows Field Airport 23155	1941-2016	1968-2014	35.43	-119.05	376,380	150	83	84

a – *percent of winters with >90% hourly data*

b – *percent of winters with >65% daily data*

Abbrievations. Meteorology (Met), Oxides of Nitrogen Concentration (NO_x), Latitude (Lat), Longitude (Lon).

Table 3. Trends in Wintertime Meteorology (1980-2016) and NO_x Concentration (1980-2014)

Location	Latitude	Fog Days		Min Temp		Precipitation		DPD		Wind Speed		NO_x[b]	
		Mann-Kendall Results for Fog Predictor Variables											
	°	H	*p*	H	*p*	H	*p*	H	*p*	H	*p*	H	*p*
Redding	40°3'	-	-	0	1.2E-01	1	3.0E-02	-	-	-	-	-	-
Red Bluff	40°9'	1	1.8E-04	0	2.4E-01	0	1.0E-01	1	1.2E-02	1	4.8E-02	-	-
Chico[a]	39°5'	-	-	-	-	-	-	-	-	-	-	1	1.5E-05
Sacramento	38°3'	1	9.1E-06	0	4.4E-01	0	6.9E-01	1	7.0E-03	1	6.7E-07	1	7.1E-07
Stockton	37°5'	1	7.3E-05	0	6.3E-01	0	3.3E-01	1	3.9E-02	1	1.5E-04	-	-
Modesto	37°4'	-	-	-	-	-	-	-	-	-	-	1	2.4E-06
Fresno	36°5'	1	1.3E-06	0	8.3E-02	0	1.3E-01	1	3.0E-03	1	8.2E-07	1	3.2E-12
Visalia	36°2'	-	-	-	-	-	-	-	-	-	-	1	4.6E-07
Bakersfield	35°3'	1	6.0E-05	0	4.6E-01	0	2.6E-01	1	3.0E-03	1	4.3E-07	1	1.3E-08
		Sen Slopes and Percent Change for Fog Predictor Variables[c]											
	°	days yr-1	% Δ	°C yr-1	% Δ	mm yr-1	% Δ	°C yr-1	% Δ	m s-1 yr-1	% Δ	ppb yr-1	% Δ
Redding	40°3'	-	-	-	-	-8.4 ± 9.14	-36	-	-	-	-	-	-
Red Bluff	40°9'	-0.43 ± 0.21	-90	-	-	-	-	0.048 ± 0.04	33	-0.011 ± 0.010	-10	-	-
Chicoa	39°5'	-	-	-	-	-	-	-	-	-	-	-0.64 ± 0.22	-61
Sacramento	38°3'	-0.80 ± 0.23	-80	-	-	-	-	0.042 ± 0.02	42	-0.033 ± 0.010	-37	-1.2 ± 0.54	-58
Stockton	37°5'	-0.77 ± 0.33	-62	-	-	-	-	0.035 ± 0.03	35	-0.022 ± 0.013	-23	-	-
Modesto	37°4'	-	-	-	-	-	-	-	-	-	-	-1.0 ± 0.44	-50
Visalia	36°5'	-	-	-	-	-	-	-	-	-	-	-0.85 ± 0.28	-51
Fresno	36°2'	-0.87 ± 0.25	-70	-	-	-	-	0.049 ± 0.03	45	-0.024 ± 0.007	-33	-1.4 ± 0.23	-63
Bakersfield	35°3'	-0.61 ± 0.25	-76	-	-	-	-	0.064 ± 0.04	42	-0.027 ± 0.009	-33	-1.4 ± 0.32	-57

a – *record limited from 1980-2008*

b – *record limited from 1980-2014*

c – *only significant trends reported*

Note. H-test results of 1 demonstrate failure of the null hypothesis at 0.01 significance level. Results of H = 0 verify the null hypothesis, indicating no trend. *Abbrievations*. Minimum Temperature (Min Temp), Dew Point Depression (DPD), Oxides of Nitrogen Concentration (NOx), p-value (p).

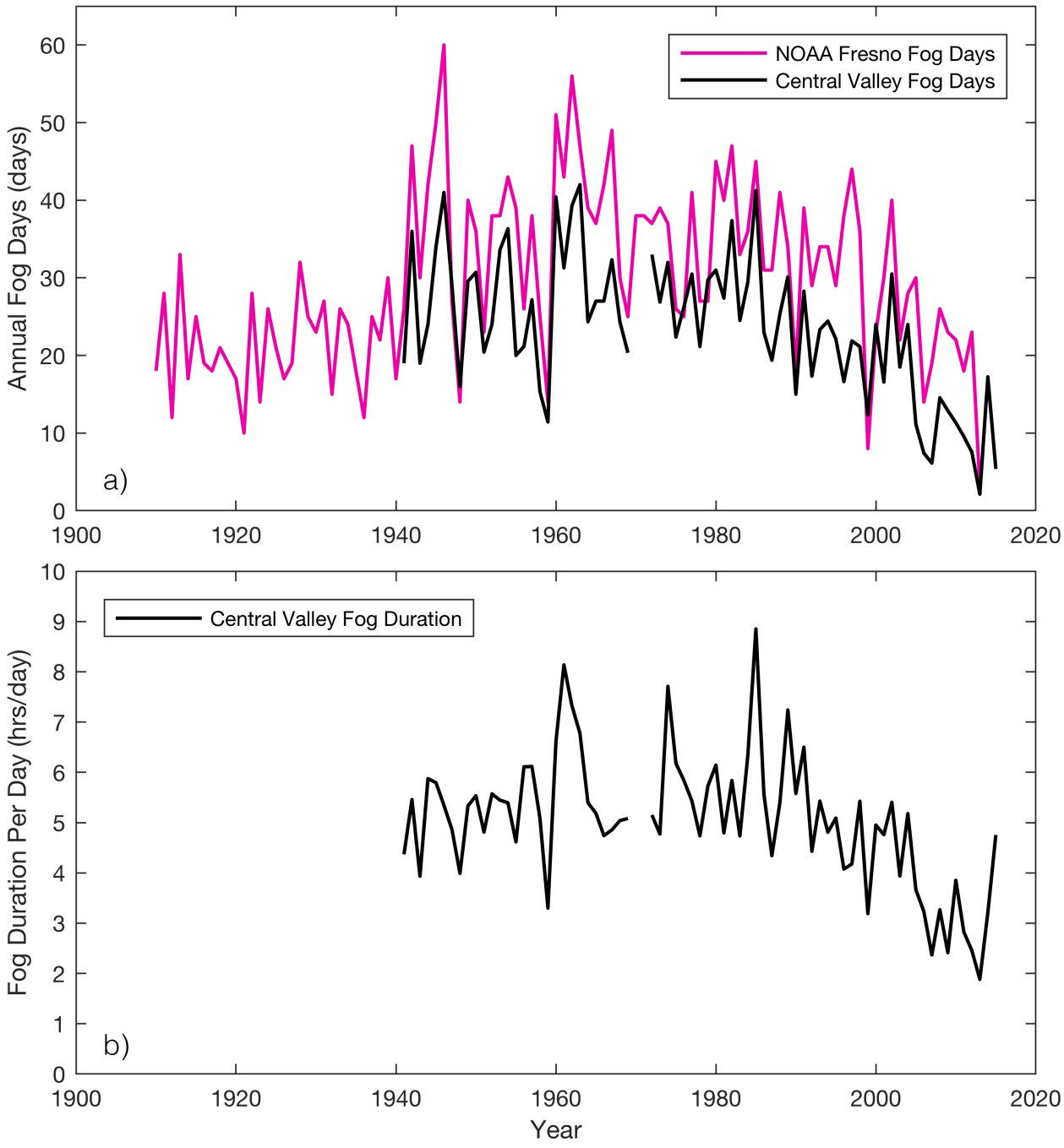

Figure 2. a) NOAA record of fog days for Fresno (1909-2014) plotted with mean Central Valley fog days derived from hourly NCDC records (1940-2016) and b) average duration of fog episodes per fog day (1940-2016).

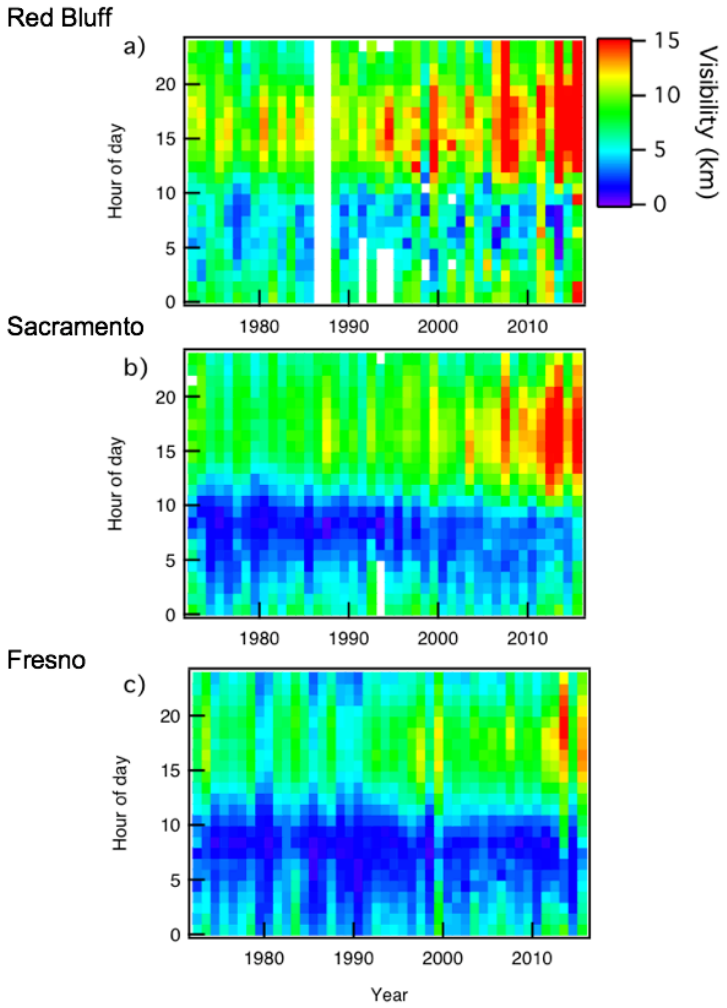

Figure 3. Time series of diurnal trend in wintertime visibility (km) for a) Red Bluff (40°N), b) Sacramento (38°N), and c) Fresno (36°N), from 1970-2015. Y-axis is hour of day from 0-24 in local standard time. Cool colors represent periods of low visibility, typically dominated by heavy wintertime fog.

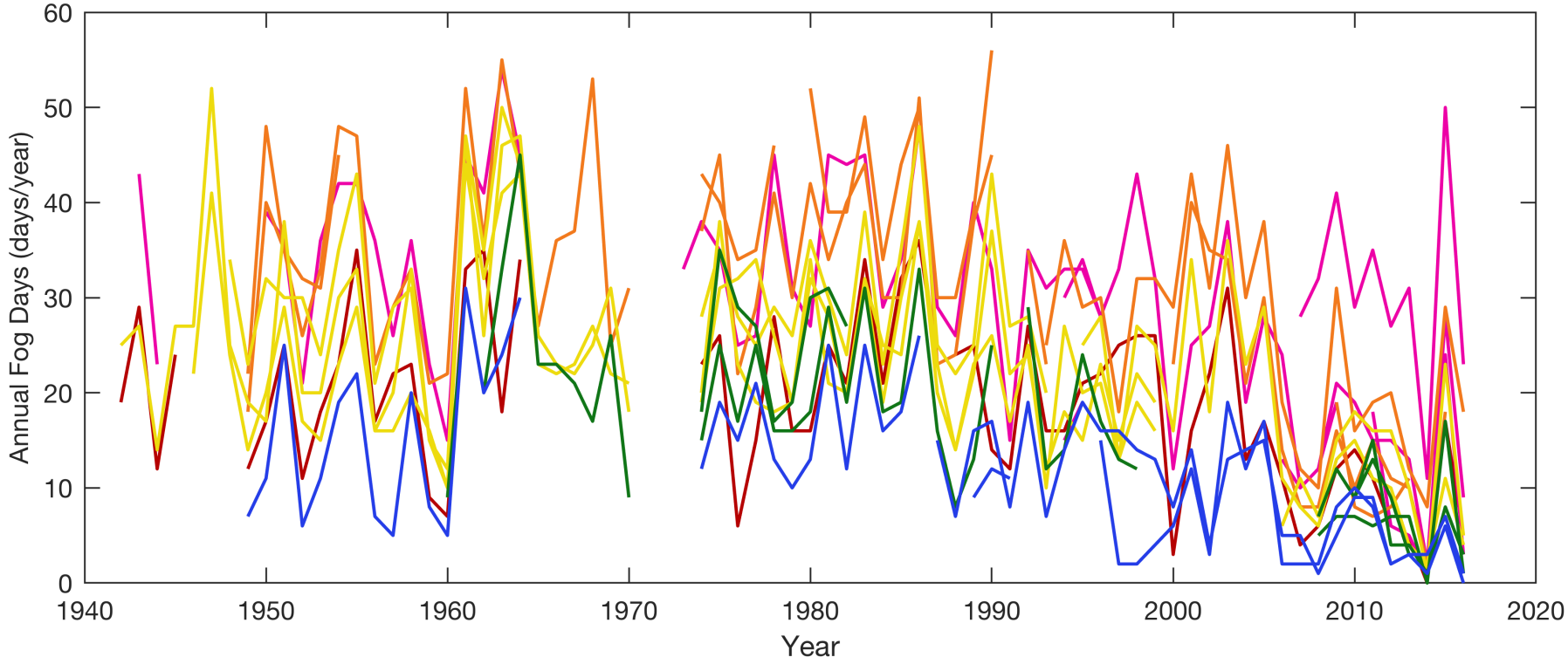

Figure 4. Plot of annual wintertime (November-March) fog days from 1940-2016 using NCDC hourly meteorological database, with color gradient as defined in Figure 1. Rainbow color code represents latitude in 1° bins of sites from 35° N (red) to 40° N (blue). Dense fog defined as a day with visibility < 400 meters for any length of time. Years with < 90% reporting are excluded.

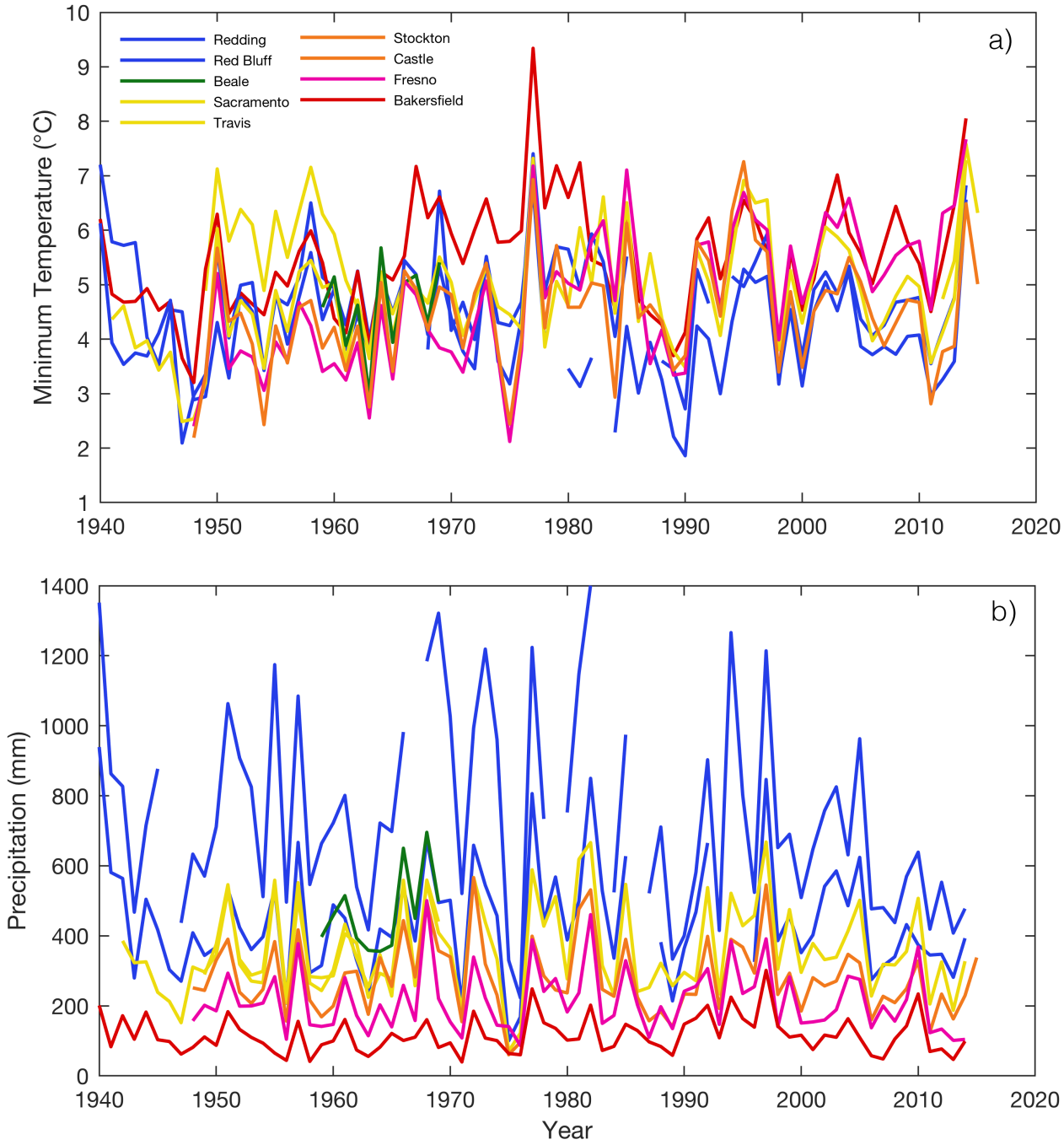

Figure 5. Time series of annual average fog season (Nov-Mar) meteorology from 1940-2016 from NCDC records for a) minimum temperature and b) precipitation. Rainbow color code represents latitude in 1°bins of sites from 35°N (red) to 40°N (blue).

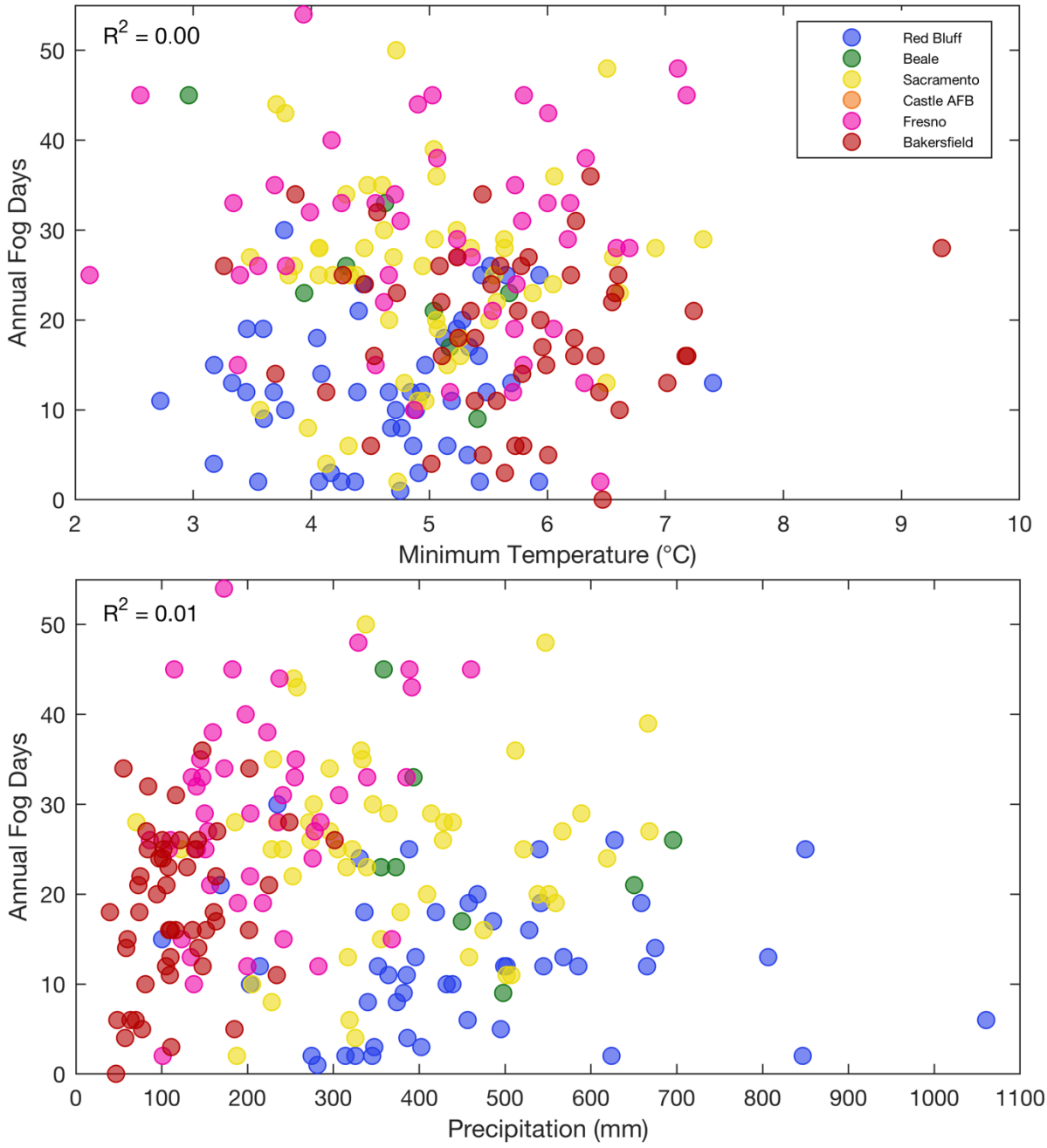

Figure 6. Annual Fog Days plotted against climate variables for a) minimum temperature and b) precipitation. No significant correlation found for either variable. Color coding represents change in 1 °of latitude, beginning at 40 °N with cool colors representing northern cities and warm colors representing southern.

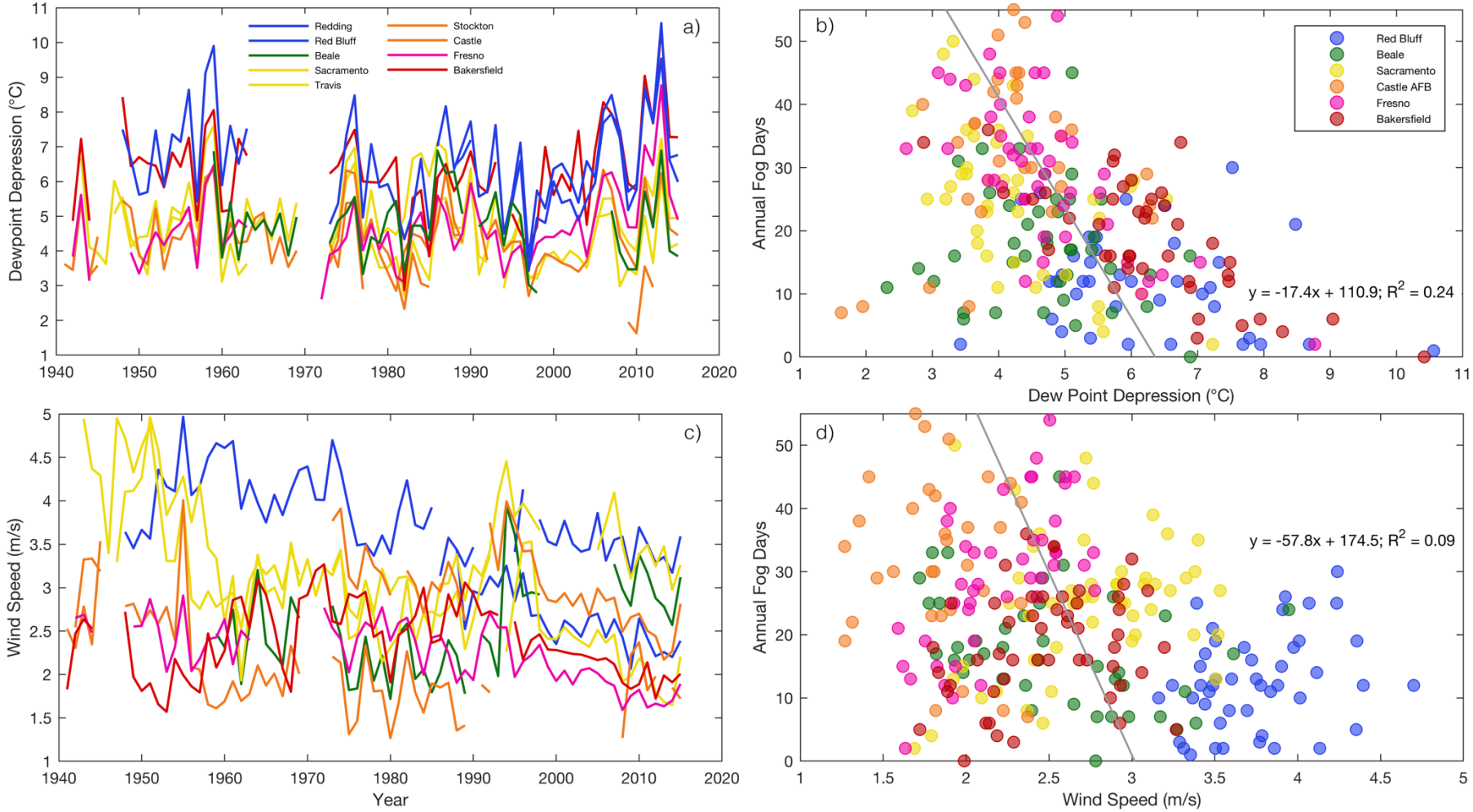

Figure 7. Time series of average a) dew point depression and c) wind speed for the annual fog season (November-March) from 1940-2016. Annual fog days plotted against b) dew point depression and d) wind speed. Rainbow color code represents latitude in 1° bins of sites from 35° N (red) to 40° N (blue).

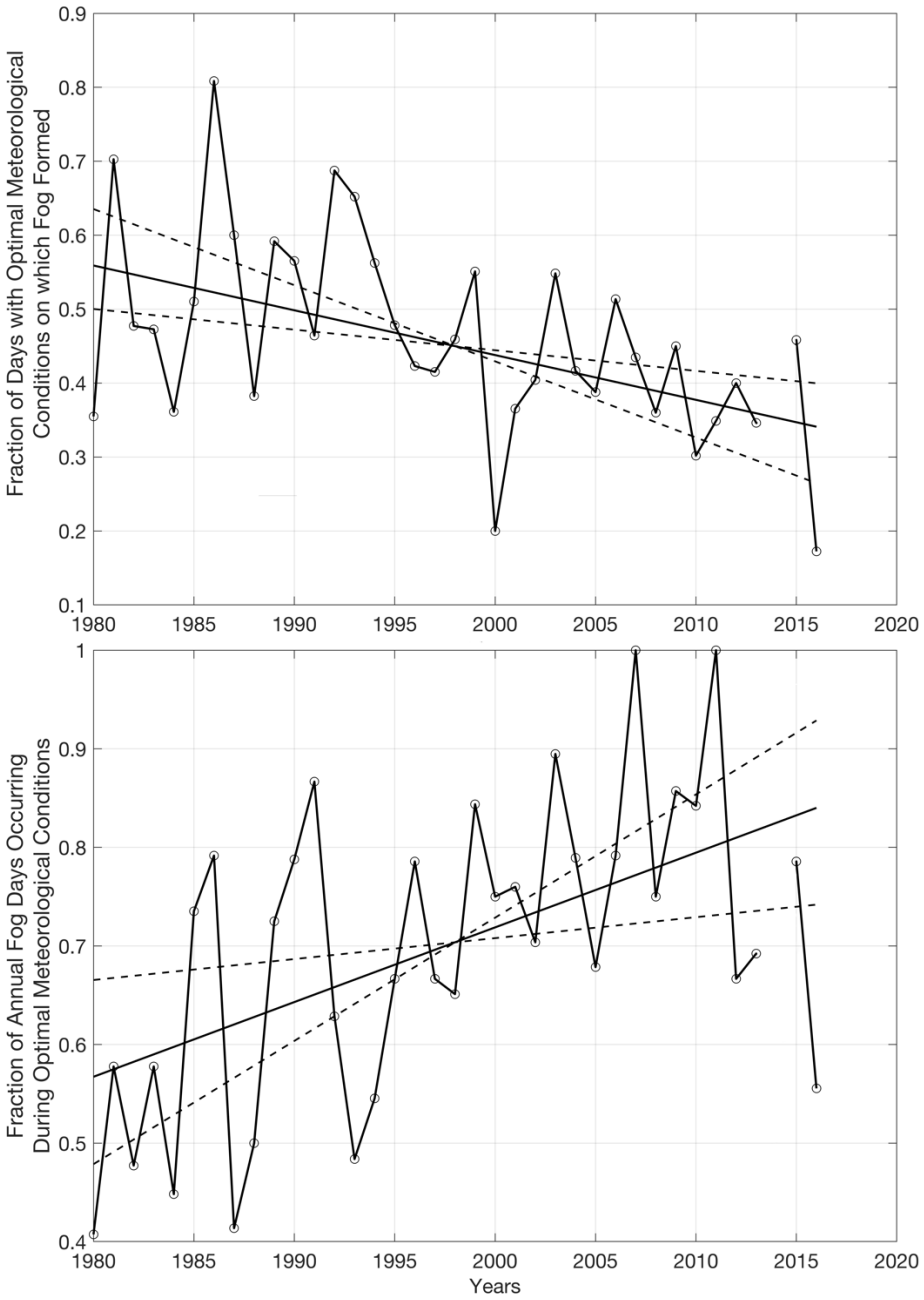

Figure 8. Historical trend for a) the fraction of days with optimal meteorological conditions where fog actually occurs (sum of fog days during optimal conditions divided by number of days with optimal conditions), and b) the fraction of total dense radiation fog days that occurred under the optimal fog meteorological conditions (sum of fog days under optimal conditions divided by total number of fog days). Optimal meteorological conditions defined as dew point depression < 4.2 °C and wind speed < 2 m/s. Solid lines represents Sen slope fits, with dashed lines showing upper and lower confidence intervals. Year 2014 was excluded because too few fog days occurred to make the statistics robust (less than 5).

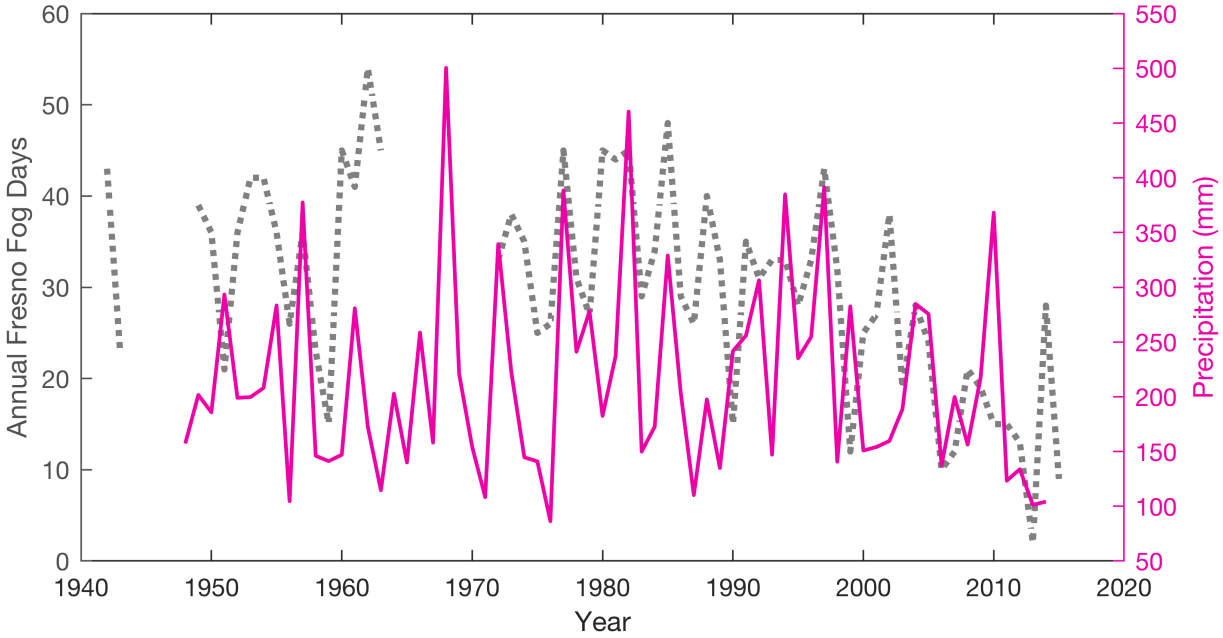

Figure 9. Time series of precipitation (pink) for Fresno plotted with annual fog days (dotted grey line) (1940-2016).

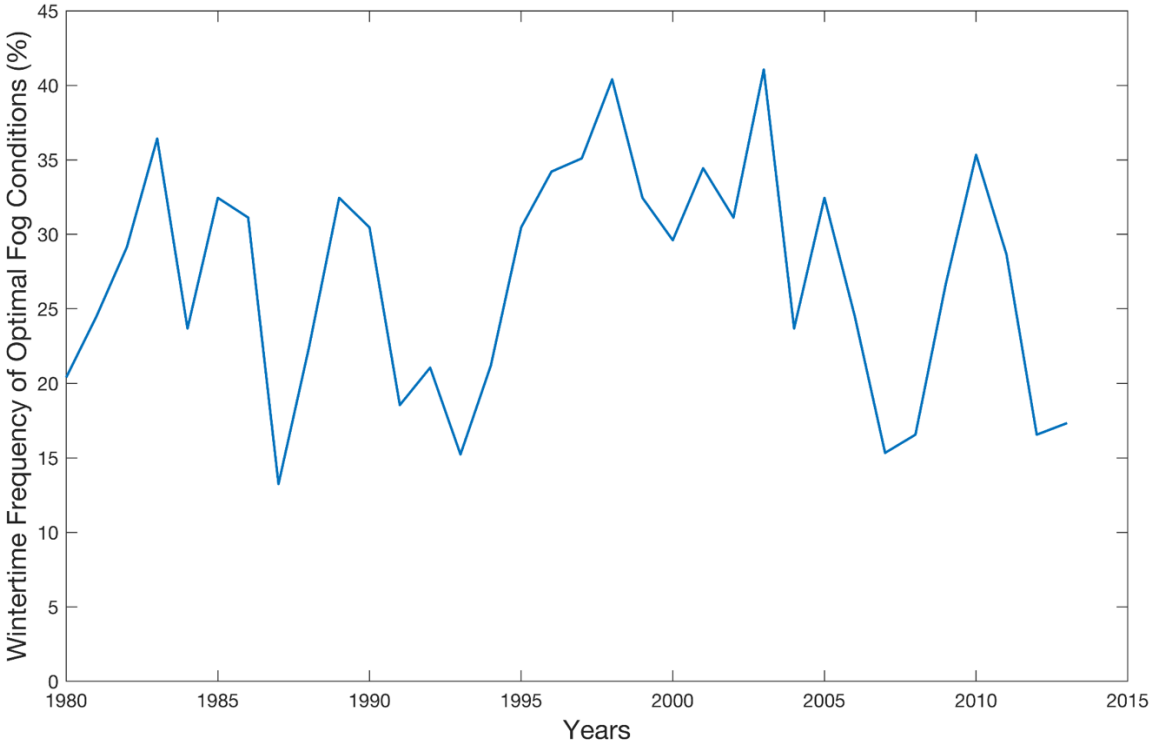

Figure 10. Historical trend of the frequency of days, as a percentage of the total, where dew point depression was < 4.2 °C and wind speed was < 2 m/s, which are optimal conditions for dense radiation fog formation.

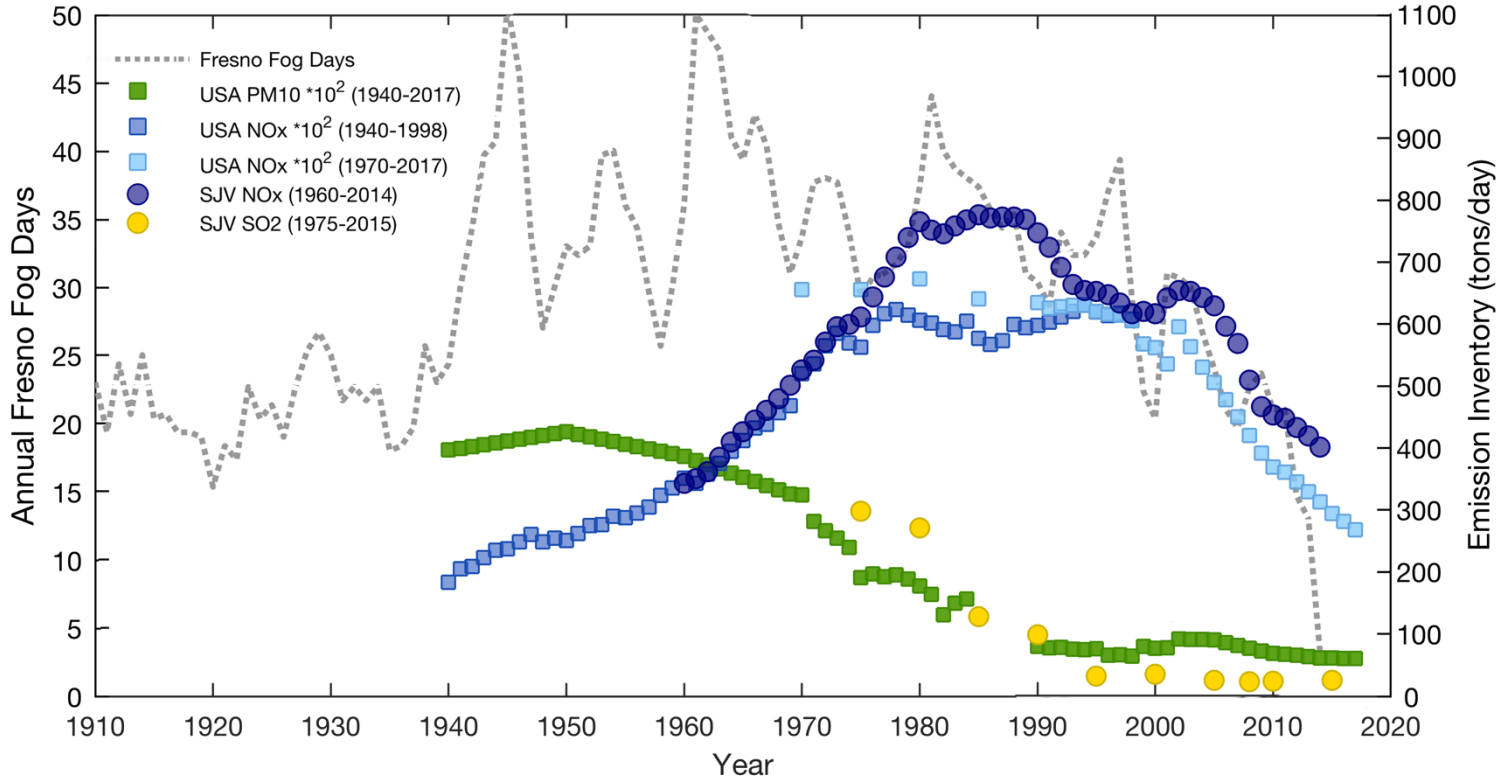

Figure 11. Times series of smoothed Fresno fog days from NOAA records (grey dotted line) plotted with national (square) and local (circle) emission inventories in tons/day. NO_x inventories represented by shades of blue points: two national NO_x inventories, ranging from 1940-1998 and 1970-2017 and one local San Joaquin Valley NO_x inventory from 1960-2014. National PM_{10} estimates from 1940-2017 represented by green squares. Local SO_2 estimates from 1975-2015 represented by yellow circles.

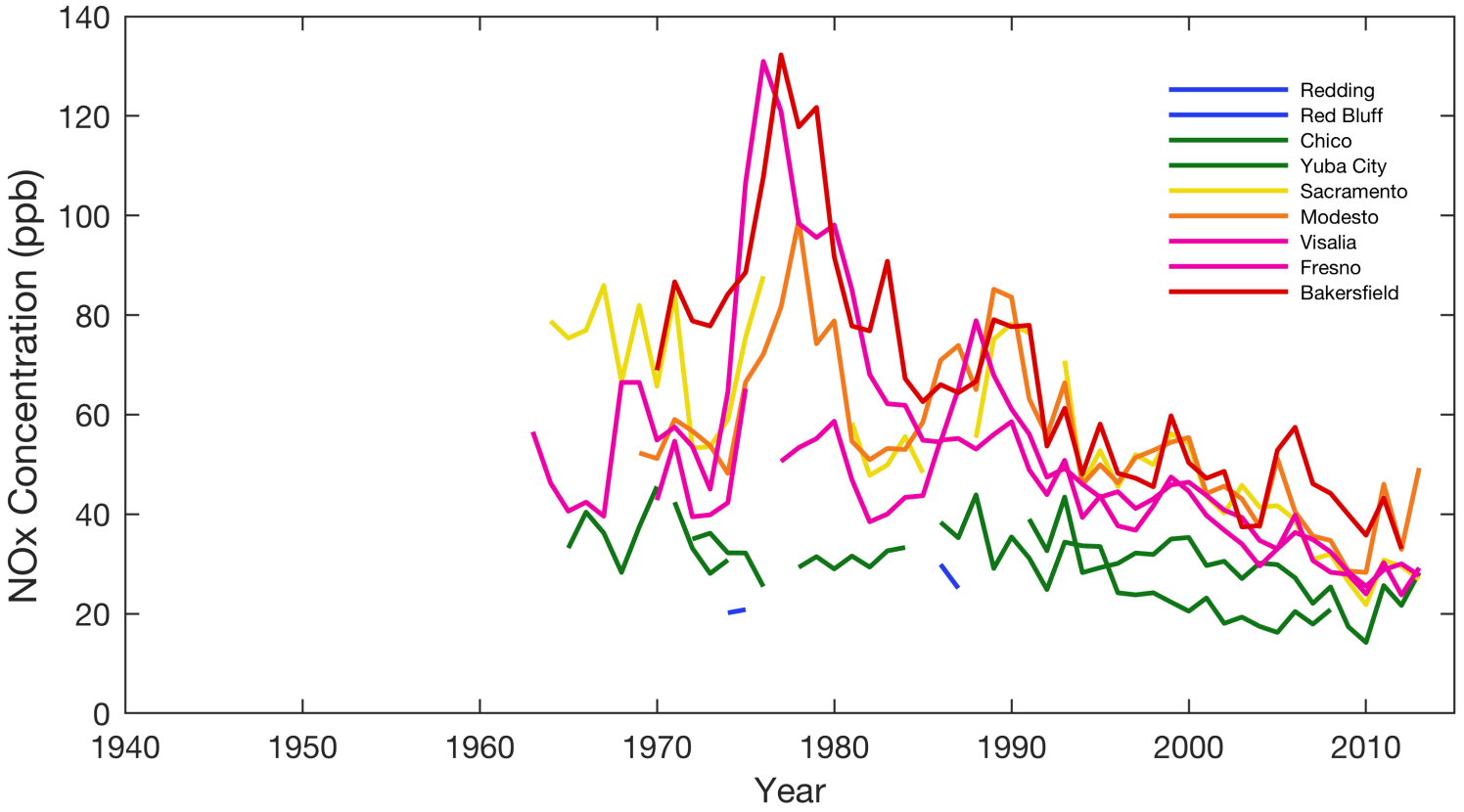

Figure 12. Time series of wintertime (Nov-Mar) NO_x concentration from 1962-2014 from the CARB archive. Color coding represents change in 1° of latitude, beginning at 40°N with cool colors representing northern cities and warm colors representing southern.

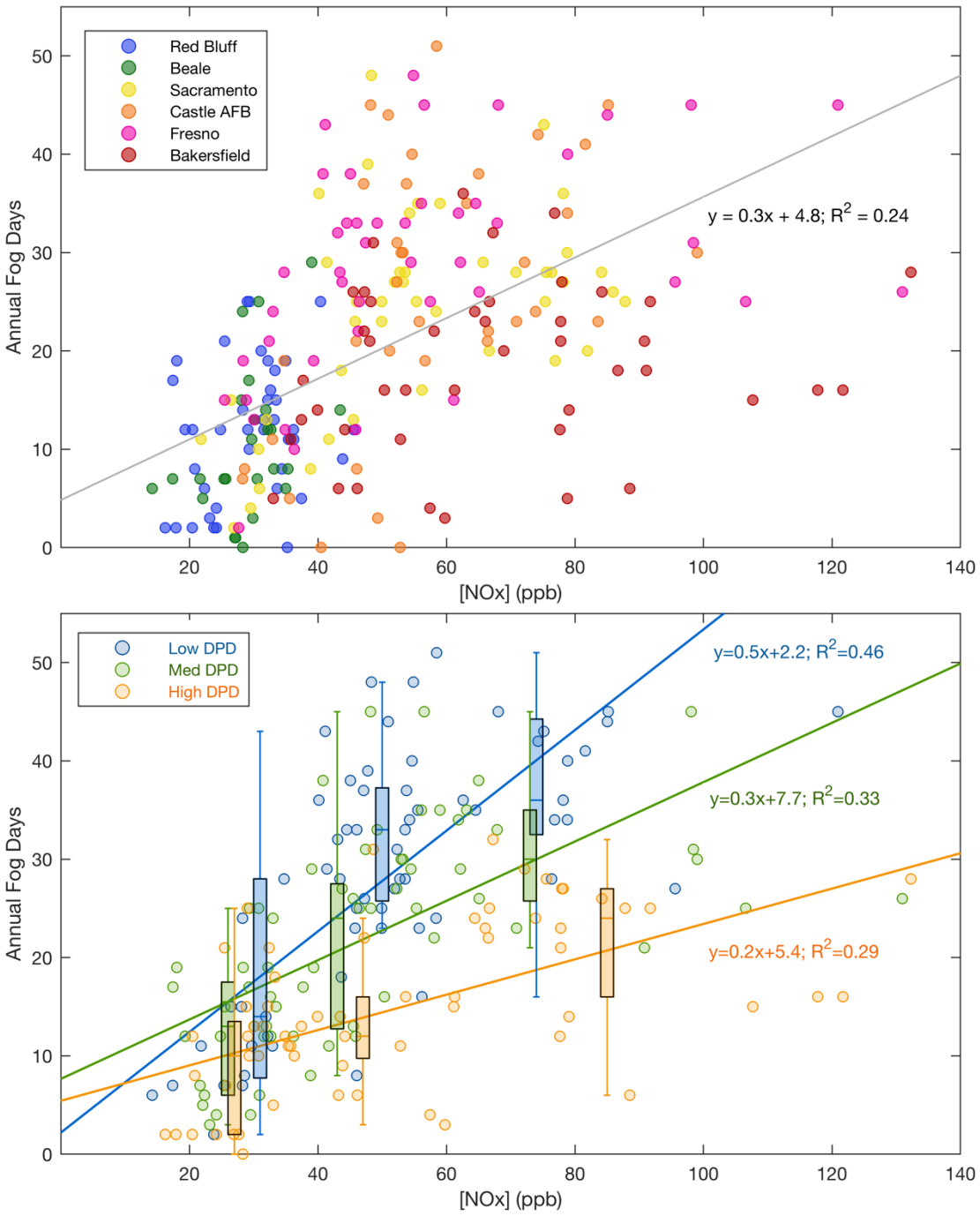

Figure 13. a) Annual Fog Days plotted against NO_x concentration (ppb), with the color coding representing 1° latitude and a fog day defined as any day where visibility < 400 m. b) Correlation between fog days and NO_x segmented by three DPD quantiles, where blue represents the lowest quantile of DPD (1.6 °– 4.2 °), green represents medium DPD (4.3 °– 5.6 °), and orange represents high DPD (5.7 °– 9.0 °). Fog day error bars demonstrated by the overlaid box plots for 3 quantiles of NO_x (low, medium, and high) per DPD bin. Total regression line displayed in both figures, where the coefficient of determination (R^2) is calculated by squaring Pearson's r to represent the explanatory robustness of the predictor variable.

Table 4. Separating high and low frequency coefficients of determination for visibility versus dew point depression, wind speed, and NO_x. +/- indicates positive and negative correlations, respectively.

	Visibility
High Frequency R^2	
DPD	0.29 (+)
[NOx]	0.10 (-)
Wind Speed	0.22 (+)
Low Frequency R^2	
DPD	0.16 (+)
[NOx]	0.38 (-)
Wind Speed	0.11 (-)

Chapter 3:

Unraveling the influence of pollution and climate variability on radiation fog frequency in California's Central Valley and Italy's Po Valley

Abstract: Temporal trends in dense fog frequency remain a puzzling global phenomenon. Italy's Po Valley and California's Central Valley have experienced an average 76% and 50% decline in fog events since 1980, respectively. There is insufficient explanatory robustness in climate as the sole driver of this trend, thus research into contributions from additional likely drivers is needed, such as air pollution. Air pollution emissions contribute to the cloud condensation (CCN) formation necessary to create clouds and fog. Effective regulatory strategies in both regions have resulted in sulfur dioxide emissions being drastically reduced and nearly eliminated, as well as 60-65% decline in oxides of nitrogen (NO_x), thus reducing the CCN available for fog formation steadily over the past 3-4 decades. I used generalized additive models to identify the most significant climate and air pollution variables affecting day to day changes in visibility, an indicator of dense fog, and compare the trends over time in these two analogous regions. Over 56-65% of the variance in visibility was consistently explained by variability in dew point depression, pollution concentration, wind speed, and precipitation. Variability in dew point depression (DPD), which incorporates both water availability and temperature, has the most pronounced influence on daily time scales. The explanatory value of NO_x concentration has 33-70% of the explanatory robustness of DPD (depending on the site) when investigating days close to the dewpoint (DPD < 3.5℃). This suggests that fog frequency is specifically sensitive to fluctuations in CCN number concentration when meteorological conditions are favorable to fog formation (e.g. when DPD is low). While DPD is a primary driver of daily variability, the significant influence of NO_x concentration on the visibility response suggests that rapid pollution declines in both valleys are primarily responsible for the diminishing fog frequency since 1980

1. Introduction

Italy's Po Valley and California's Central Valley both have histories of extremely low visibility caused by wintertime radiation fog. This valley fog, which commonly forms during the coldest part of the day from November – March, plays an important role in local climatic conditions by reducing radiative cooling, moderating surface temperatures, and blocking incoming solar radiation. In the Central Valley, the valley fog is associated with some positive impacts for farming by ensuring sufficient winter chill for many fruit crops contributing to the agricultural economy (Baldocchi and Waller, 2014; Luedeling et al., 2009). However, fog episodes can limit horizontal visibility to only a few meters, with serious consequences to ground and aviation transportation (Ashley, 2015; Bendix, 1993). Polluted fogs also have damaging impacts on human health, infrastructure, and vegetation (Mariani, 2009).

In recent decades, both regions have concurrently experienced rapid declines in the frequency of fog events. In the Po Valley, rural and urban stations in Bologna observed a 47% reduction in hours of dense fog since the mid-1980s (Giulianelli et al., 2014). Similarly, Central Valley sites observed a 46 – 90% decline in fog events over the same period (Baldocchi & Waller, 2014; Gray et al., 2019; Herckes et al., 2015). While many studies have identified trends in radiation fog frequency, most have only postulated, but not tested, possible causes. Possible contributors to this decrease include: a) increasing temperatures due to urban heat island (Lee, 1987; Suckling & Mitchel, 1988) or climate change (Cordero et al., 2010), b) changes in the number of stagnation events (Caserini et al., 2016), and c) reduction in the availability of hygroscopic cloud condensation nuclei (CCN) due to effective air pollution regulation (Charlson et al., 2001). Investigating the relative contributions of changing climate and air pollution variables on declining fog episodes is important for providing insights into the causes of continued trends.

Both the Po and Central Valley are characterized as highly polluted regions (American Lung Association, 2016; European Environment Agency, 2014), owing to emissions from their large populations, vehicular transportation, intensive agricultural, livestock, and industrial activities, combined with regularly occurring episodes of stagnant valley air. The orography and meteorological conditions that support fog formation – high pressure systems, strong temperature inversions, and anomalously low wind speeds (Agenzia Regionale per la Protezione Ambientale, Emilia-Romagna, 2013; Bianco et al., 2011; Caserini et al., 2016; Herckes et al., 2015; Underwood et al., 2004) – also present challenges for controlling concentrations of primary air pollutants such as sulfur dioxide (SO_2), nitrogen oxides (NO_x), and ammonia (NH_3), and the secondary particulate matter they produce. Reactions of SO_2, NO_x, and NH_3 directly contribute to the formation of ammonium nitrate (NH_4NO_3) and ammonium sulfates ($(NH_4)_2SO_4$ and NH_4HSO_4) which are important contributors to fine particulate matter, causing frequent regulatory exceedances. Particulate nitrate and sulfate are also very hygroscopic and of the ideal size range for cloud condensation nuclei at low supersaturation (Petters & Kreidenweis, 2007). Cloud and fog-droplet literature indicate high availability of nitrate and sulfate and their gas-phase precursors can impact the formation, composition, persistence, and density of radiation fog (Andreae et al., 2008; Gultepe et al., 2007; Kulmala et al., 1995; Kulmala et. al., 1998).

Air pollution in both these regions has declined at a similar rate and over a similar period as fog frequency due to regulatory intervention. In the Po Valley, substantial reductions in primary

emissions since the 1980s contributed to declining trends in particulate matter with aerodynamic diameter 2.5 micrometers or less ($PM_{2.5}$), most significantly in the winter (Cusack et al., 2012; Putaud et al., 2014). Bigi and Ghermandi (2016) determined this trend was largely attributable to a regulatory forced renewal of vehicles with more advanced emission controls and efficient engines – an impact which is also seen in decreasing fuel sales. Additionally, a decline in emissions from industrial combustion due to technological improvements influenced the trend (Bigi and Ghermandi, 2016). Similarly, the Central Valley has experienced concurrent reductions in primary emissions and secondary inorganic aerosols (Pusede et al., 2015) due to engine modifications, such as the implementation of the three-way catalytic converter in the 1980s, along with state-mandated checks on engine performance and buy-backs of high polluting vehicles. Improvements in diesel-fueled trucks, industrial stack controls, and home heating have also contributed to cleaner air (Frost et al., 2006; McDonald et al., 2012).

With such rapid environmental changes occurring concurrent to increasing population and changing climate, applying multivariate analysis to determine and quantify the drivers of this change provides a way to evaluate the most important factors changing dense fog frequency in the Po and Central Valley. Recent studies have also investigated the competing effects of temperature and aerosol loading. For instance, Central Valley meteorology analysis shows no trend in the occurrence of favorable conditions for fog formation since 1980, yet the fog continues to decline (Gray et al., 2019). Instead, the study indicates that long-term trends in fog better correlate both spatially and temporally with seasonally-averaged air pollution concentration than with climate variables (Gray et al., 2019). As inorganic aerosol number concentration fell, so did the hygroscopicity of CCN sources and the amount of soluble gases dissolved into the water droplets – both of which previously aided fog formation occurring at nontraditional activation conditions (RH < 100%). With reductions of pollution, Central Valley fog has become less frequent and more sensitive to temperature and water availability, with nearly all fog days occurring during the most favorable meteorological conditions, unlike 35-years ago (Gray et al., 2019). This is similar to studies in New Delhi, which found that when pollution load increased rapidly, fog formation occurred at unexpectedly high dew point depression (DPD > 1°C) suggesting a synergistic effect between pollution and meteorology (Tiwari et al., 2011). When considering declining fog globally, Klemm (2016) modeled the compounding effects of climate change and air pollution in five air basins, finding that a 10% reduction in emissions is equivalent to 0.1°C increase in temperature.

Here, I apply Generalized Additive Models (GAMs) (Hastie and Tibshirani, 1990) to meteorology and pollution observations from the Central Valley and Po Valley to better quantify the relative explanatory value of potential predictor variables on visibility and develop a more robust understanding of the nonlinear relationships contributing to fog formation with the ultimate goal of elucidating causes of its declining trend.
`

2. Methods

2.1. Study region and data

To provide input for the GAM models described below, predictor variables for each site were selected based on known and suspected contributors of fog and processed using flags for data quality control. Hourly meteorological data was downloaded from the National Climatic Data

Center (NCDC) for airports adjacent to Milan in the Po Valley (*Figure 1*) and Sacramento, Fresno, and Bakersfield (*Figure 2*) in the Central Valley (https://www7.ncdc.noaa.gov/CDO/cdoselect.cmd).

Hourly-averaged temperature, dew point, wind speed, and sea level pressure were downloaded from the NCDC. Dew point depression (DPD), which is calculated by subtracting dew point from ambient temperature, was also derived from hourly data. For the Central Valley, corresponding airport measurements of daily maximum/minimum temperature and precipitation sums were downloaded, from which 1 and 2-day lagged precipitation was also derived (https://www.ncdc.noaa.gov/cdo-web/datatools/lcd). Seasonal impacts were accounted for in the model using day of year (winter season) and length of night (length of radiative cooling time) calculated using the Herbert Glarner formula based on day of year and latitude (https://www.mathworks.com/matlabcentral/fileexchange/20390-day-length). Year and Julian day were also tested inputs to capture potential time trends from processes not represented in weather and pollution covariates.

The Po Valley model used daily data downloaded from Lombardia Regional Environmental Protection Agency (Agenzia Regionale per la Protezione Ambientale, ARPA) for the primary pollutants NO_x and SO_2, as well as total suspended particles (TSP), a now-retired measurement for particles with historically long records. By contrast, California models only included daily NO_x concentration from the California Air Resources Board (ARB) (https://www.arb.ca.gov/adam/). I selected monitoring stations within the urban plume of each local airport which had long enough historical data records, compared each station for consistency, and removed severe outliers. The wintertime mean pollution concentration for each city was calculated by averaging over multiple monitoring stations within the city limits (15, 8, 11, and 9 for Milan, Sacramento, Fresno, and Bakersfield, respectively), each of which were operational for varying lengths of time. For the Central Valley, daily measurements of TSP or PM_{10} were unavailable from a comparable source due to the use in California of multiday, rather than daily, filter sampling for aerosols. Central Valley SO_2 could not be included in modeled daily visibility because it was nearly always below detection limit during the period of inquiry due to effective regulatory measures and limited coal utilization. Fog sampling studies confirm that Central Valley droplets are associated with nitrate-dominated CCN (Collett et al., 2002). I considered the potential importance of formation periods from gas precursors to secondary aerosol by introducing 1 and 2-day lags in pollution in the model.

Predictor variables were analyzed for the response of visibility. Airport visibility observations were initially measured using the Surface Aviation Observation guidelines, in which meteorologists used field markers to manually determine visibility. After 1996, the Automated Surface Observation System was implemented at airports internationally and visibility is now automatically recorded using a forward scatter visibility sensor which measures the attenuation of light at 20-second intervals. With the new guidelines, sites have an either 11.3 kilometer (km) or 16 km detection ceiling on observations; thus, all measurements over the period of inquiry are limited to 11.3 km maximum visibility to remain consistent. The visibility of greatest interest in dense radiation fog measurements are days where the visibility falls below 400 meters (m) (~ 0.25 miles). The correlation between number of wintertime fog events and seasonally-averaged visibility is high (r^2 = 0.92 and r^2 = 0.54 for Milan and Sacramento, respectively) (*Figure 3 and 4*), indicating that visibility is strongly influenced by fog events in these regions.

Data quality flags identified multiple instrumentation artifacts in the Milan meteorology observations from the Linate airport. Wind speed measurements were disproportionately low prior to 1992, during which > 2000 hours of wind speed equal to 0 m/s were observed at airports throughout the Po Valley, while wind speed was almost never (< 5 hours) equal 0 m/s after 1992. Such a steep drop in occurrence is unrealistic and suggests instrumentation or observational method changes. Additionally, DPD observations demonstrated varying instrumentation ceiling effects and detection limits from 1998-2009 that were not consistent throughout the data set. Lastly, precipitation had a low observation rate with many NaNs in the dataset. Thus, observations for wind speed, RH, temperature, and precipitation were acquired from local ARPA stations. Multiple Milan ARPA sites (Brera, Cassano, Marche, Juvara, Turbigo) were tested for consistency with the reliable years of Linate Airport data. Site similarity was determined using the tau test, where the Kendall rank correlation coefficient was calculated to measure the association between data sets. The highest tau coefficient was found for Juvara, at only 3 km from Linate airport, with a $\tau = 0.73$ for DPD observations (*Figure 5*) and $\tau = 0.72$ for wind speed (*Figure 6*). At Juvara, wind speed was slightly lower on average and DPD slightly higher, likely owing to its more urban surroundings. Precipitation had a $\tau = 0.62$, which was deemed acceptable due to the challenges in recording precise volumes in rain gauges. Based on these data quality challenges, as well as limitations on the distribution and length of air quality sites, Milan is the only site representing the Po Valley usable in our model.

Daily meteorology and air pollution variables were calculated by averaging over hourly observations taken every three hours (eight measurements per day). Data were included only when seven of eight measurements per day were available to calculate a daily average. Records were analyzed for data quality, particularly prior to station decommissioning when unrealistic outliers were most common. Instrumentation malfunction was primarily addressed by removing outliers using the Interquartile Range Rule, with which the interquartile range is first calculated and an outlier is defined as any value falling outside of 1.5 times the first and third quartile. This removed < 5% of any variable and did not appreciably change any mean.

2.2. Trend analysis

Trends in fog days and air pollution are reported for Central Valley (consistent with Gray et al., 2019), and for the Po Valley, where a fog record of this length and distribution has not previously been described in the literature. Annual days of dense fog are summed for each fog season (November-March) for any day where visibility falls below 400 m for an hour or longer. Due to the episodic nature of fog, I required each month to have > 90% of hourly reporting in order to sum over the month. Availability of sufficient data for all five months was required to create a seasonal sum. Visibility and pollution averages had comparatively less strict reporting thresholds since they are continuous observations. Monthly averages were calculated if > 65% of daily averages (derived from hourly observations) were available. This threshold was determined by random sampling t-tests of large iterations and requiring deviation from the mean be < 5%.

Trends were calculated using the non-parametric two-tailed Mann-Kendall trend test and the Theil-Sen estimator (http://www.mathworks.com/matlabcentral/fileexchange/authors/23983). The Mann-Kendall trend test compares the null hypothesis (H_0), which would indicate no trend in the data, against the alternative hypothesis (H_1), which would imply a significant trend (Mann, 1945; Kendall, 1955). An output of H = 1 suggests that the null hypothesis failed and there is a

statistically significant trend at the $\propto = 0.01$ significance level. Once a trend was detected, I used the Theil-Sen estimator, which is a non-parametric technique for fitting a line while minimizing the impact of outliers (Theil, 1950; Sen, 1968). I found the trend using Sen's slope (Q_i) which is determined by calculating the median of all the slopes between pairs of points over the period:

$$Q_i = \frac{(x_j - x_k)}{(j - k)} \; for \; i = 1, \ldots n$$

where x_j and x_k are data at times j and k, and n is the number of points. The mean of Q_i over all n values is Sen's slope, which, along with a y-intercept, allows a best fit to be calculated.

The Theil-Sen estimator was used to determine the average change in visibility and air pollution over the available record. In particular, regionally-specific fog trends are reported for the Po Valley for annual fog days and visibility. Regions were distinguished using cluster analysis classifications to group cities based on their visibility trends (*Figure 1*). Cluster analysis was performed using the R package TSclust and based on temporal correlation as a measure of time series proximity (Chouakria and Nagabhushan 2007), applying a temporal correlation threshold of 0.25.

Table 1 provides summary statistics for the available observational data inputted into the GAM model for Milan, Sacramento, Fresno, and Bakersfield. Because of the episodic nature of precipitation, it was input into the model as a categorical variable, with 1 indicating a day in which rain occurred and 0 indicating a day in which rain did not occur. All other predictor variables were input as continuous variables.

2.3. Model description

GAM is a nonparametric regression technique which determines a smoothed fit between each response and predictor (without requiring a prori information about the fit) using thin plate regression splines (Wood, 2006). The flexibility inherent in GAMs allows the relationship between the predictor and response to be determined fully by the data, possibly limited by smoothing terms and link functions. Since the model is additive, the interpretation of each individual graph does not depend on the values of the other variables, thus allowing independent conclusions to be drawn from the graphical responses, holding all other inputs constant. The technique can also capture nonlinear patterns that better describe data that might typically be missed. The general formula for our visibility models is:

$$\ln(visibility) = a + s_1(x_1) + \ldots + s_n(x_n) + \varepsilon$$

where a is the intercept, $s_{1\text{-}n}$ are the smooth functions of the continuous predictor variables $x_{1\text{-}n}$, and ε is the residual error. The model was run using the mgcv package in R (https://cran.r-project.org/web/packages/mgcv/mgcv.pdf) and using a logarithmic link function.

2.4. Predictor variable selection

To select predictor variables for input to the model, used an iterative six step process inspired by Barmpadimos et al., 2011, Jackson et al., 2009, and Sartini et al., 2013.

Step 1: A univariable model was created for each covariate, along with an Akaike Information Criterion (AIC) (Akaike, 1974) estimator. The univariable models are ranked in order of lowest AIC. Each model is also tested to determine the basis dimension, *k*, which is the number of knots included in the smoothed spline. Beginning with *k*-1 (the degrees of freedom in the model), the number of knots is iteratively decreased with the goal of having the maximum number of knots included in the spline while also maintaining the lowest AIC score. AIC is estimated using the following equation:

$$AIC = - 2 * \log L + k * edf$$

where L is the maximized value of the likelihood function for the estimated model, k is the penalty parameter, and edf is the effective degrees of freedom of the model. AIC is a term estimated for model quality and selection by evaluating the compromise between goodness of fit of a model versus model simplicity. A model that is over fit has higher effective degrees of freedom in the regression spline, and is thus more wiggly, though possibly without physical meaning. AIC prioritizes both fit and simplicity. As in Barmpadimos et al., 2011, I ranked based on AIC over deviance explained to ensure that the models had meaningful results. The model with the lowest AIC score after determining smoothing terms is selected.

Step 2: The remaining covariates are iteratively added to the univariable model following the procedure in step 1, one at a time. The model with the lowest AIC is selected.

Step 3: To confirm the value of the original variable added, the covariate selected in Step 1 is removed and each of the remaining are individually tested in the model. If this new combination results in a lower AIC than the model in Step 2, the current combination is selected.

Step 4: The current predictor inputs are tested for collinearity using the Variance Inflation Factor (VIF) (Freund and Wilson, 1998). Collinearity occurs when two model inputs have a linear relationship, which results in redundancy and makes it challenging to correctly identify each variable's input. For example, average temperature and maximum temperature have a VIF > 1000, because these variables vary linearly. I used a VIF cut off of 5, in accordance with Montgomery and Peck, 1992. VIF was calculated with the 'car' package in R (https://cran.r-project.org/web/packages/car/car.pdf).

Step 5: The above steps are repeated for the mutually adjusted models with the addition of one covariate at a time. The steps are continued until the AIC does not lower with additional inputs, while also being aware of how each additional input impacts the r^2 of the model.

Step 6: The robustness of the model is verified by ensuring each covariate has a p-value significant at the 1% significance level, as well as by analyzing the model residuals using gam.check (*Figures 7-10*). Model residuals were plotted against variables not included in the model to investigate any remaining relationships.

An alternative method outlined in Jackson et al., 2009 that selects variables based on deviance explained, rather than AIC, was also tested. This method selected the same variables in slightly different order.

2.5. Predictive modeling for likely conditions

The most useful output for traditional GAM models is an r^2 value and individual plots of the smoothed fits for each of the covariates, as well as p-values denoting the fit significance. These plots represent the response of the dependent variable (visibility) over the range of inputted values of the predictor variable. Typically, the y-axis response units are represented as a ratio relative to the mean value of visibility over the course of the record. It is more meaningful for the y-axis to be transformed into kilometers, as represented by the original dependent variable. This requires reconstructing each covariate plot using the *predict* function in the mgcv package (https://stat.ethz.ch/R-manual/R-devel/library/mgcv/html/predict.gam.html).

The predictive fit is constructed for each individual covariate by holding the remaining covariates in the model at a set of likely conditions (e.g. the median value). The predictive function allows us to then recreate the model fit on the response scale, as well as transform the original output to calculate the confidence intervals.

2.6. Interaction terms

Past studies on Central Valley fog sensitivity indicate there is greater explanatory value in investigating pollution and DPD in concert (Gray et al., 2019). This analysis suggested that the most definitive effect of aerosol concentration can be seen when analyzing pollution at low DPD conditions, because only when the temperature reaches dew point can CCN be activated, therefore impacting fog. Instead, additional primary pollutants, and thereby aerosols, at high DPD conditions might increase haziness or have no effect on visibility at all. In addition, air pollution might affect visibility by scattering solar radiation (Manara et al., 2019), an impact independent from its contribution to CCN number concentration. Thus, isolating the effect of predictive variables under low DPD conditions allowed a better description of air quality impact on fog formation.

As such, DPD as an interaction term was tested with all pollution covariates in the model. Interaction terms in GAM models can be introduced by including a *by* term in the spline, which indicates that the spline will be fit for the covariate in question by each level specified, thus showing how the response changes over certain categories. In this case, two levels of DPD were selected: DPD < 3.5℃ and DPD > 3.5℃. This threshold was determined by varying over multiple quantiles at all sites and investigating the maximum and minimum responses. A daily averaged DPD of 3.5℃ is high enough to represent the low DPD in warmer, drier sites, while also being low enough to maximize the dependent variable response.

3. Results

3.1. Trends in fog and pollution

The Po Valley fog trend, averaged over 9 airport stations (*Table 2*), shows a statistically significant 50% decline in fog days (visibility < 400 m) since 1980 (*Figure 15a*). This decline is consistent at locations throughout the valley (*Table 3*), which were subdivided into the regions North, East, and South based on a cluster analysis of their meteorological characteristics (*Figure 11*). The regional fog day decline is largest in the North, which is the foggiest region where 5 of the 9 airport stations

report from. The North saw a 54% decline, compared with a 42% decline in the South and 28% decline in the East, the least foggy region (*Figure 16a*). Fog hours have declined at a faster rate than fog days (- 65% decline in total hours), because the duration of fog episodes is also declining, from an average of 7.8 hours per fog day in 1980 to 5.7 hours in 2016 (*Figures 12 and 13*). The fog decline was persistent even when investigating less dense fog by applying visibility thresholds of 650 and 1150 meters (.4 and .7 statute miles) rather than the normal definition of 400 meters (0.25 statute miles).

Wintertime fog decline is concurrent with consistent increases in average visibility. The most pronounced improvement was also seen in the North (74%) where average fog season visibility increased from 4.2 km in 1980 to 7.3 km in 2016. The South and East saw a statistically significant 56% and 29% increase in visibility, respectively (*Figure 16b*). *Table 4* shows the changes by site based on the Theil-Sen estimator.

The Po Valley observed similar rates of decline in pollution concentration, beginning with SO_2. Wintertime average SO_2 concentration decreased from 175 ppb in the late 1970s to < 5 ppb by 2010 (*Figure 4c*). From 1980-2010, TSP declined by 81% and NO_x concentration, the dominant inorganic pollutant contributing to wintertime PM in recent decades (Chow et al., 2006; Pusede et al., 2016), has declined by 61%.

While the Po Valley has nearly double the average fog days of the Central Valley, the patterns of fog and pollution decline are very similar. Fog season peaks in January at both locations, but begins earlier in the Po Valley than Central Valley. The Central Valley observed 76% fewer fog days from 1980 to 2016 (Gray et al., 2019). The Central Valley has also seen similar concurrent decreases in primary pollutants. Average NO_x concentration declined 65% since 1980 (*Figure 15d*), with Sacramento, Fresno, and Bakersfield seeing a 64%, 70%, and 66% decrease, respectively. Since 1980, SO_2 concentration declined at an exponential rate, rather than linear, with emission inventory estimates in 1995 an order of magnitude lower than that in 1975 (298 tons per day vs. 32 tons per day. As such, using the linear Theil-Sen approach from 1980-2016 is inappropriate. From 1980-1995, the southern valley saw an 89% decline in SO_2 emissions, since which it has been near constant, falling an additional 6 tons per day by 2015

These trends are most meaningful when investigated with regional aggregates, because temporal availability for each site can be uneven, particularly given our strict requirements for data averaging. For instance, in the Central Valley annual NO_x concentration is not available at every site for each year; thus, some yearly-averages are more weighted to one location over another. See *Figure 14* for specific location availability. Additionally, the spatial distribution of sites is typically limited to airports that are adjacent to urban regions. However, the fog decline has also been identified in rural areas in other studies (Baldocchi and Waller, 2014; Giulianelli et al., 2014).

3.2. GAM model results

Figures 5 – 8 show the GAM model fit results for Milan, Sacramento, Fresno, and Bakersfield, locations for which are described in *Table 5*. *Table 6* reports the covariates selected for each model in the typical order of deviance explained, all of which were highly statistically significant. In addition to reporting total r^2, I analyze the explanatory value of each variable by calculating the modeled visibility response over 90% of all covariates. A day of data is only evaluated in the model

if all covariates are reported that day, which limits the temporal length of the model depending on data availability. The r^2 results range from 0.65 (Milan) to 0.56 (Bakersfield), which is consistent with other studies investigating long-term trends in meteorology and pollution (Barmpadimos et al., 2011). The common covariates selected for all sites were DPD, NO_x, wind speed, and precipitation. Average temperature and dew point were both tested in the models, but had a much lower deviance explained than DPD, even when added concurrently. Only in Sacramento was the addition of the variable length of night, which represents the hours from sunset to sunrise during which radiative cooling from the surface would occur, important to the model. In the Milan model, where daily observations of SO_2 and TSP were available, both pollutants were selected in addition to NO_x. All three pollutants passed the VIF test for collinearity.

3.2.1. Dew point depression

DPD has the most pronounced impact on visibility for all sites. As expected, days with DPD close to zero are associated with low visibility with very narrow confidence intervals (*Figure 17–20*). In the Central Valley, the slope from 0 – 4℃ shows a steep rise in visibility response, only to gradually flatten and have little impact at warmer, dryer temperatures. The slope of Milan DPD is less severe, but the response shape is similar. Sites exhibit a 7.6 – 8.9 km increase in visibility response over 90% of the DPD range. Interestingly, the site with the lowest median DPD (3.5℃), Milan (*Table 1*), has the highest r^2, and the site with the highest (5.2℃), Bakersfield, has the lowest r^2.

3.2.2. Pollution

NO_x concentration has the next most relevant explanatory value at all sites, for which the visibility response declines near-linearly with declining concentration. This relationship is emphasized by investigating the relationship between visibility and NO_x concentration in two bins: one in which DPD < 3.5℃ and another where DPD > 3.5℃. The interaction term provides some delineation between the influence of increasing NO_x in fog-supportive conditions versus haze-supportive conditions. The first output, $NO_x^{DPD < 3.5℃}$, shows the response of visibility to the total range of NO_x (in the context of the mutually adjusted model) should all that NO_x react as it does when DPD < 3.5℃. The second output, $NO_x^{DPD > 3.5℃}$, fits the range of NO_x as it does when DPD > 3.5℃. Thus, the interaction term allows us to separate the response by two sets of conditions. In all four GAMs, daily DPD falls below 3.5℃ for 26 -51% of the time, allowing the model sufficient data for fitting both terms. Additionally, I tested the explanatory value of NO_x using 1-and-2 day lag values to consider aerosol formation time, as well as modeled NO_x as a factor using ranges of quantiles; however, the interaction term yielded the best results.

The fitted response of visibility for $NO_x^{DPD < 3.5℃}$ exhibits a much steeper slope (*Figure 17-20*) and more pronounced decline in visibility with increasing concentration (-5.6 to -3.0 km) versus DPD > 3.5℃ (-2.8 to -0.55 km). The fit is very similar for Sacramento, Fresno, and Bakersfield. Sites with higher NO_x concentration, such as Milan with a median 110 ppb and Bakersfield with a median 63 ppb (in comparison with 41 and 43 ppb) (*Figure 3*), demonstrate a more pronounced impact on modeled visibility, suggesting the magnitude of its impact grows linearly with additional pollution. Milan's $NO_x^{DPD < 3.5℃}$ has 70% of the explanatory value of DPD (+ 7.9 km *vs*. - 5.6 km) and Bakersfield has 53% of the explanatory value of DPD (+ 8.0 km *vs*. - 4.2 km) in comparison to 40% and 33% for Sacramento and Fresno.

When investigating the $NO_x^{DPD > 3.5℃}$ fit, there is an apparent gradient in which the more polluted the site, the larger the visibility impact of NO_x during dry conditions. For instance, the most polluted site, Milan, has a 2.8 km decreasing impact on visibility for NO_x on days where DPD > 3.5℃, followed by Bakersfield (-2.4 km), Fresno (-1.7 km), and Sacramento (-0.55), in descending order of median concentration. I can infer that this is capturing much of the impact of NO_x concentration on haze.

In Milan, SO_2 was selected for the model, but with tempered results due to the timespan of the model. While SO_2 observations date back to 1971, the Milan model begins in 1989 based on the data availability of other critical covariates. In the 1970s, concentrations above 200 ppb were not uncommon, but by the early 1990s it had nearly halved. By 1995, SO_2 concentration was typically below 20 ppb, and by 2005, below 5 ppb. This exponential rate of decline, particularly in the presence of other potential CCN sources, yields a counterbalancing result, as seen in *Figure 17*. For 90% of the range of SO_2 values, SO_2 causes a modest -1.2 km decline. Pronounced low visibility impact is only seen at the maximum, anomalous values of SO_2 observed during the 20 years of the model.

Prior to 1990, the contribution of SO_2 to sulfate aerosols had much more explanatory value for visibility. *Figure 21* compares the visibility response by decade for 4 univariable SO_2 models. While these models lack the influence of other covariates, the diminishing impact of SO_2 as concentration declines is evident. Thus, it is estimated that SO_2 concentration had a larger role historically not evident in the mutually adjusted Milan model.

In fact, SO_2 can only be accurately modeled for Milan when the covariate *year* is included (*Figure 17*). Without this addition, SO_2 exhibits an inexplicable response where visibility is slightly increasing with higher SO_2 concentration, which does not make physical sense. However, when *year* is added, it modifies the trend signature from the SO_2 fit and improves the overall deviance explained by 3%. The response of visibility in the *year* fit does not have direct interpretable meaning, but instead captures visibility variations in the model not explicitly accounted for with fine resolution meteorology and pollution data. For instance, these could include variations in micrometeorology that impact radiative cooling, such as historical changes in surface roughness and turbulence, frequency of inversion layers, or porosity of surrounding surfaces.

Total suspended particle is a now-retired measurement technique with a somewhat variable size-selectivity of 20 – 50 μm., depending on the sampling head design. This large size range is not ideal for investigating fine particles such as CCN, with a typical size range of 0.2 μm, since it represents a mass dominated by coarser particles. However, measurements for TSP began in 1977, when concentration was 6-to-10 fold higher than the typical range in 2010, allowing for a more robust investigation of its impact on visibility over a long time period. Numerous studies have investigated an equivalent ratio between $PM_{2.5}$, PM_{10}, and TSP, most often finding that ratios varied considerably by sites and seasons based on pollutant source (Brook et al., 1997; Eeftens et al., 2012). However, these studies also found that despite site differences in ratio, $PM_{2.5}$-to-PM_{10} was highly correlated (Brook et al., 1997; Eeftens et al., 2012; Harrison et al., 1997), with Milan comparisons finding a wintertime correlation of 0.97 (Marcazzan et al., 2001). As such, I use TSP as a proxy for CCN, but with acknowledgement of the limitations.

The TSP fit shows a largely-linear declining response of visibility as particulate concentrations

increase, with the most pronounced impact on visibility when TSP < 50 μm/m^3 and then tapering off at higher concentrations. A decline in visibility of 4.1 km is estimated over 90% of the range of TSP values.

The more robust daily pollution record in Milan allowed further testing of DPD interaction terms on SO_2 and TSP. *Figure 22* compares the responses of NO_x, SO_2, and TSP varied by the two levels of DPD responses. *Table 7* compares the visibility response of the original variable to visibility when varied by the DPD interaction term (all within the mutually-adjusted model). For each variable, the explanatory robustness of visibility increases when investigating the response for DPD < 3.5°C. NO_x and TSP exhibit similar patterns with concentration on days with DPD > 3.5°C having only ~1/3rd of the impact of concentrations on days with DPD < 3.5°C. SO_2 on low DPD days doubles the negative visibility response, though it is still less than half that of NO_x and TSP under the same conditions. Increasing SO_2 concentration on warmer, dryer days does not negatively influence the visibility response at all, and in fact shows a 1.1 km increase in visibility over 90% of the SO_2 data, but with larger confidence intervals.

These results suggest that gaseous precursors to aerosol formation (NO_x and SO_2) have a more pronounced impact on visibility when conditions are closer to the dew point, likely in part because of their contribution to hygroscopic, submicron aerosol formation or dissolution in droplets encouraging activation at RH close to 100% (Kulmala et al., 1995; Laaksonen et al., 1998). Despite the negligible role of coarse particles in fog formation, low DPD also enhanced TSP results, likely because it correlates with that of fine particles. Past research has found that fine particles better described trends in mass variability and was a significant portion of PM_{10} mass and approximately 1/3rd of TSP mass (Brook et al., 1997). In Milan specifically, research found that fine particle mass, which has the highest correlation with SO_4^{2-}, NO_3^-, and NH^{4+}, was two times that of coarse (2.5 – 10 μm) in PM_{10} measurements (Marcazzan et al., 2001), which suggests that the visibility response to $TSP^{DPD < 3.5°C}$ could be indicative of changes in CCN.

However, I ultimately chose to vary NO_x by DPD over SO_2 and TSP for several reasons. The severe decline in SO_2 makes the model response unreliable, particularly with recent measurements near detection limit, and the visibility response is minor with regards to 90% of the SO_2 measurements. The TSP fit and response to the interaction term are similar to NO_x, but the measurement technique is less reliable and contains an uncertain number of coarse particles. Lastly, the Po Valley is now nitrate dominated in the winter and varying NO_x by DPD yields more comparable results with the Central Valley.

3.2.3. Wind speed

Wind speed has a less pronounced, but statistically significant impact on visibility response at all sites. When daily averaged wind speeds are low, visibility is lower. The increase in visibility response is most evident in wind speed from 0 – 2 m/s at all sites, then neutralizes at higher speeds. Such a low wind speed range is relevant to the formation of radiation fog, because the rate of radiative cooling is very sensitive to turbulence. Wind speed is also important for the dilution of urban emissions. Hence higher wind speeds increase visibility by 1.1 – 2.7 km in the four models. Milan wind speed is noticeably lower than the Central Valley, in which 95% of the days modeled had wind speed < 2 m/s. Meanwhile, Milan wind speed has the lowest explanatory value, perhaps because the variance is so low. In the Central Valley, the visibility response for wind speed in

Bakersfield and Fresno is double that of Sacramento. While all Central Valley sites have a median wind speed near 2 m/s, Sacramento has a larger variance and maximum, owing to higher prevalence of wintertime storms.

3.2.4. Length of night

Length of night was tested in all sites, but only had significant explanatory value in Sacramento, suggesting that a longer period of radiative cooling after sunset is necessary for fog to form. In past work, I have shown a diurnal trend in which fog forms later into the early morning in recent years than when fog frequency was at its maximum (Gray et al., 2019). Given that Sacramento is the least polluted location, there are fewer hygroscopic gases dissolved in atmospheric moisture forcing activation to occur under nontraditional conditions (RH< 100%). Thus, temperatures need to cool further in order to reach activation, possibly making the length of radiative cooling a more relevant covariate.

3.2.5. Precipitation

Due the episodic nature of precipitation, it is included in the model as a binary categorical variable, simply indicating whether it rained on a given day or not. To account for the role of winter storms, particularly as a moisture source prior to high pressure systems in the wintertime which is known to promote fog formation, I also modeled 1-and-2 day lag times, but without significant results. Sacramento has the most frequent rain events at 31% of the winter season, similar to Milan, whereas Bakersfield has rain on only 19% of the days. The modeled response indicates that days with precipitation improve visibility at all sites, ranging from a 1.3 – 2.4 km. Bakersfield and Fresno have a 1 km greater improvement in visibility than Milan and Sacramento on days with rain events. Improved visibility may be due to wet deposition of pollution or increased turbulence decreasing the likelihood of radiation fog forming on the same day. A larger impact on visibility is seen in the less rainy locations, possibly because there is a longer duration for particles to accumulate and be rapidly deposited.

4. Summary and conclusions

This investigation of wintertime visibility in the Po and Central Valley analyzes known and suspected drivers of fog formation for their relative contribution to daily visibility with the ultimate goal of elucidating causes of the diminishing radiation fog season. Investigating the competing effects of changing temperature versus aerosol loading was of important interest, particularly given the 60-95% reduction in wintertime inorganic pollution concentration seen in both regions. Concurrent with these reductions in NO_x, SO_2, and particulate concentration, a 50% decline in Po Valley fog and 76% decline in Central Valley fog occurred since 1980. Meanwhile, changing climate and continued urbanization present possible obstacles to fog formation.

Site-specific generalized additive models explain 56-65% of the daily visibility variance with a combination of meteorology and pollution covariates for Milan (1989-2010) and Sacramento, Fresno, and Bakersfield (1973-2016). DPD has the largest explanatory value at all sites, which is physically intuitive since DPD must fall to near-zero for fog formation, and fog is a significant presence during the winter. NO_x concentration, the now-dominant inorganic pollutant in both regions, was investigated for its role as a precursor to hygroscopic aerosols. Explanatory value of NO_x was enhanced by investigating the fit under daily conditions with temperature close to dew

point (DPD < 3.5°C) and significantly higher than dew point (DPD > 3.5°C). Our primary interest was the visibility response for NO_x when DPD is low, as this is more likely to be impacting fog formation, rather than contributing to further haze. More polluted sites reported a stronger visibility response than less polluted sites, which is in agreement with other investigations of high pollution regimes that found spikes in pollution loadings clearly aided CCN activation under nontraditional conditions (DPD > 1°C) (Tiwari et al., 2011). In Milan, NO_x impact on visibility is approximately 2/3rds that of DPD, and in Bakersfield, it is ½. Meanwhile, for Sacramento and Fresno, NO_x has ~ 1/3 the impact of DPD. Meanwhile, wind speed and precipitation have minimally positive impacts on daily visibility and are likely much smaller drivers in the overall trend. While DPD is a primary driver of daily variability, the large impact of NO_x concentration on the visibility response suggests that rapid declines in both valleys (61-65%) has had an important impact on the diminished fog season since 1980.

There remains significant reduction potential for precursor pollutants, particularly for NO_x in the Po Valley. Continued mitigation strategies will likely contribute to an improvement in fog, which would support transportation safety and have broad commercial and productivity benefits. In addition, the Po Valley is estimated to warm by 2.4 – 4.4K, depending on emission scenario, by the end of the 21st century (Caserini et al., 2016), which will likely increase DPD and impact fog formation further.

5. Figures and tables

Figure 1. Map of eight Po Valley sites color coded using cluster analysis. Clusters defined geographically by north (Turin, Milan (Linate Airport and Malpensa Airport), Bergamo, Brescia), east (Treviso, Venice), and south (Bologna, Rimini). Star indicates Milan site used in GAM model.

Figure 2. Map of three Central Valley sites investigated in GAM models. Stars indicates all three sites used in GAM model.

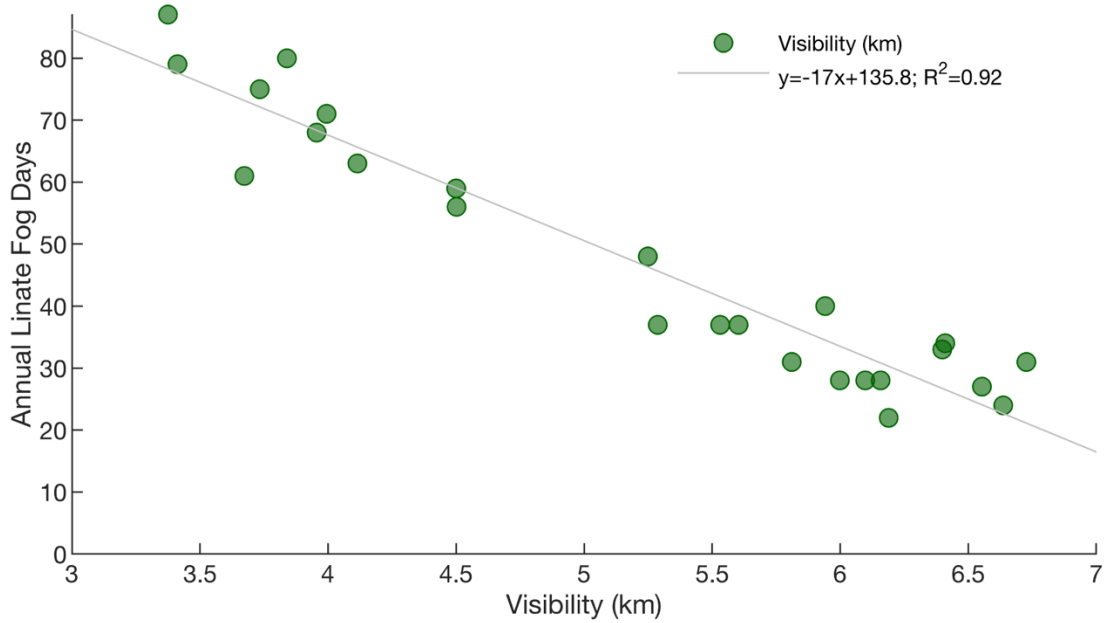

Figure 3. Linate annual fog days (days where visibility < 400 meter for 1 hour) versus daily average visibility.

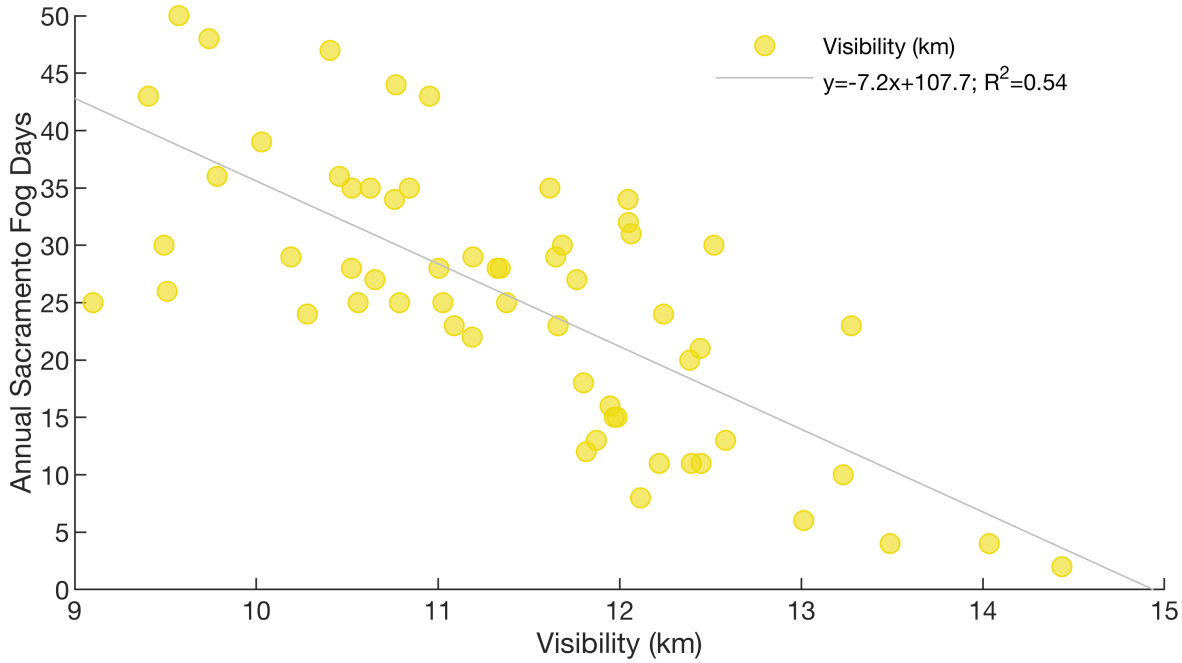

Figure 4. Sacramento annual fog days (days where visibility < 400 meter for 1 hour) versus daily average visibility.

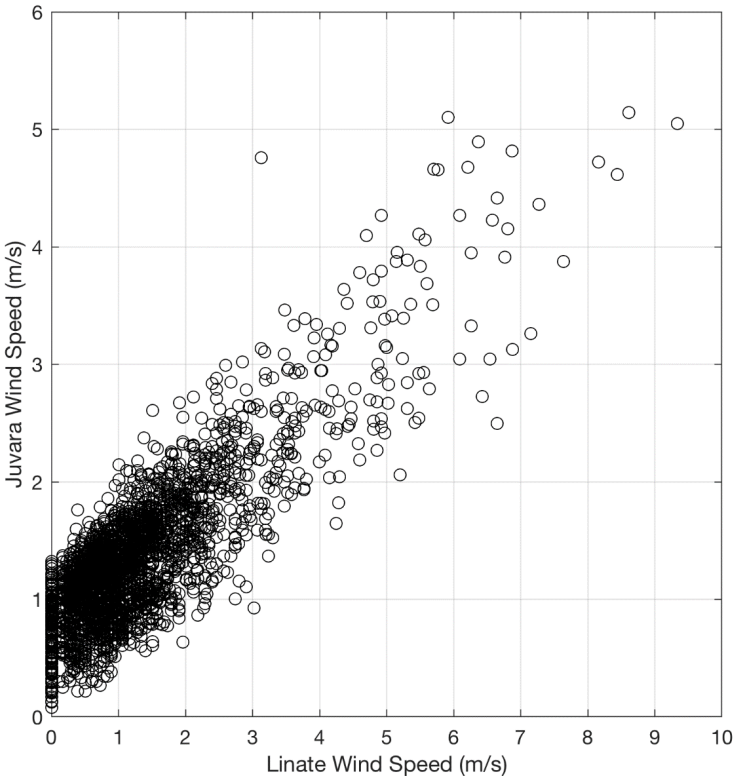

Figure 5. Plot of wind speed (m/s) at Juvara versus Linate demonstrating correlation between sites ($\tau = 0.72$).

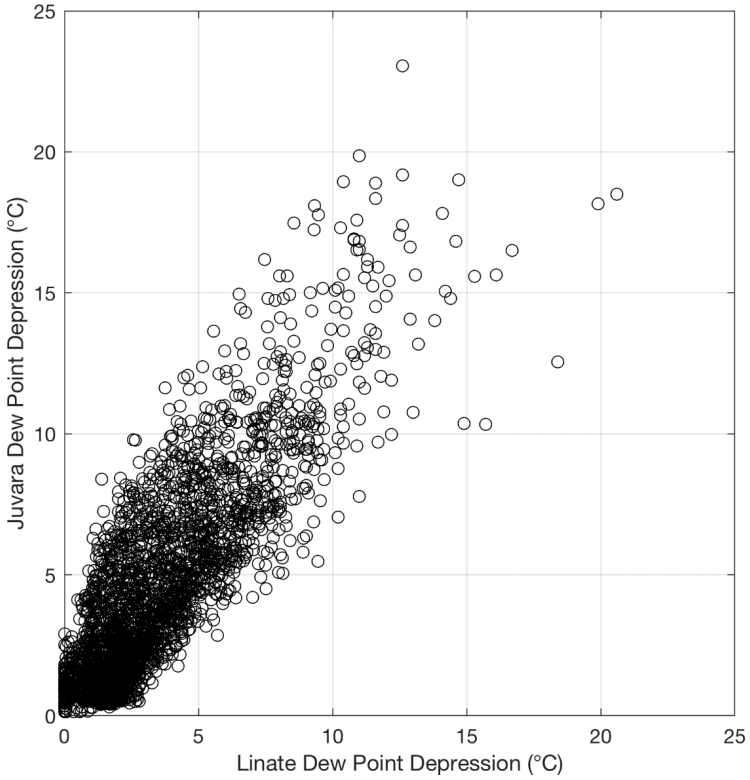

Figure 6. Plot of dew point depression (°C) at Juvara versus Linate demonstrating correlation between sites ($\tau = 0.73$).

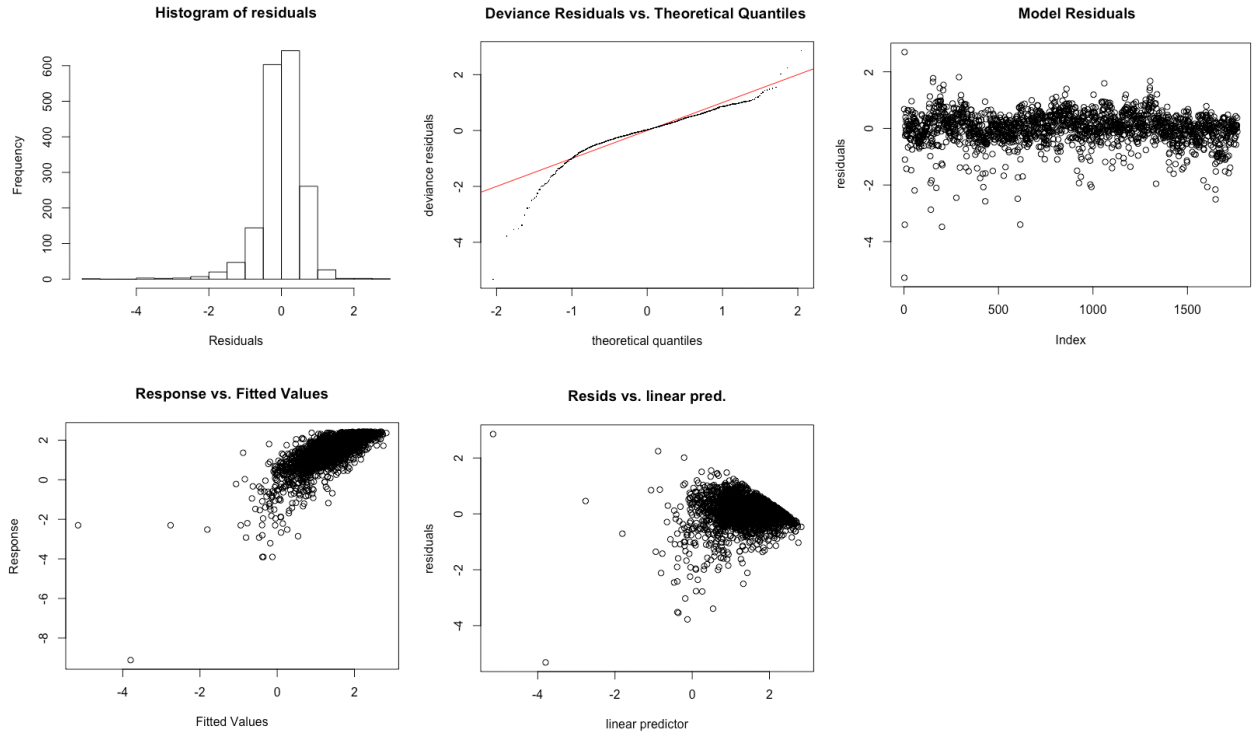

Figure 7: Gam.check output for Milan model.

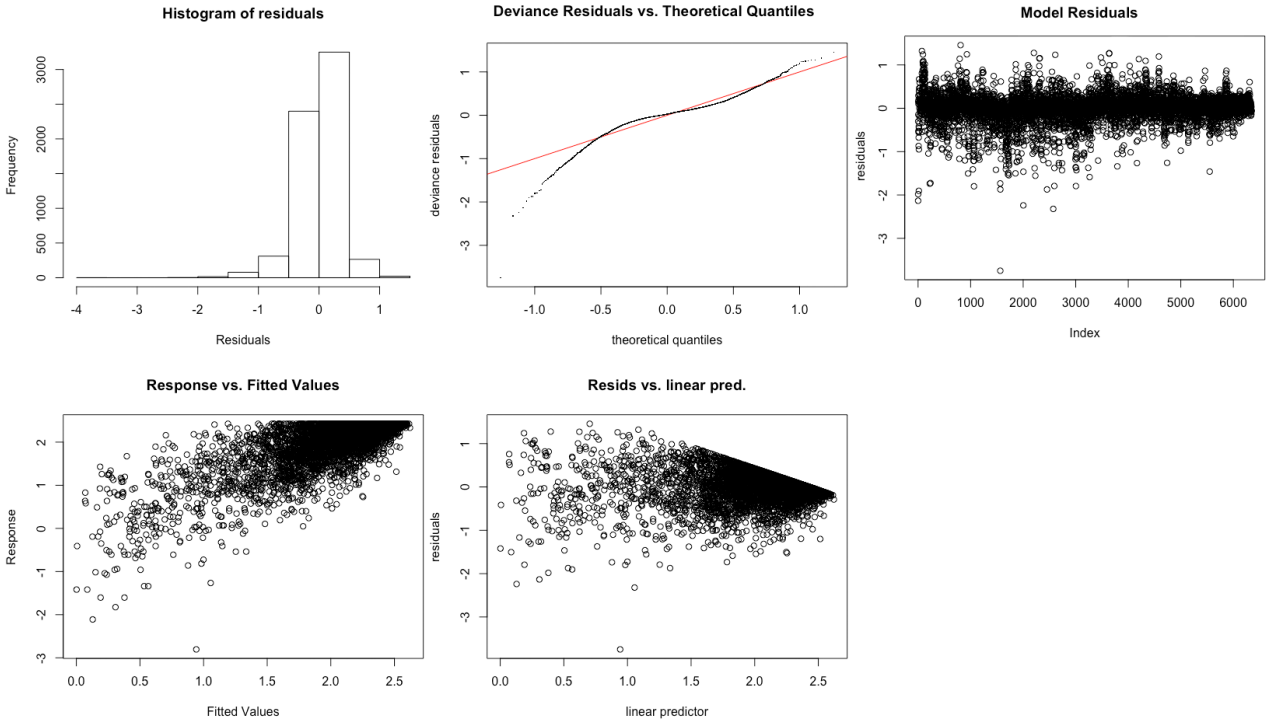

Figure 8: Gam.check output Sacramento model.

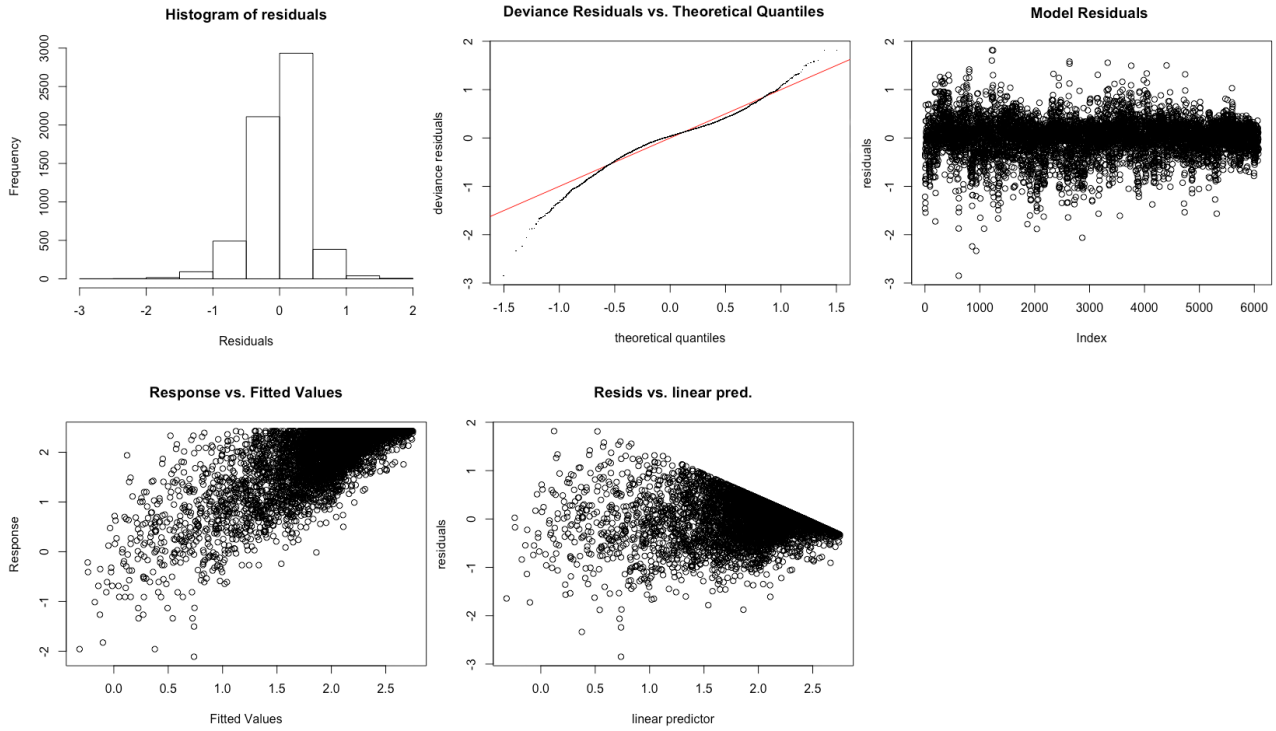

Figure 9: Gam.check output for Fresno model.

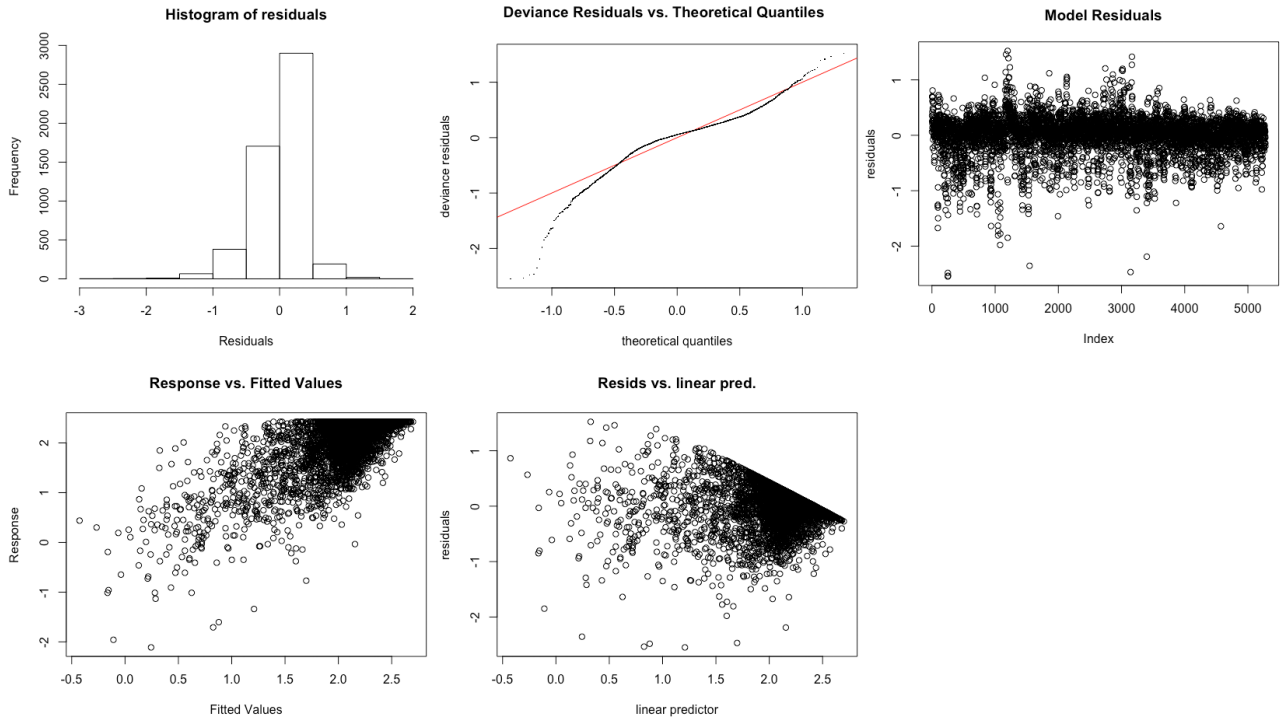

Figure 10: Gam.check output for Bakersfield model.

Table 1. Data Summary Statistics

Location	Visibility (km)	DPD (°C)	Dew Point (°C)	Avg Temp (°C)	Max Temp (°C)	Min Temp (°C)	SLP (mb)	Wind Speed (m/s)	NOx (ppb)	SO_2 (ppb)	TSP ($\mu g/m^3$)
Milan											
Minimum	0.0	0.19	-11	-3.8	-	-	992	0.1	18	0.0	8.8
Median	4.5	3.5	2.3	6.9	-	-	1019	1.3	110	8.1	68
Maximum	11	15	14	18	-	-	1043	2.6	300	110	270
Sacramento											
Minimum	0.10	0	-5.1	-0.36	3.3	-6.1	1005	0.0	0.0	-	-
Median	10	3.4	5.9	9.8	15	5.0	1020	2.3	41	-	-
Maximum	11	11	16	20	27	16	1034	7.1	190	-	-
Fresno											
Minimum	0.12	0	-4.2	-0.56	3.3	-6.1	1007	0.0	3.2	-	-
Median	9.5	4.1	5.7	10	16	5.0	1020	2.0	43	-	-
Maximum	11	12	16	21	29	16	1033	5.1	260	-	-
Bakersfield											
Minimum	0.12	0	-4.6	0.97	3.9	-5.0	1006	0.0	3.3	-	-
Median	10	5.2	5.5	11	17	5.6	1020	2.2	63	-	-
Maximum	11	15	15	22	31	16	1032	4.6	230	-	-

Abbreviations. Dew Point Depression (DPD), Oxides of Nitrogen Concentration (NO_x), Sulfur Dioxide (SO_2), Total Suspended Particles (TSP), SLP (sea level pressure)

Table 2. Po Valley Fog Day Sites

Location	Start Year	End Year	Lat (◦)	Lon (◦)	Elevation (m)
Bergamo	1966-09-08	2017-01-01	45.7 N	9.70 E	238
Bologna	1964-08-11	2017-01-01	44.5 N	11.3 E	37.5
Brescia	1966-09-04	2017-01-01	45.4 N	10.3 E	102
Milan - Linate	1931-01-04	2017-01-01	45.5 N	9.28 E	108
Milan - Malpensa	1965-02-04	2017-01-01	45.6 N	8.73 E	234
Rimini	1945-04-08	2017-01-01	44.0 N	12.6 E	12.5
Turin	1964-08-11	2017-01-01	45.2 N	7.65 E	301
Treviso	1966-09-01	2017-01-01	45.7 N	12.2 E	18.0
Venice	1961-03-01	2017-01-01	45.5 N	12.4 E	2.10

Table 3. Po Valley Fog Day Trend (1980-2016)

Location	Slope	1980	2016	% Change	Mean
Torino	-0.50	33.0	15.5	-53	25.3
Linate	-0.88	56.9	26.1	-54	38.6
Malpensa	-1.6	69.0	11.5	-83	43.9
Treviso	-0.18	39.7	33.4	-16	36.8
Venezia	-0.50	43.5	26.0	-40	36.0
Rimini	-0.36	36.8	24.3	-34	30.0
Bologna	-0.59	46.7	26.0	-44	38.0

Table 4. Po Valley Visibility Trend (1980-2016)

Location	Slope	1980	2016	% Change	Mean
Torino	0.08	4.89	7.59	55	6.24
Linate	0.08	4.08	6.83	68	5.83
Malpensa	0.13	3.15	7.66	140	5.53
Treviso	0.05	5.03	6.64	32	5.82
Venezia	0.04	5.91	7.13	21	6.49
Rimini	0.06	5.02	7.03	40	6.08
Bologna	0.08	4.06	6.96	72	5.53

Table 5. GAM Model Inputs

Location	Years	Lat (◦)	Lon (◦)	Elevation (m)	n
Po Valley					
Milan	1989-2010	45.45	9.28	108	1764
Central Valley					
Sacramento	1963-2014	38.51	-121.50	4.6	6346
Fresno	1963-2014	36.78	-119.72	102	6075
Bakersfield	1973-2014	35.43	-119.05	150	5277

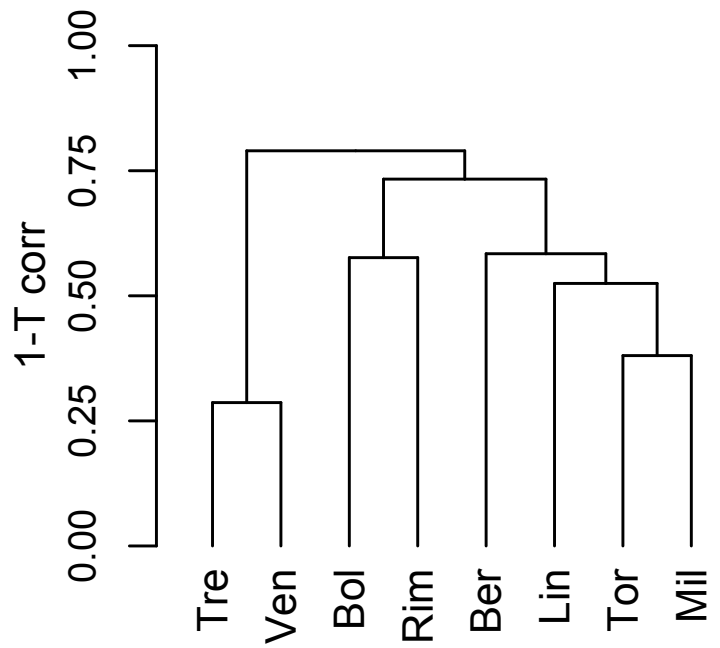

Figure 11. Results of cluster analysis for prominent sites in the Po Valley.

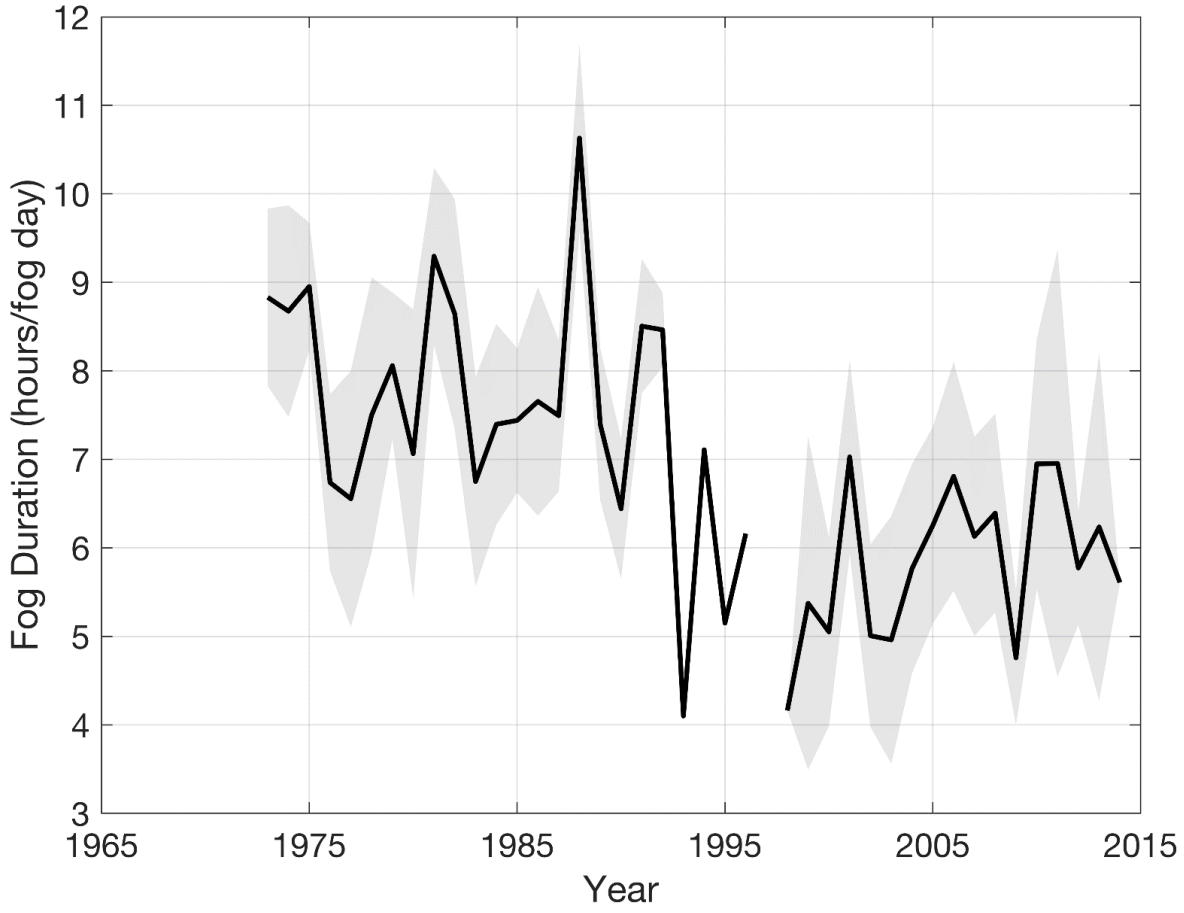

Figure 12. Plot of trend in average number of fog hours (visibility < 400 meters) for all sites in the Po Valley. Grey shading represents standard deviation of sites.

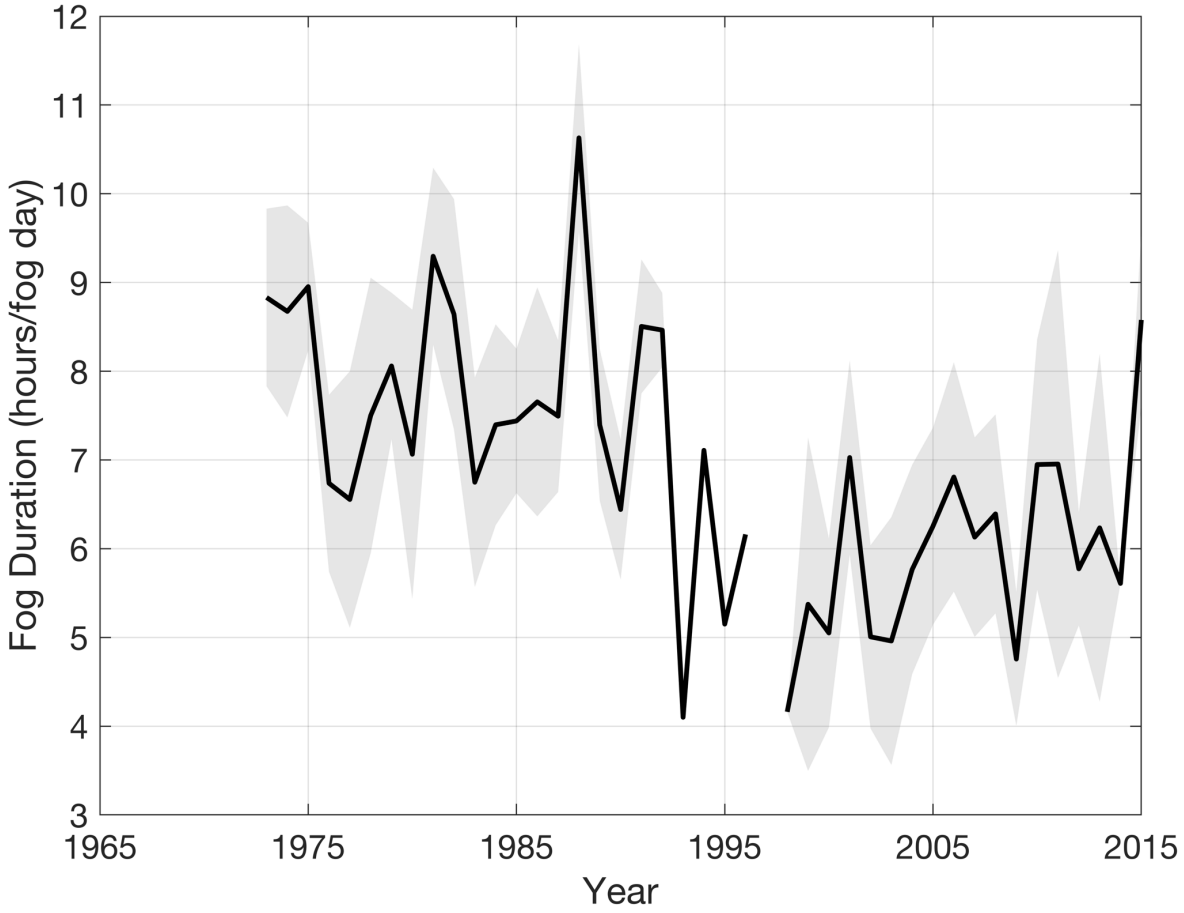

Figure 13. Plot of trend in average duration of fog episode per day for all sites in the Po Valley. Calculated by dividing number of fog hours per season by number of fog days. Grey shading represents standard deviation of sites.

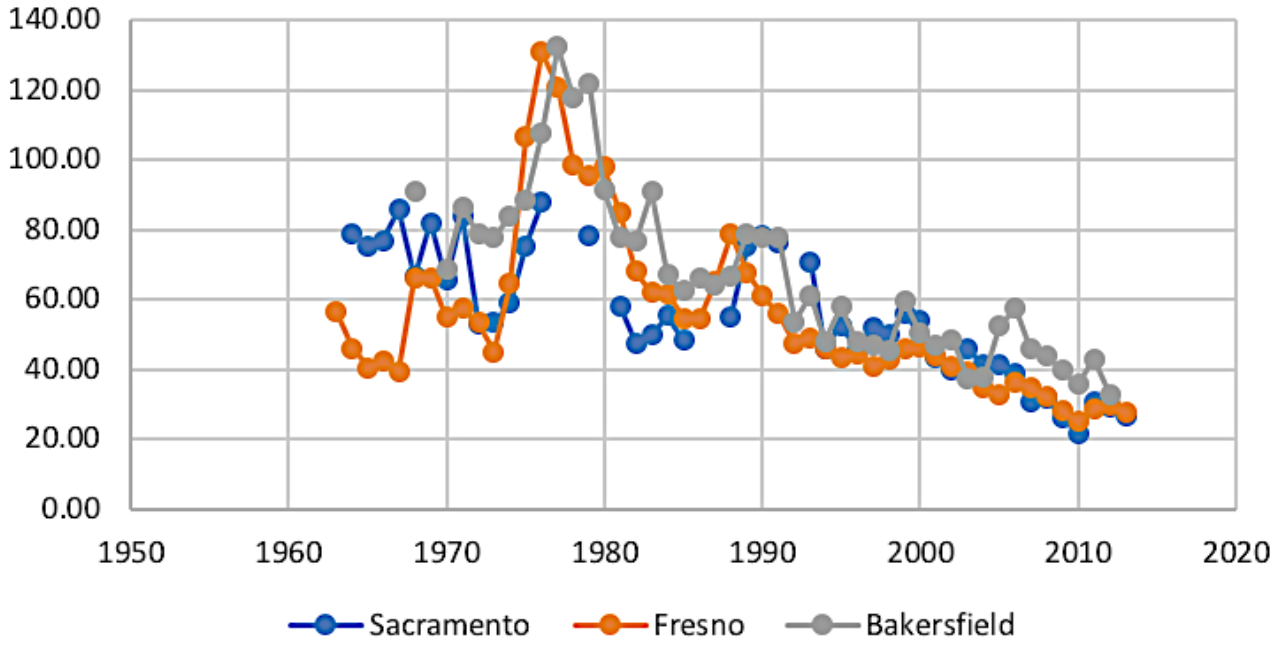

Figure 14. Plot of trend in NOx concentration (ppb) for Sacramento (blue), Fresno (orange), and Bakersfield (grey) from 1963-2015. Points represent years with >65% days reported per month. Plot shows how averaging can be weighted toward some locations over others.

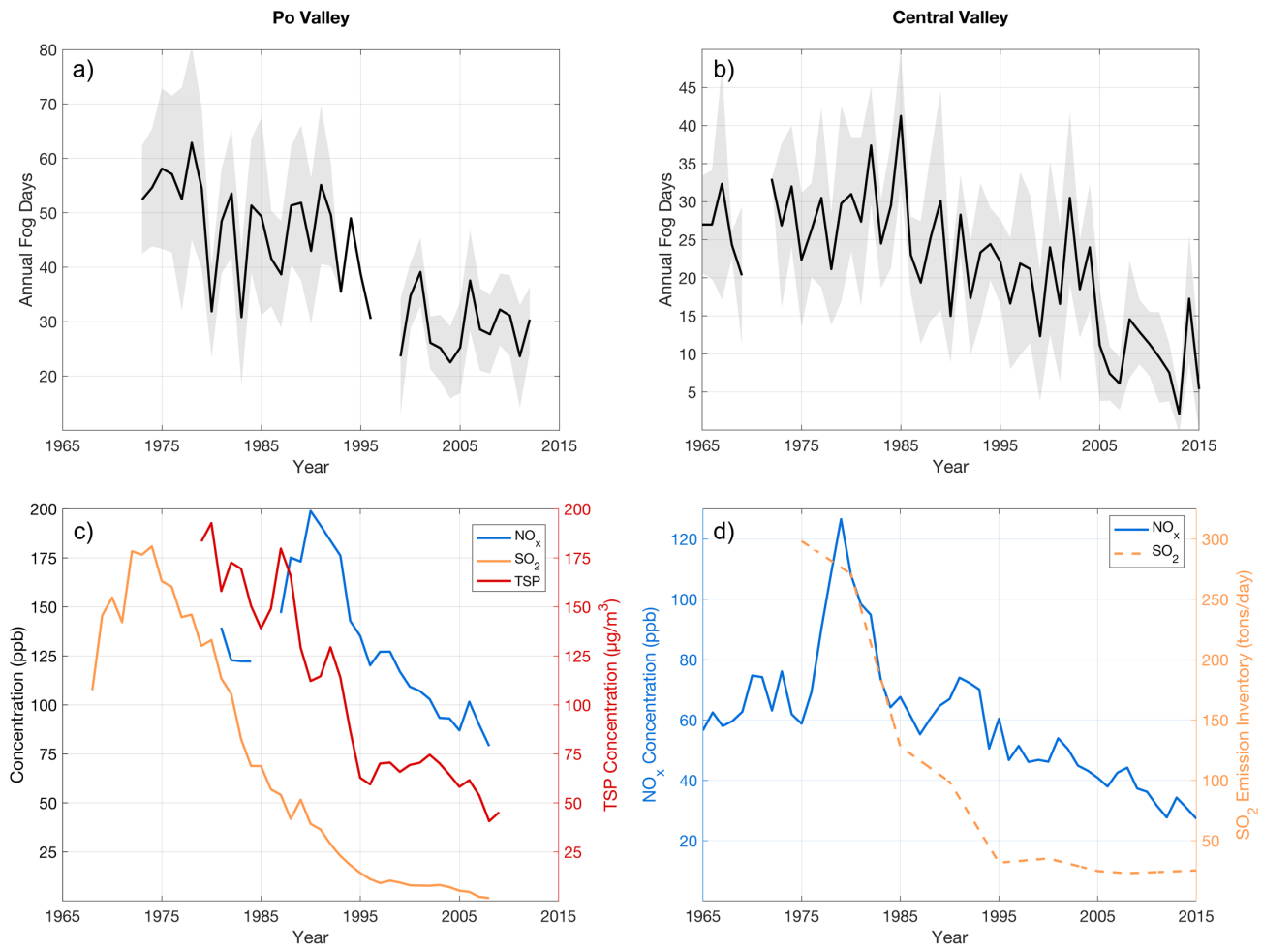

Figure 15. Trends in annual fog days (sum of days with 1 hour of visibility < 400 m) and pollution from 1965-2015. Panel a and b show the trend in annual fog days for nine Po Valley observation sites (Turin, Milan - Linate, Milan – Malpensa, Bergamo, Brescia, Bologna, Rimini, Treviso, and Venice) and nine Central Valley observation sites (Redding, Red Bluff, Beale, Sacramento, Travis, Stockton, Castle Air Force Base, Fresno, Bakersfield). Panel c shows the Po Valley (Milan) trend in oxides of nitrogen (NO_x) (blue) and sulfur dioxide (SO_2) (orange) concentration (ppb), as well as the concentration ($\mu g/m^3$) of total suspended particles (TSP) (red). Panel d shows trend in NO_x concentration for Central Valley (averaged for Sacramento, Fresno, Bakersfield), as well as an SO_2 emission inventory (tons/day) from the California Air Resources Board.

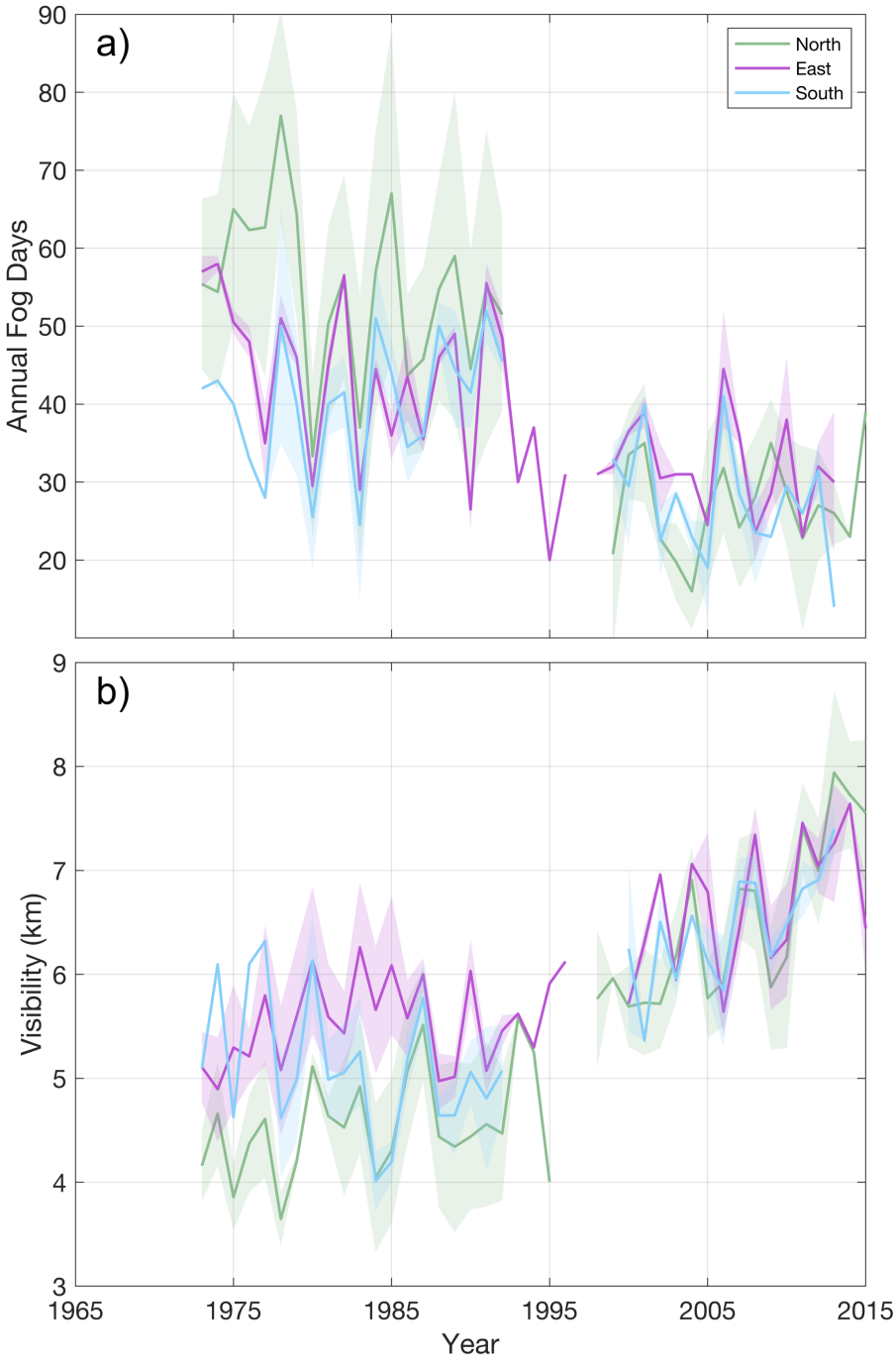

Figure 16. Panel shows Po Valley trend in annual fog days (top) and visibility (bottom) for clusters defined geographically by North (Turin, Milan (Linate Airport and Malpensa Airport), Bergamo, Brescia), East (Treviso, Venice), and South (Bologna, Rimini). Shading represents standard deviation of sites.

Table 6. GAM Model Results

	Continuous Variables								*Categorical Variable*
Location	DPD	$NO_x^{DPD < 3.5°C}$	$NO_x^{DPD > 3.5°C}$	SO_2	TSP	Wind Speed	Year	Night Length	Precipitation
Milan[a]									
r^2 = 0.65									
90% Range	0.58 - 11°C	43 - 250 ppb	43 - 250 ppb	1.4 - 41 ppb	27 - 160 µg/m^3	0.6 - 2.0 m/s	1991-2009	-	* 28%
Visibility Impact	(+) 7.9 km	(-) 5.6 km	(-) 2.8 km	(-) 1.2 km	(-) 4.1 km	(+) 1.1 km	(-) 3 km	-	(+) 1.3 km
Sacramento[b]									
r^2 = 0.62									
90% Range	0.81 - 8.3°C	10 - 109 ppb	10 - 109 ppb	-	-	0.53 - 5.6 m/s	-	12.3 - 14.3 hr	* 31%
Visibility Impact	(+) 7.6 km	(-) 3.0 km	(-) 0.55 km	-	-	(+) 0.86 km	-	(-) 1.3 km	(+) 1.3
Fresno[b]									
r^2 = 0.61									
90% Range	1.0 - 9.3°C	13 - 130 ppb	13 - 130 ppb	-	-	0.62 - 4.2 m/s	-	-	* 23%
Visibility Impact	(+) 8.9 km	(-) 3.0 km	(-) 1.7 km	-	-	(+) 2.7 km	-	-	(+) 2.4 km
Bakersfield[b]									
r^2 = 0.56									
90% Range	1.3 - 12°C	19 - 160 ppb	19 - 160 ppb	-	-	1.1 - 3.8 m/s	-	-	* 19%
Visibility Impact	(+) 8.0 km	(-) 4.2 km	(-) 2.4 km	-	-	(+) 2.4 km	-	-	(+) 2.4 km

a – 1989 - 2010
b – 1973 - 2014

Abbreviations. Dew Point Depression (DPD), Oxides of Nitrogen Concentration (NO_x), Sulfur Dioxide (SO_2), Total Suspended Particles (TSP).

** – % of winter days with rain events*

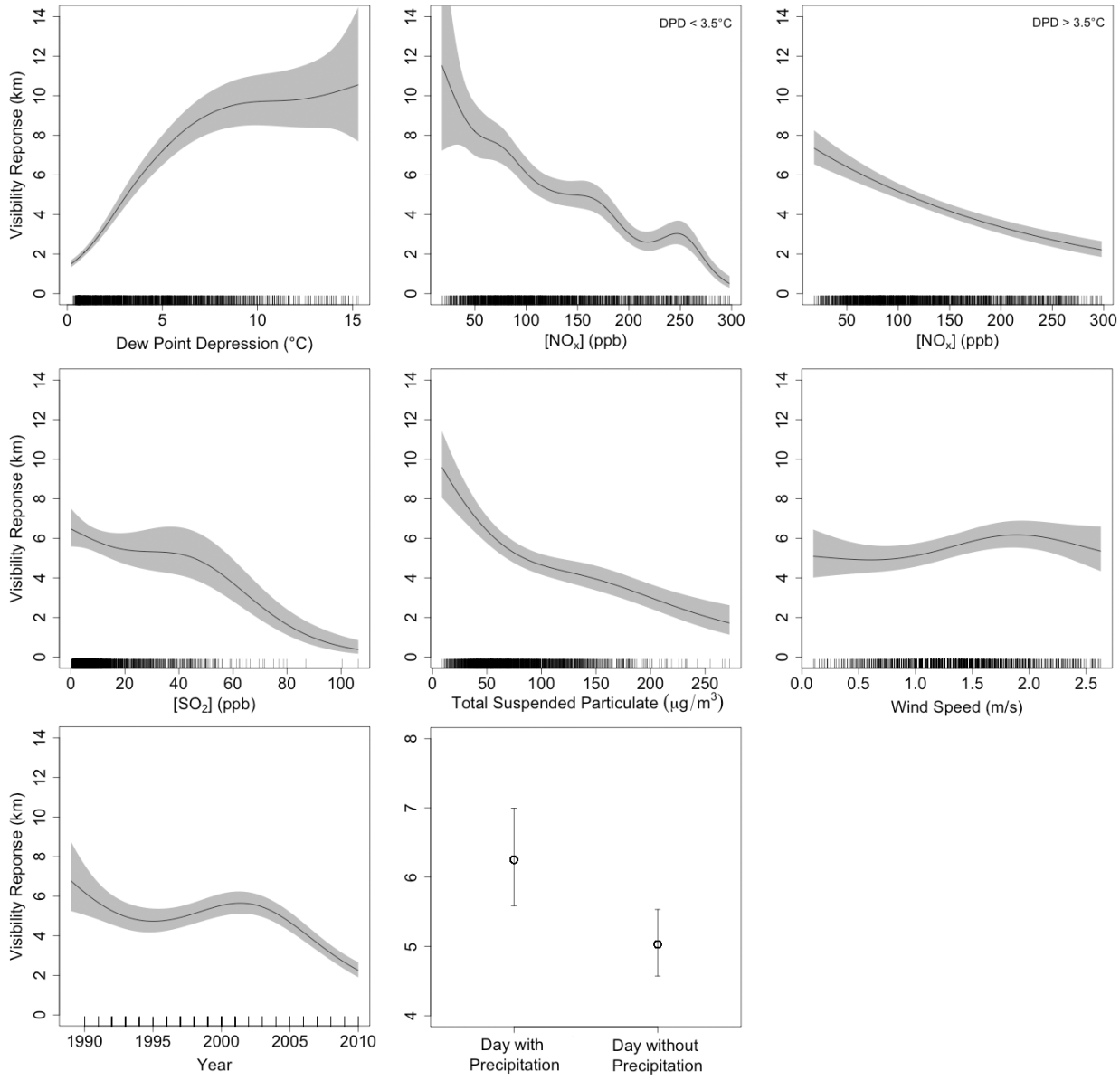

Figure 17. GAM model results for Milan from 1989 – 2010 where each plot represents the partial response on visibility (km), all of which additively contribute to the total regression. Y-axis labeled from 0-14 kilometers with the exception of precipitation, which has a narrower y-axis and is modeled as a categorical variable comparing days with and without precipitation. Grey shading represents confidence intervals two times the standard error. NO_x response is separated by interaction terms, with the first plot indicating the response of [NO_x] should all inputs have occurred with DPD < 3.5℃ and the response of the second indicating response should all values occur when DPD > 3.5℃.

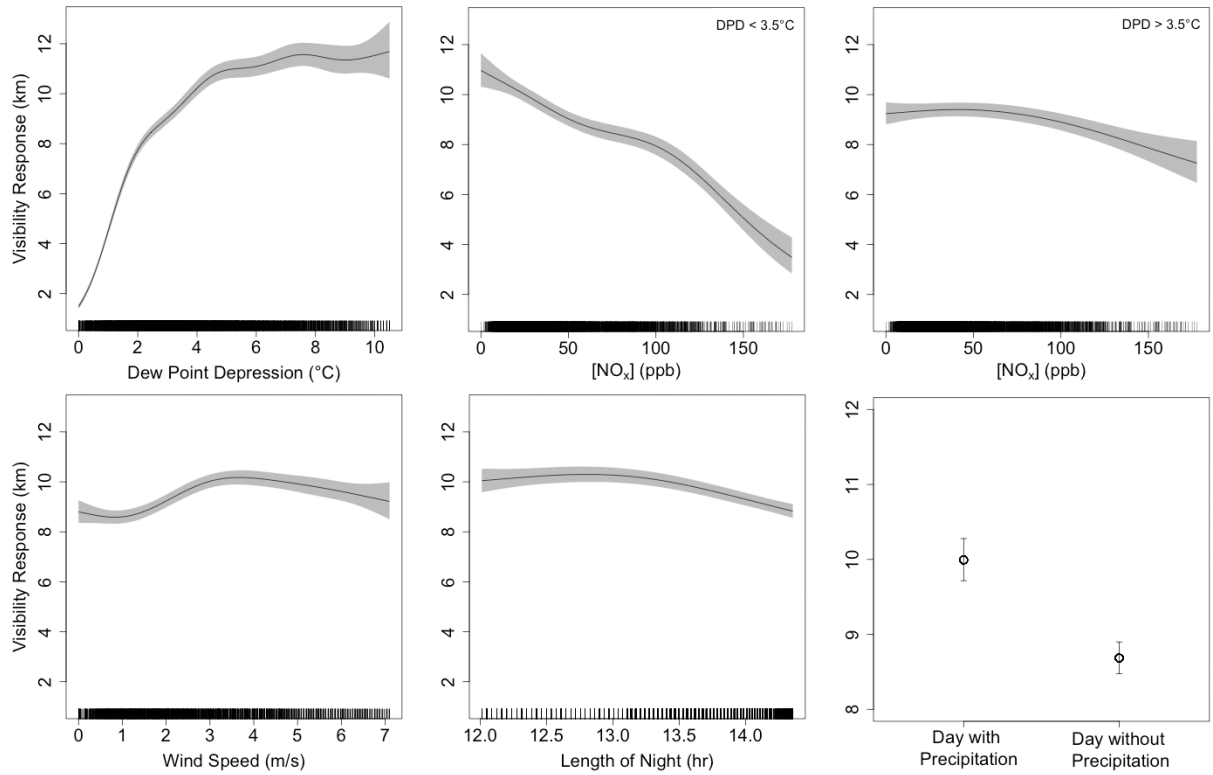

Figure 18. GAM model results for Sacramento from 1973-2016 where each plot represents the partial response on visibility (km), all of which additively contribute to the total regression. Y-axis labeled from 0-13 kilometers with the exception of precipitation, which has a narrower y-axis and is modeled as a categorical variable comparing days with and without precipitation. Grey shading represents confidence intervals two times the standard error. NO_x response is separated by interaction terms, with the first plot indicating the response of $[NO_x]$ should all inputs have occurred with DPD < 3.5℃ and the response of the second indicating response should all values occur when DPD > 3.5℃.

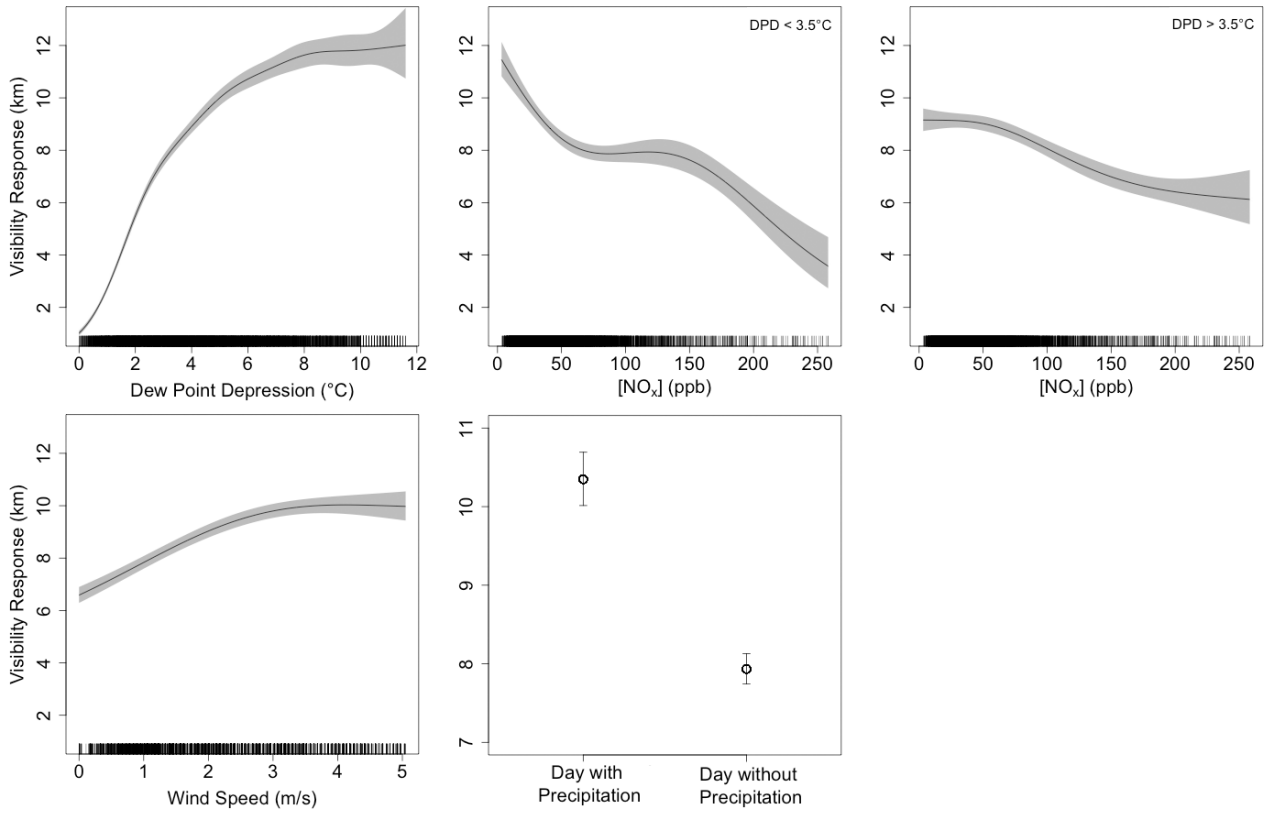

Figure 19. GAM model results for Fresno from 1973-2016 where each plot represents the partial response on visibility (km), all of which additively contribute to the total regression. Y-axis labeled from 0-13 kilometers with the exception of precipitation, which has a narrower y-axis and is modeled as a categorical variable comparing days with and without precipitation. Grey shading represents confidence intervals two times the standard error. NO_x response is separated by interaction terms, with the first plot indicating the response of [NO_x] should all inputs have occurred with DPD < 3.5℃ and the response of the second indicating response should all values occur when DPD > 3.5℃

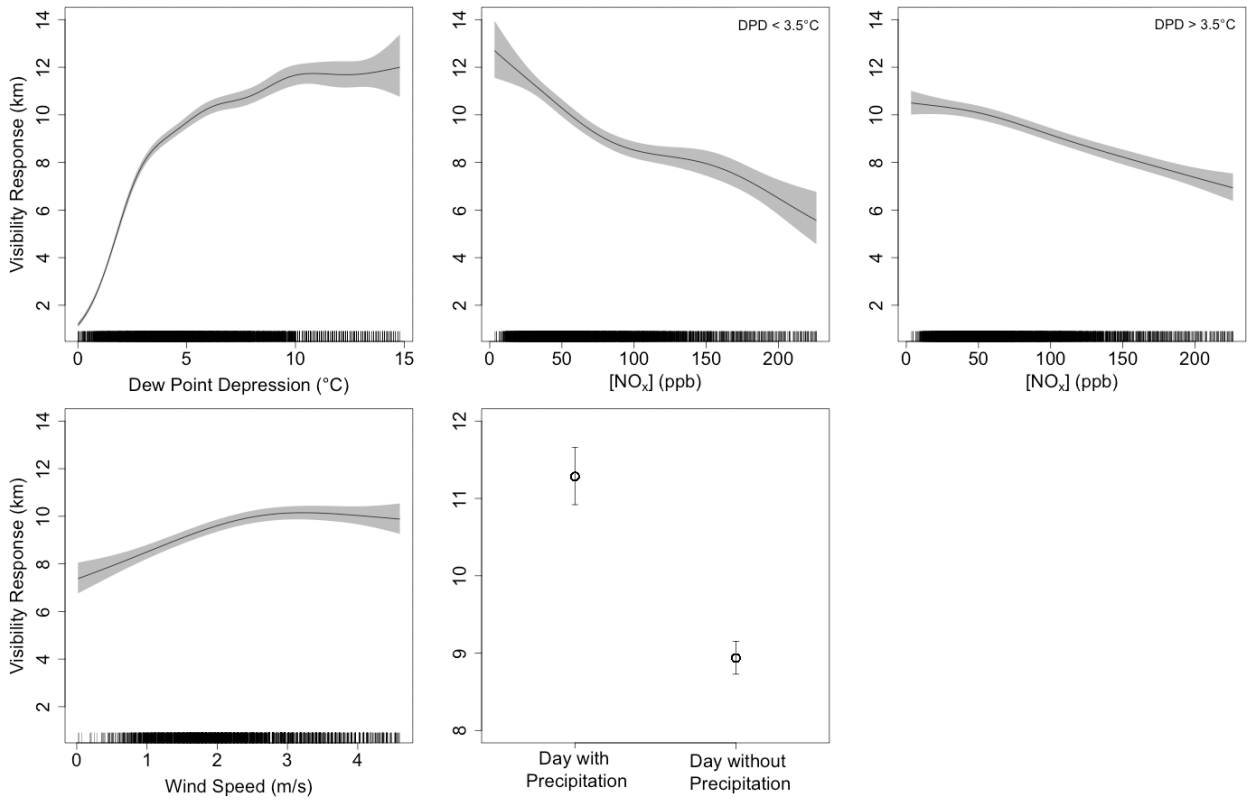

Figure 20. GAM model results for Bakersfield from 1973-2016 where each plot represents the partial response on visibility (km), all of which additively contribute to the total regression. Y-axis labeled from 0-12 kilometers with the exception of precipitation, which has a narrower y-axis and is modeled as a categorical variable comparing days with and without precipitation. Grey shading represents confidence intervals two times the standard error. NO_x response is separated by interaction terms, with the first plot indicating the response of [NO_x] should all inputs have occurred with DPD < 3.5℃ and the response of the second indicating response should all values occur when DPD > 3.5℃.

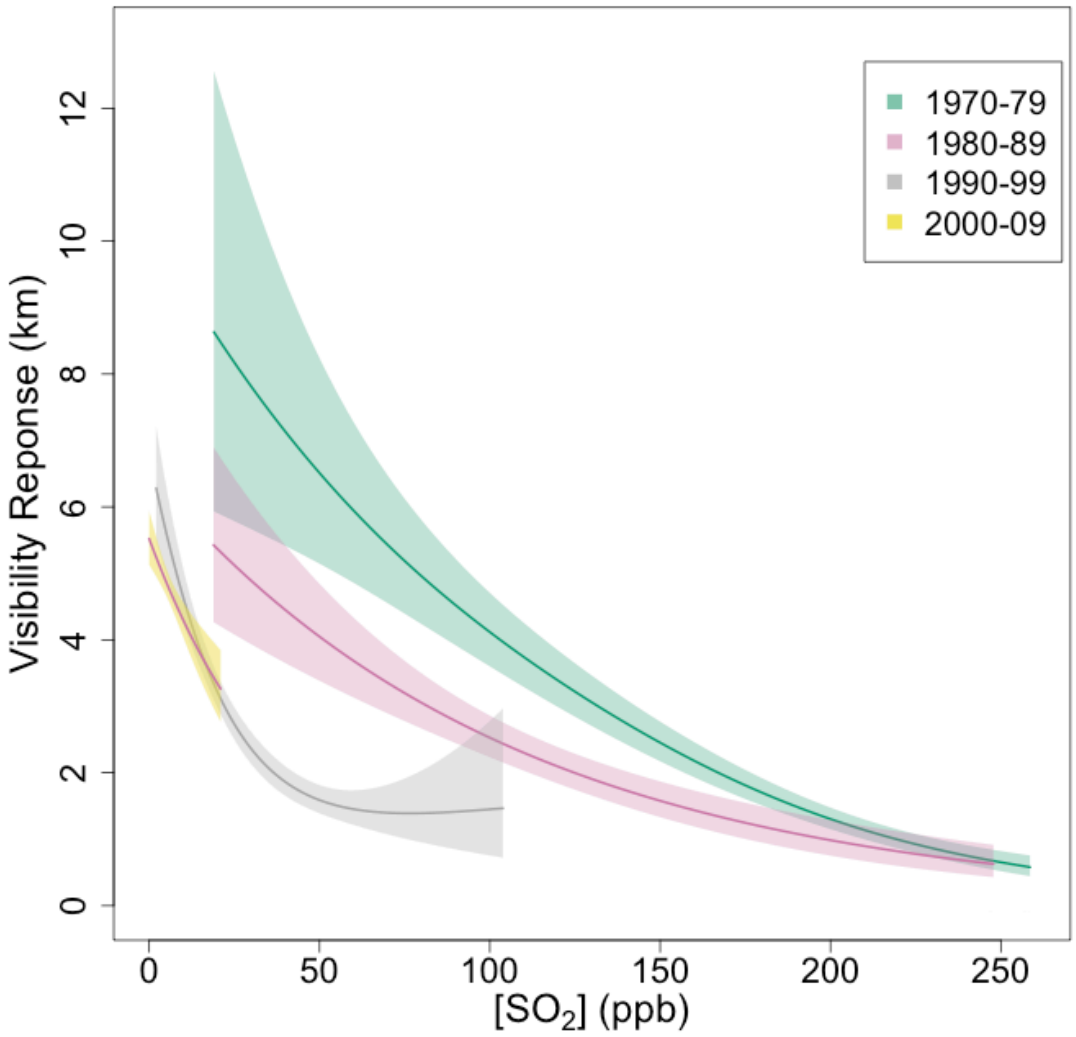

Figure 21. Plot of univariable visibility response to sulfur dioxide (SO_2) separated by each decade of observation

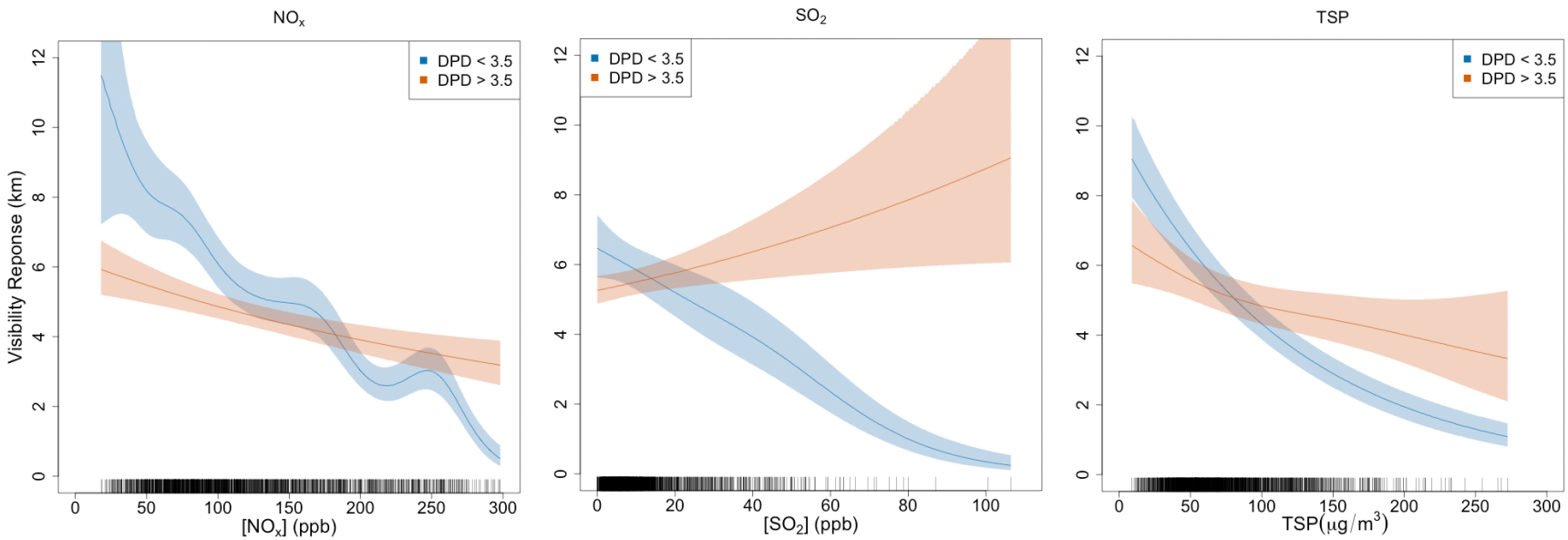

Figure 22. Plots of the visibility response to air pollution (oxides of nitrogen (NO_x), sulfur dioxide (SO_2), and total suspended particle (TSP)) varied over two levels of dew point depression (DPD). Blue lines represent pollutant response when DPD < 3.5 ℃ and orange represents pollutant response when DPD > 3.5 ℃.

Table 7. Milan Air Pollution Interaction Term Comparison

Location	NO_x	$NO_x^{DPD < 3.5℃}$	$NO_x^{DPD > 3.5℃}$	SO_2	$SO_2^{DPD < 3.5℃}$	$SO_2^{DPD > 3.5℃}$	TSP	TSP $^{DPD < 3.5℃}$	TSP $^{DPD > 3.5℃}$
Milan									
90% Range	43-250 ppb	43-250 ppb	43-250 ppb	1.4 - 41 ppb	1.4 - 41 ppb	1.4 - 41 ppb	27 - 160 µg/m^3	27 - 160 µg/m^3	27 - 160 µg/m^3
Visibility Range	7.4-3.5 km	8.6-3.0 km	5.6 - 3.5 km	6.4 - 5.2 km	6.4 - 3.9 km	5.3 - 6.4 km	8.0 - 3.8 km	7.8 - 2.7 km	6.1 - 4.4 km
Net Impact	(-) 3.9 km	(-) 5.6 km	(-) 2.1 km	(-) 1.2 km	(-) 2.5 km	(+) 1.1 km	(-) 4.1 km	(-) 5.0 km	(-) 1.7 km

Abbreviations. Oxides of Nitrogen Concentration (NO_x), Sulfur Dioxide (SO_2), Total Suspended Particles (TSP)

Chapter 4:

Trends in frequency, rate, and severity of Central Valley fog-related traffic accidents

Abstract: Decades of multicar pile ups along California's Central Valley highways made the region widely-known for the frequency and severity of its fog-related accidents. Despite prevention measures dating back to 1973, no long-term evaluation of the trend in accidents has been conducted. This chapter analyzes descriptive statistics and trends in fog-related accidents from 1996-1997 to 2015-2016 fog seasons, primarily focusing on the four largest counties: Sacramento, San Joaquin, Fresno, and Kern. The Central Valley saw a 65% decline in fog-related accidents over 20 winters, the variance of which is best explained by the sharply declining trend in seasonal fog hours over the same period. Annual frequency of fog hours (visibility < 650 meters), as summarized each fog season (November-March) explain an average of ~80% of the annual variability in fog-related accidents for the counties studied, suggesting that the declining trend in fog is a strong determinant in the declining trend in accidents. The decline in fog-related accidents occurred despite a 6-15% increase in vehicle-kilometers driven from 2002-2016 in the four counties. The subsequent improvement in visibility results in annual fog-related injuries falling by 72%, with the valley seeing an average of 550 fewer injuries from fog accidents in 2015-2016 than in 1996-1997.

Further, at least two counties, Sacramento and San Joaquin, also show declines in the rate of accidents per fog hour, suggesting that improvements to vehicle safety, roadway notifications, and traffic diversion may make detectable impacts. Additionally, there is evidence that fog-related accidents grew less severe over the 20-year study when investigating the frequency of accidents in five collision severity categories relative to the total fog accidents each season. In Sacramento, Fresno, and Kern County, trends in less serious accidents are increasing at the expense of more dangerous collisions, which are decreasing.

The study found no trend in the number of collisions per fog-related accident, relative to the number of accidents each year, suggesting that when accidents occur, the probability of multicar pile ups remains the same. Additionally, the frequency of fatal accidents shows no trend, suggesting there continue to be important opportunities for roadway and vehicle safety improvements.

The human safety and commercial benefits to a reduction in fog-accidents and the resulting roadway delays is well documented. The declining trend in dense fog in this region has had the most pronounced impact on the declining frequency of fog-related accidents. Past chapters implicated changing regional air pollution concentrations as a critical driver in the long-term trend of fog frequency. The strong link between the historical number of Central Valley fog events and trends in pollution concentration provides a measure of how regulations of emissions that led to decreases in aerosol concentration, and thereby wintertime fog frequency, also led to the declining trend in fog-related accidents.

1. Introduction

In the United States, 21% of accidents and 23% of fatal crashes are due to the presence of adverse weather conditions, which cost a minimum of $22 billion USD annually from the resulting emergency services, property damage, medical costs, productivity loss, and delayed traffic (Ashley et al., 2015; Blincoe et al., 2002; Pisano et al., 2008; USDOT, 2018). The cumulative annual travel delay for snow, ice, and fog alone is estimated at 544 million vehicle-hours (United States Department of Transportation (USDOT), 2018).

While rain is responsible for the largest proportion of weather-related accidents, fog-related accidents are responsible for many of the most severe crashes (Abedel Aty et al., 2011). Studies of Florida collisions found that fog was implicated in one-in-five accidents involving 10 or more vehicles and, when present, resulted in accidents with more serious injuries than during clear conditions (Abedel Aty et al., 2011, Hamilton et al., 2014). Adverse fog conditions are responsible for 9% of weather-related accident fatalities in passenger vehicles and 12% in commercial vehicles, resulting in 464 peopled killed per year, on average (2007-2016) (Pisano et al., 2008; USDOT, 2018). For perspective, that is comparable to the annual number of fatalities from hurricanes, tornadoes, floods, heat, cold, and lightning combined (averaged from 2009-2018) (National Weather Service (NWS), 2019). While extreme weather hazards may anomalously result in more fatalities in a given year, the consistent year-over-year danger fog poses deserves attention.

Fog events are less common than other driving hazards; the complex variables and episodic nature of fog results in it being underreported by weather advisories, further exacerbating the risk it poses to drivers. In a five-year study (2007-2011), Ashley et al., 2015 found that 72% of national vision-obscured fatalities occurred when no visibility-related weather advisory had been issued. This effect was most pronounced in warmer months, but even at its least, in February, fog advisories were not issued prior to ~50% of fatal fog-related accidents, which is a much higher percentage of unwarned fatalities than other accident types (Ashley et al., 2015; Black and Ashley, 2010).

The presence of fog reduces visual contrast and obscures details of the road, making it difficult for drivers to perceive depth and speed. This is made more challenging given that traditional high beams reflect off the suspended water droplets, only further obscuring vision. Studies indicate that driver response to fog can be hazardous and unpredictable. Drivers perceive the lead car to be 60% farther away in foggy conditions than clear; coupled with overconfidence based on roadway conditions, such as retroreflective lanes, they may fail to sufficiently reduce travel speed to avoid unexpected events (Carvallo et al, 2001; Buchner et al., 2006; Brooks et al., 2011). Abdel-Aty et al., 2011 found fog-related accidents most commonly occurred on high-speed roads, undivided roads, roads with no sidewalk, and two lane rural roads. Simulated studies also found that road type impacts driver's response to decreasing visibility (Rosey, 2017). On average, low visibility causes a 10-12% speed reduction and 12% reduced road capacity (Agarwal et al., 2005; Pisano and Goodwin, 2002), the effects of which are further amplified in dense radiation fog where visibility is reduced to only a few meters.

Radiation fog complicates driving due its patchy, heterogenous density patterns, causing visibility to rapidly drop without warning. Such was the case in Fresno in November 2007 when a fog-related accident resulted in a mile-long, 108-vehicle pile-up, including 18 semi-trailer commercial

trucks. The accident caused 63 injuries, resulted in at least two deaths, and closed the highway for over 12 hours. Notably, the last vehicle collided ten minutes after the initial crash, highlighting how obscured potential collisions can be to oncoming drivers before reaching the hazard. Fog covered only ~10% of the valley that morning, so commuters and commercial drivers were unsuspecting (Lin and Weiss, 2007). Commercial vehicles are particularly vulnerable to more severe accidents, since they require more stopping distance, respond poorly to unpredictable speed variance, and impose a more dangerous collision upon impact (Pisano et al., 2008; Ashley et al., 2015).

Past works have identified dense radiation fog as the leading cause of weather-related traffic accidents in California, within which the Central Valley is a national hotspot for fatalities from vision-obscured accidents (Ashley et al., 2015; USDOT, 2017). The Central Valley has a high volume of roadway traffic due to both commercial transportation and residential commuting. Low population density throughout a majority of the valley increases commuting distance. Wintertime visibility conditions are historically dangerous enough that many school districts have wintertime guidelines in place to implement a "fog day," delaying school until roads are safe enough for bus transportation. Depending on the district, visibility below 60-90 meters (m) at 0500 LT results in a delay of school (Appleton, 2018). Rural school districts, such as those in southwest Fresno, have had up to 15 fog days in a single school year (Appleton, 2018).

The persistence of fog in the Central Valley, known regionally as tule fog, is aided by two primary attributes: wet winters with intense but infrequent storms, permeated by persistent anticyclonic periods of dry, sunny conditions and very stable winds (Herckes et al., 2015). After increases in soil moisture from early winter rainfall, radiative cooling on long, cloudless nights allows atmospheric moisture close to the surface to cool to dew point and condense, forming fog droplets (Underwood et al., 2004). The bowl-like topography of the 720-kilometer (km) long valley, flanked on either side by two north-south oriented mountain ranges, keeps surface winds low and supports strong inversion layer development into the morning (Bianco et al., 2011; Holets & Swanson, 1981).

The Central Valley, though characterized by its agricultural economy and largely rural roadway network, is a region in transition. The urban population of the valley is growing at a rate significantly greater than the state or national population. Analyzing a sample of 10 counties in the Central Valley, Congressional Research Service (CRS) maps indicate that from 1980-2003, population density in the valley increased from 75 person per square mile to 131, and valley-wide population grew by 75% (CRS, 2005). For comparison, during this period, the United States increased by only 28% and the state of California by 50%. Projections suggest that the Central Valley population will continue to expand rapidly, with an expected tripling of 2003 population by 2040 (Struglia et al., 2003). Total vehicle-kilometers traveled in this region reflect this growing population.

In the midst of increasing roadway traffic, the Central Valley has also experienced a significant decline in the frequency of wintertime fog, with sites throughout observing a 46-90% decline in fog events since 1980 (Baldocchi & Waller, 2014; Gray et al., 2019; Herckes et al., 2015). Previous chapters have linked the decline in fog frequency with concurrent regulation-induced declines in air pollution experienced throughout the valley (Gray et al., 2019). A reduction in primary air

pollutants lead to a reduction in secondary inorganic aerosols, most commonly ammonium nitrate (Pusede et al., 2016), which is of the correct size and chemical composition to make efficient cloud condensation nuclei for atmospheric moisture to condense on (Petters & Kreidenweis, 2007). Thus, previous work found that a reduction of 10 parts per billion (ppb) in oxides of nitrogen (NO_x), the limiting precursor to aerosol nitrate formation, results in a reduction of approximately five fog days per year (Gray et al., 2019). Decreasing trends in fog and air pollution are reflected throughout the valley, such as in Fresno where a decline of 49 ± 8 ppb in NOx since 1980 occurred concurrent to a loss of 31 ± 9 fog days per season (Gray et al., 2019). This driver in fog decline, along with increases in dew point depression and urban expansion, is expected to continue decreasing fog frequency in the future.

During the 20-years of this study, the California Department of Transportation (Caltrans) also implemented new strategies for warning drivers about the presence of fog. In 2009, a pilot program for a fog warning system installed sensors in approximately one kilometer increments along a 21-kilometer stretch of California Highway 99, which carries 100,000 vehicles per day (USDOT, 2017). The declining tule fog trend makes the efficacy of the sensors challenging for Caltrans to assess (Lavelle, 2014); this coupled with infrastructure and budgetary constraints postponed any expansion of the system. However, commuter's increased access to weather alerts through smart phones and experimental forecasting websites, such as the NWS Experimental Fog Severity Index, has further empowered drivers to take precautionary measures (Morss et al., 2008; NWS, 2019).

Lastly, fleet turnover during the study period implies that a higher percentage of vehicles with sophisticated crash-avoidant technology now share the road. Features such as lane departure warnings and forward collision warnings have theoretical safety benefits, but studies have failed to objectively demonstrate their real world benefit – which would prove even more challenging in foggy conditions with obscured vehicle sensors (Hamilton et al., 2014; Mehler et al., 2014). Additionally, vehicle safety during accidents has gradually improved year-over-year since 1996. A study by the National Highway Traffic Safety Administration (NHTSA) found that owning an 18-year or older vehicle increased the risk of accident fatality by 71%. Further, as a result of improved safety features, owning an older vehicle was more dangerous in the past than today: an eight-year old car increased the risk of fatality by 37% in 2005, but only 33% for an eight-year old car in 2010 (NHTSA, 2013).

The unique conditions of the Central Valley, in which the number of fog events has declined, yet the population and traffic volume continue to increase, make it an important venue to explore trends in fog-related accidents. This study analyzed fog-related accidents in the Central Valley for the period 1996-2016. The purpose of this chapter is to provide an exploratory and descriptive analysis of the fog-related accident database and identify relationships and questions that might steer future roadway-weather studies and support legislative measures.

2. Methods

2.1. Data acquisition

Data for this investigation consist of roadway accident descriptions, daily roadway mileage estimates, and visibility observations. The data originate from three sources:

The roadway accident data set was downloaded from the California Highway Patrol Accident Investigation Unit through their Statewide Integrated Traffic Records System (SWITRS) (https://www.chp.ca.gov/programs-services/services-information/switrs-internet-statewide-integrated-traffic-records-system). Using the collision data set, accidents were limited to three districts (3, 10, and 6) that encompass a majority of the Central Valley and filtered by accidents where fog was a primary contributing factor for 1996 -2016. The SWITRS collision data provide information on date, hour, day of week, number of vehicles per accident, collision severity, and number of injuries and fatalities. Data were temporally scaled to the hour of accident occurrence to match the scale of meteorological observations. Annual summaries of data were compiled for the fog season from November – March (NDJFM), meaning a small percentage of fog-related accidents outside the typical season (< 4%) were not included.

Estimates for daily roadway mileage were obtained from the Caltrans Highway Performance Monitoring System (https://dot.ca.gov/programs/research-innovation-system-information/highway-performance-monitoring-system) and converted to kilometers. In order to determine an estimate for the fog season, the daily vehicle-kilometers driven was multiplied by the length of the fog season (151 or 152 days, depending on leap year). Since Caltrans estimates daily roadway mileage annually, any analysis with roadway mileage was computed with Jan-Dec (JFMND) fog accident summaries, rather than seasonal summaries (NDJFM).

Visibility observations were downloaded from the National Climatic Data Center (https://www.ncdc.noaa.gov/cdo-web/datatools/lcd) for airport stations throughout the Central Valley and temporally scaled to one-hour intervals. Seasonal summaries of fog days, fog hours, and fog duration were derived by investigating instances when visibility fell below 400, 650, and 1150 meters (0.25, 0.4, and 0.7 miles). Traditionally, dense radiation fog is defined as visibility < 400 meters (0.25 miles) (National Oceanographic and Atmospheric Administration, 2005), but less dense fog can still be dangerous to motorists, as well as useful for estimating patchy fog conditions away from the point-source visibility measurements. Seasonal fog days and hours were determined by summing the instances visibility fell below those markers. Annual fog duration was derived by dividing the number of fog hours by number of days of fog. I required each season (NDJFM) to report all five months, in which each month reports > 90% of hourly observations. Visibility was measured according to the Automated Surface Observation System, whereby visibility was automatically recorded using a forward scatter visibility sensor, measuring the attenuation of light at 20 second intervals (National Oceanographic and Atmospheric Administration, 2005). Data was processed with flags for quality control to remove noticeable instrumentation artifacts.

The episodic nature of radiation fog requires frequent and complete reporting to fully capture the trend, and thus, only a few stations met these requirements over the 20-year period. I matched these stations with the corresponding counties in the collision data set, focusing most of the site-

specific research on the counties of Sacramento (District 3), San Joaquin (District 10), Fresno (District 6), and Kern (District 6) (*Table 1*).

2.2. Trend analysis

Trends were found using the non-parametric two-tailed Mann-Kendall trend test and the Theil-Sen estimator (http://www.mathworks.com/matlabcentral/fileexchange/authors/23983) (Burkey, 2006; Sen, 1968; Theil, 1992), which tests the null hypothesis (H_0), which would indicate no trend in the data, against the alternative (H_1), which indicates a significant trend (Mann, 1945; Kendall, 1955). I investigated trends at the 95% confidence interval, where an output of H=1 implies that the null hypothesis failed and there is a significant trend at $\propto = 0.05$. The Theil-Sen estimator then determines a best fit line by calculating the median of all slopes between pairs of points over the period. One advantage of this technique is that it minimizes the impact of outliers. The mean of all slopes over n values is Sen's slope (Qi):

$$Q_i = \frac{(x_j - x_k)}{(j - k)} \; for \; i = 1, \ldots n$$

where x_j and x_k are data at times j and k, and n is the number of points.

Similarly, Kendall's Tau was used to determine correlation between two variables by measuring the strength of the dependence between two columns of ranked data (Sen, 1968). The best fit line was calculated using orthogonal least squares regression, which minimizes the orthogonal distance from the observed data points to the regression line and is ideal for analysis with randomness in both the dependent and independent variables (https://www.mathworks.com/matlabcentral/fileexchange/16800-orthogonal-linear-regression).

2.3. Analysis description and assumptions

I first describe the spatial and temporal distribution of selected fog-related accident parameters. In 3.3.1, histograms, frequency tables, and trend analysis are presented to describe and classify fog-related accidents for the entire valley.

Section 3.3.2 presents investigation of site-specific fog-related accidents, pairing counties with adjacent airport meteorological stations. Fog-related accident trends are determined for each county, including the trend in these accidents in relation to annual vehicle-kilometers traveled. The study then investigates how the trend in fog frequency impacts fog-related accidents annually to determine the trend variability associated with fog rates versus other safety improvements. In doing so, the trend in fog-related accident per hour is calculated to explore whether roads become safer for drivers during fog episodes over time. Lastly, this section explores how the density of fog, as found by hourly visibility measurements at local airports, effects accident frequency.

Section 3.3.3 presents the distribution of accident severity and its site-specific trends over time. The relationship between visibility and accident severity, as well as number of collisions per accident is investigated. Trends in annual injuries and fatalities also provide additional insight into changes in accident severity.

This analysis requires a number of assumptions inherent in large data sets that are subject to human recording errors. Trends in statistics and severity distribution assume that all fog-related accidents in the Central Valley were reported to the police; however, it is estimated that 57% of crashes go unreported (Pisano et al., 2008). I assume here that this ratio is stable throughout the dataset. Police accident reports may involve errors, such as misclassifying the cause of accident or presence of a visibility hazard. Incorrectly recording the hour of accident would result in this analysis associating the wrong hour of visibility from a local airport with it, possibly misrepresenting the visibility conditions in averages. Notably, the SWITRS contains unresolvable errors in the categorizing of accident severity, as well as misreporting of injuries, from the fog season of 2001-2002 to 2005-2006. Thus, these years were left out of descriptive analysis for severity and injuries.

Lastly, the identifier of fog events, visibility, is observed at one point source for each county, which ultimately may be >100 km away from the location of the accident. Airports are typically adjacent to urban centers, where the urban-clear island effect likely begins evaporating radiation fog first (Underwood et al., 2004). Therefore, our visibility estimates may be higher than what was experienced at the sites of collision, particularly in the larger counties, such as Fresno and Kern.

3. Results and discussion

3.1. Spatiotemporal analysis

From October 1996 to April 2016, 19,850 fog-related accidents occurred in districts 3, 10, and 6, which span the majority of the Central Valley (*Figure 1*), of which ~38% resulted in injury. The majority of fog collisions over the 20-year period incurred property damage only, as classified by police reports, but 33% resulted in minor or visible injuries and 5% in severe or fatal injuries (*Figure 2*). In total, 844 deaths were reported and at least 9,471 injuries, which is likely an underestimate due to misreporting in the SWITRS record system from 2001-06. Relative to its population, District 3 has the lowest total of fog-related accidents during the study (*Table 1*). Comparatively, District 10 (central) and 6 (south) have 2.5 and 2.6 times as many fog-related accidents per person, respectively.

Notably, counties within the study region at high median elevation experience far fewer fog-related accidents than those at comparatively low elevation. Nearly all counties with less than 1% of the total fog-related accidents are found in regions with a median elevation greater than 300 m (*Table 1, bolded*). Rare exceptions to the impact of elevation are seen in counties with low populations, such as Glenn and Colusa County. These counties account for less than 1% of the fog-related accidents but have high rates of fog accidents per person (2 and 3 times that of Sacramento County, respectively). An additional exception, Placer County, has a median elevation of 806 m, yet accounts for 2% of fog collisions because it spans horizontally from the western low elevation valley into the eastern mountain ranges.

Unlike typical motor vehicle accidents, which peak during the summer months when roadway volume peaks, fog-related accidents peak from September to February (Ashley et al., 2015). In the Central Valley, where precipitation is primarily limited to frontal storms between December and March (Killam et al., 2014), fog events and the resulting accidents are almost exclusively in the

winter months (*Figure 3a*). ~70% of all fog-related accidents occur in December (31%) and January (38%) during the height of the tule fog season when long nights allow for maximum radiative cooling. This mid-winter maximum in fog accidents is much more concentrated than the national distribution, which found that 28% of fog-related fatalities occurred in December and January (Ashley et al., 2015). November and February are the next most common months for fog-related accidents, at 17% and 10%, respectively (*Table 2*). Diurnally, fog-related accidents peak during morning rush hour and before solar radiation can evaporate the fog layer between 0600 – 0800 local time (LT), with a clear maximum (21%) at 0700 LT (*Figure 3b*). This differs from the majority of accidents, which peak during evening rush hour (Ashley et al., 2015). Contrary to national results for fog-related accidents (Hamilton et al., 2014), Central Valley fog collisions are not more common on weekdays than weekends (*Figure 3c*). Instead, there is a maximum on Friday, followed by Saturday, with a minimum on Sunday, likely influenced by low commercial and commuter traffic.

In total, the districts of the Central Valley saw a statistically significant 65% decline in fog-related accidents between the 1996-1997 and 2015-2016 fog seasons (*Figure 4*).

3.2. County-specific analysis with fog data

The county-specific investigation focused primarily on counties with high-resolution visibility data at a local airport (Sacramento, San Joaquin, Fresno, and Kern County) (*Figure 5, white stars*), with supplementary analysis for counties closely-adjacent to a high-reporting airport (Stanislaus and Tulare County) (*Figure 5, grey stars*). Of the 23 counties in districts 3,10, and 6, the six investigated make up 72% of the fog-related accidents from 1996-2016, as well as 72% of the total population (*Table 2*).

Table 3 describes the primary counties and airports analyzed, representing regions of high population and vehicle-travel. On average, each county travels 5.8 billion vehicle-kilometers each year, with the highest being nearly 8 billion annually in Sacramento County, which also has the highest population and population density (*Table 3*). Sacramento, San Joaquin, Fresno, and Kern County experience an annual wintertime average of 120 fog-related accidents per county from 1996-2016. Dense fog is a frequent phenomenon in these regions (*Figure 6b*). The median airport visibility during fog-related accidents is only 600 m, with 1-in-15 fog-related accidents occurring when local airport visibility was zero meters.

The primary counties investigated in this study – Sacramento, San Joaquin, Fresno, and Kern – observed a statistically significant decline in fog-related accidents from 1996-2016, from a 65% decline in Sacramento to a 72% decline in Kern (*Table 4*). *Figure 6a* demonstrates that the high variability in fog-related accidents each year covaries from county to county.

3.2.1. Fog-related accidents scaled to kilometers-traveled

The decline in fog-related accidents occurred despite a ~ 6-15% increase in vehicle-kilometers driven from 2002-2016 in three of the four primary counties analyzed (*Table 5*). When summed for all four counties, this represents a 0.5% increase in roadway volume per year, except for a notable decline after the 2007-2008 financial crisis (*Figure 7*).

Using these estimates, I can determine the number of fog-related accidents per kilometer per year from 2002-2015. This calculation not only scales counties of differing areas relative to their population and commercial function, but also more accurately reflects the improved trend in fog-related accidents relative to the increased amount of travel. *Table 6* shows the recalculated trend in fog-related accidents per calendar year (JFMND) for comparability with the roadway volume data (limited to 2015). Although the southern counties of Fresno and Kern have an area 6 and 8 times larger, respectively, than that of Sacramento County, they have ~10% the population density; thus, vehicle-kilometers traveled in each county are comparable (*Table 3*).

Roadway volume per person is also much higher in Fresno and Kern County. For instance, Kern has 59% the population of Sacramento County, but drives 68% of the kilometers per fog season. Thus, relative to population of Sacramento, Kern roads see 780 million more kilometers, or ~870 kilometers more per person. The increased roadway traffic relative to their population seen in Kern and Fresno (273 million extra miles) may be attributed to longer commuting distances due to low population density or a higher volume of commercial transport, which is common along its highways. Sacramento County also has the lowest annual rate of fog-related accidents per kilometer, when averaged from 2002-2015. Fresno has the highest rate of accidents per kilometer (2.3 times higher than Sacramento), followed by Stockton (2.1 times higher), and Bakersfield (1.3 times higher) (*Figure 8*).

When summed for all four counties from 2002-2015, the rate of fog-related accidents per kilometer declined by 80% (*Figure 8*). The largest change in fog accidents per kilometer was in Sacramento (*Table 6*). From 2002-2015, fog-accidents per vehicle-kilometer decreased by 73%, a 10% larger decline than the fog decrease over that same period (*Table 6*). While other sites did not see as significant of an enhancement in the declining trend when considering the 2 billion additional kilometers driven in 2015 relative to 2002, all declining trends in rate of fog-related accidents remained the same or strengthened the declining trend.

3.2.2. Impact of fog frequency on fog-related accidents

A significant decline in the frequency of fog during this period has greatly contributed to the reduction in accidents. When investigating fog seasons from 1996-2016, fog hours declined significantly at Sacramento, Stockton, Fresno, and Bakersfield airport. The four airports saw a 91% decline from 1996-2016 in the frequency of dense fog hours (*Figure 6b*), traditionally defined as visibility < 0.25 miles (400m). Less dense fog events, defined as visibility < .4 miles (650 m) and < .7 miles (1150 m) also declined by~ 50% over the twenty-year period (*Figure 6b*). Examining multiple visibility thresholds is critical for this study due to the large footprint of each county, particularly Fresno and Kern. The heterogenous density patterns common to radiation fog make it likely that visibility may differ at a local airport despite being dense enough on county roadways to cause accidents. This is evident in *Table 7*, which examines the visibility during fog-related accidents at adjacent airports. When summarizing the frequency of accidents occurring at the three distance thresholds (400, 650, and 1150 meters), 55 and 59% of accidents in Sacramento and San Joaquin County occur when local airport visibility is < 650 m, compared with 48 and 39% for the much larger counties of Fresno and Kern (*Table 7*). This is further demonstrated in *Figure 9* which shows the annual frequency of accidents occurring compared to the adjacent airport

visibility. Sacramento, San Joaquin, and Fresno accidents most commonly occur when visibility is < 1 km (61, 65, 53%, respectively), whereas Bakersfield's (Kern County's) visibility distribution is notably higher, with a majority occurring when airport visibility is < 2 km (53%) (*Table 8*). While this could indicate more dangerous roadway conditions, it is more likely that visibility is higher at the airport than the collision site at the time of the accident and that this impact is most prominently seen in the larger counties, such as Kern County, which is nearly ten times larger than Sacramento.

The discrepancy between airport visibility and visibility at accident sites has grown more pronounced over the course of the study, suggesting that patchiness in radiation fog throughout the valley has increased since 1996. *Figure 10* shows the trend in airport visibility from 1996-2016 for Sacramento, San Joaquin, Fresno, and Kern County. Average visibility during fog-related accidents increased from 1996-2016, most notably in Sacramento and Fresno County, which saw a 78 and 130% increase in visibility respectively. In recent years, it is common for the airport visibility to reach 5-7 km during an accident elsewhere in the county, suggesting that the valley fog is becoming patchier and the local airport less representative of conditions throughout *(Figure 10)*. Chapter 1 showed that diurnal trend in fog events changed over time, with dense fog evaporating sooner in the morning than in past decades (Gray et al., 2019), which would likely begin at the urban centers and dissipate outward. Underwood et al. 2008 studied the formation of urban clear islands in cities throughout the valley, finding that lower relative humidity due to urban surfaces resulted in earlier evaporation of fog. However, the dissipation pattern varied with each event, suggesting it would be challenging to determine a visibility correction factor based on distance from the airport.

Despite this, fog hours and fog-related accidents are highly correlated, and total annual fog hours in all counties are an excellent predictor of incidence of fog-related accidents. *Figure 11* shows annual fog hours plotted against the annual total for fog-related accidents (NDJM) for the primary counties (Sacramento, San Joaquin, Fresno, and Kern), as well as for the counties adjacent to high-reporting airports (Stanislaus and Tulare). Notably, correlating with annual fog hours rather than number of fog days or average duration of fog episodes captures more of the variance. When restricting comparison to the strictest definition of dense radiation fog (visibility < 400 m), annual fog hours explain 72-88% of the variance in fog-related accidents (*Figure 11a*). However, increasing the threshold to visibility < 650 m captures more of the variability, increasing to 71-91% (*Figure 11b*). *Figure 11c* tests the correlation with visibility < 1150 m, which only marginally improves the r-squared, suggesting that the 650 m threshold is ideal. The 250 m increase in the definition adjusts for the differences in fog density throughout the valley and aligns with the median visibility during fog-related accidents throughout the record (600 m). Stanislaus and Tulare County correlate well with fog observations from neighboring San Joaquin and Fresno County for all thresholds tested (*Figure 11*). The strength of the relationship between fog-related accidents and annual fog hours – even despite the distance accidents occur from the local airport – suggests that a majority of the improvement in fog-related accidents in recent years has been precipitated by decreasing rates of fog.

3.2.3. Trend in rate of fog-related accidents per fog hour

In order to quantify alternative sources of improvement, such as safer roadway conditions, warning systems, and improved vehicle technology, the annual fog-related accidents were normalized by annual fog hours to investigate a change in the frequency of accidents during fog events. Fresno and Kern County, with their much larger footprints, have an average of 1.7 and 1.5 accidents per fog hour, compared with San Joaquin and Sacramento with 0.8 and 1.0 accidents per hour (*Table 9*).

Some of this difference may be accounted for by differences in area, which is better represented by vehicle-kilometers traveled per county. When scaled by average vehicle-kilometers traveled, Sacramento County has the lowest number of fog-related accidents per kilometer during each fog hour. Comparatively, during a fog hour, San Joaquin County has 1.4 times the accidents per kilometer as seen in Sacramento, followed by Kern with 1.8 and Fresno with 1.9. However, since there remains uncertainty about how area affects the rate of dissipation and total annual fog hours in the larger southern counties, conclusions cannot be made about whether these spatial differences in the southern counties are attributed to less safe roadway conditions.

Figure 12 shows the trend in the rate of fog-related accidents per fog hour per county. From 1996-2016, Sacramento and San Joaquin County demonstrate a statistically significant 46 and 49% decrease, respectively, in the rate of accidents per fog hour, suggesting that improvements to traffic safety may have an important impact (*Table 4*). It is most notable that this decline occurred in Sacramento County despite a 15% increase in roadway volume since 2002. No trend was found in Fresno and Kern County, where the rate throughout the study showed much more variability. Particularly in Kern, peaks in the trend seem most influenced by years where fog hours were proportionally much lower than the number of accidents, thus causing the ratio to spike (*Table 9*).

The 49% decline in rate of fog-related accidents per fog hour in San Joaquin County may be indicative of the Caltrans Automated Warning System (CAWS) implemented in District 10 beginning in 1996, in which 36 traffic monitoring sites, 9 meteorological stations, and 9 alert signs were first implemented in high traffic areas, creating one of the most advanced warning systems of its kind in the world (MacCarley, 1999). However, Sacramento County had the lowest rate of accidents when scaled for both drivers and fog events.

3.3. Trend in accident severity

Caltrans subdivides accident severity into five categories: property-only damage, minor injuries, visible injuries, severe injuries, and fatal. By percentages, the severity of accidents in the four counties is similar, despite differences in average visibility during fog-related accidents (*Table 10*). Median visibility calculated for the five categories of fog-related accidents demonstrates that accident severity is largely decoupled from density of fog. In all counties except Bakersfield, the median for property-only damage, as well as minor, visible, and severe injuries is nearly identical, fluctuating by less than 200 m. *Figure 13* shows the cumulative distribution for all four counties with a box whisker plot for the visibility during each accident category. The infrequency of fatal collisions skews the descriptive statistics for visibility, making it anomalously high at all locations

relative to the other four categories (*Figure 13*). Median visibility for Bakersfield investigated for the five categories is ~1- 2 km higher than the other sites.

Unsurprisingly, due to the declining rate of fog hours and fog-related accidents, there is a 61% decline in property damage collisions and 83 and 70% decline in visible and severe injury accidents from 1996-2016 when totaled for the four counties (*Figure 14*). *Figure 15* shows the trend in fog-related accident severity for the four primary counties. Fresno County, where annual injuries were double that of other counties studied, exhibited the most consistent decline in all severity categories (- 64 – 84%), except fatalities (*Table 11*). Declines in accident severity are reflected in trends of annual injuries (*Figure 16*), which was statistically significant in all counties with an average 72% decline valley-wide (*Table 4*). Notably, the frequency of fatal collisions throughout the study remains consistent despite such high declining rates in fog-related accidents, similar to the results of Ashley et al., 2015. However, the smaller sample size of fatal accidents limits the statistical robustness of this trend and should be evaluated over time with more data.

Changes in severity were analyzed relative to the number of accidents per year to investigate whether fog-related accidents are becoming less dangerous. Normalizing by the number of fog-related accidents per year showed trends in visible injuries from accidents declined in Sacramento (32%), Fresno (57%), and Bakersfield (62%) since the winter of 1996-1997 while trends in less severe accidents increased. Fresno County saw a 25% increase in property damage only accidents and Sacramento and Kern County saw a 43 and 60% increase in minor injury accidents, relative to the annual total. These three collision categories make up ~ 95% of all fog-related accidents, and thus reflect of a transition to less dangerous accidents. There is no trend for the severe and fatal categories (which account for only ~ 3 and ~ 2% of accidents, respectively), which may be the result of cumulative, less predictable factors in driver performance and road conditions.

Approximately 56% of accidents involve two collisions, whereas 35% involve one collision and 7% involve three collisions (*Table 12*). Multicar events with 7-10 collisions occur nearly every winter (*Table 12*), with collision number being as high as 108 over the 20-year study. Past assessments also identified Central Valley fog-related accidents as involving more vehicles than standard accidents (MacCarley, 1999), likely owing to low visibility conditions limiting driver's perception of distance between vehicles and distance needed for abrupt stopping (Carvallo et al, 2001; Buchner et al., 2006; Brooks et al., 2011). Notably, there is no distinguishable trend since 1996 in the number of collisions per accident, when normalized by the number of accidents in a year (*Table 12*). The lack of trend in fatalities and number of collisions per accident, relative to the number of accidents per year, suggests there remain important areas for improvement in roadway and vehicle safety.

4. Conclusion

Central Valley fog-related accidents have detrimental impacts on human safety, commerce, and productivity. Accident prevention measures began as early as 1973 with Operation Fogbound (MacCarley, 1999), but no long-term evaluation of the decline in accidents has been conducted. The annual frequency of these accidents has seen a pronounced 65% decline over the 20 winters between 1996-2016, the variance of which is best explained by the sharply declining trend in seasonal fog hours. In the six counties analyzed, the variance in fog hours, as measured by visibility

< 650 m at local airports, explained over 80% of the annual total in fog-related accidents per county. The decline in fog-related accidents occurred despite a 6-15% increase in vehicle-kilometers driven from 2002-2016 in the four counties. The subsequent improvement in visibility resulted in annual fog-related injuries falling by 72%, with the valley seeing an average of 550 fewer injuries from fog accidents in 2015-2016 than in 1996-1997.

The rate of fog-related accidents per fog episode is also decreasing for at least two of the counties: Sacramento and San Joaquin. The large areas of Fresno and Kern County make it more difficult to determine. Sacramento County has the lowest rate of fog-related accidents when both kilometers-traveled and frequency of fog hours are accounted for. There is evidence that fog-related accidents grew less severe over the course of the 20-year record in Sacramento, Fresno, and Kern County. Relative to the annual number of fog-related accidents, trends in less serious accidents are increasing at the expense of more dangerous collisions, which are decreasing. This indicates that when accidents are occurring, over time, they are less severe, suggesting that improvements to vehicle safety, roadway notifications, and traffic diversion may be making notable impacts. Yet, incidents with at least 7-10 collisions continue to occur nearly every year, leaving room for continued improvement in weather advisories.

The variability in fog is a strong determinant in the total annual number of accidents; therefore, understanding drivers of fog frequency has critical implications for the safety and economic well-being of valley residents. The strong link between the historical number of Central Valley fog events and trends in pollution concentration shows that regulatory measures that led to decreases in aerosol concentration, and thereby wintertime fog frequency, also led to significant reductions in resulting fog-related accidents. The significant reduction in accidents and injuries attributable to reductions in fog should be accounted for when considering the economic and societal benefits of air pollution mitigation.

5. Figures and tables

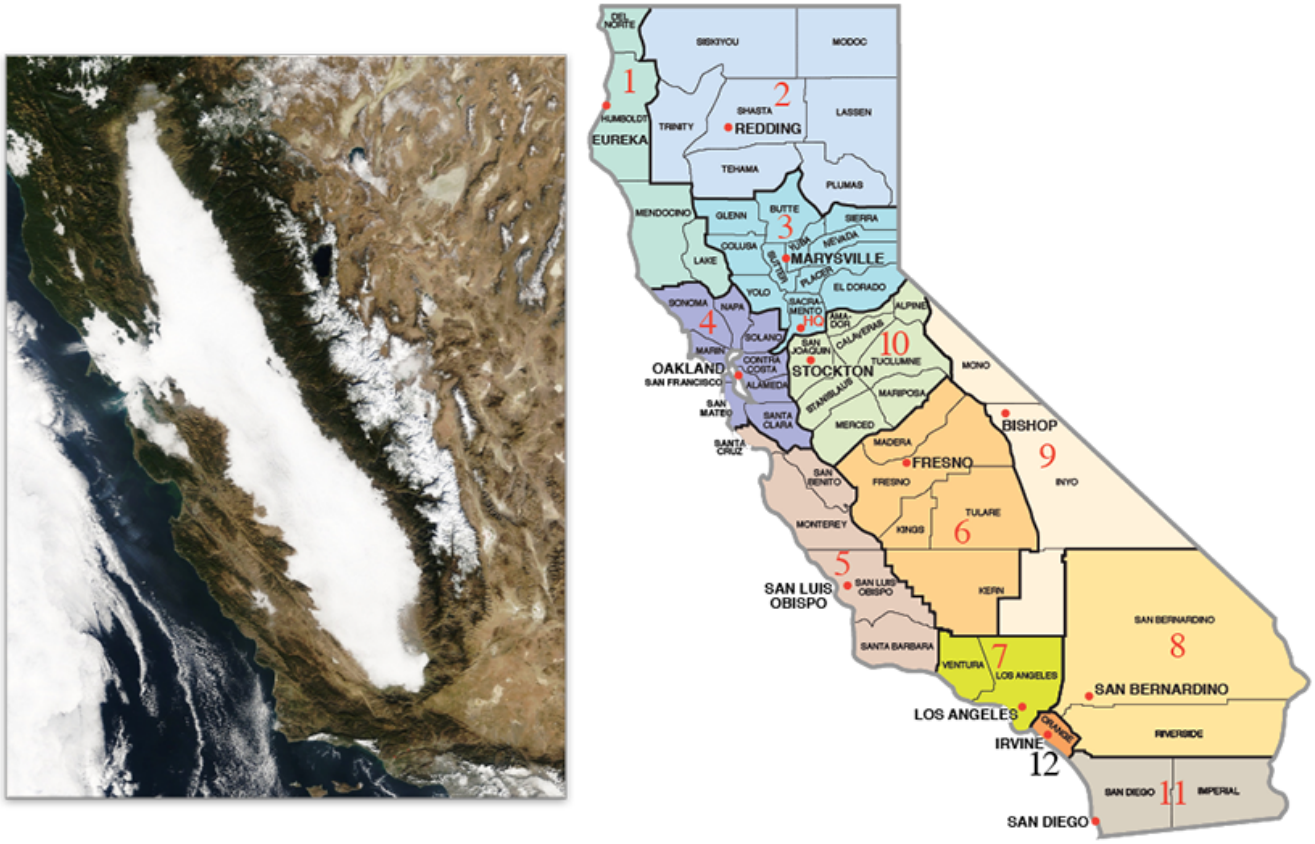

Figure 1. Terra MODIS retrieval of radiation fog event in Central Valley (left); District (numbers) and county boundaries from California Department of Transportation (right). Study focuses on counties in districts 3, 10, and 6.

Table 1. Central Valley fog-related accidents by county, 1996-2016
Data: California Highway Patrol Accident Investigation Unit Statewide Integrated Traffic Records System.

	Total Fog-Related Accidents	Percent of Central Valley (%)	Elevation (meters)	Area (km^2)	Population[a] (10^3)
District 3 (North)					
Butte	284	1.4	**398**	4,248	229
Colusa	92	.5	25	2,990	22
El Dorado	110	.6	**638**	4,434	189
Glenn	78	.4	51	3,406	28
Nevada	84	.4	**883**	2,481	100
Placer	383	1.9	**806**	3,644	386
Sacramento	2133	11	17	2,502	1,531
Sierra	7	0	**1509**	2,468	3
Sutter	284	1.4	15	1,562	97
Yolo	481	2.4	21	2,621	219
Yuba	153	.8	106	1,632	77
Total	4089	21		31,988	2,881
District 10 (Central)					
Alpine	2	0	**1852**	1,914	1
Amador	55	0.3	**379**	1,570	39
Calaveras	78	0.4	**655**	2,642	46
Mariposa	21	0.1	**735**	3,758	18
Merced	1395	7.0	46	4,996	273
San Joaquin	2396	12	16	3,623	745
Stanislaus	1924	9.7	30	3,872	548
Total	5915	29		22,375	1,670
District 6 (South)					
Fresno	3367	17	95	15,444	989
Kern	1859	9.4	137	21,088	893
Kings	1222	6.2	76	3,600	150
Madera	800	4.0	283	5,537	157
Tulare	2598	13	125	12,494	465
Total	9846	50		58,163	2,654

[a]2017 population estimate

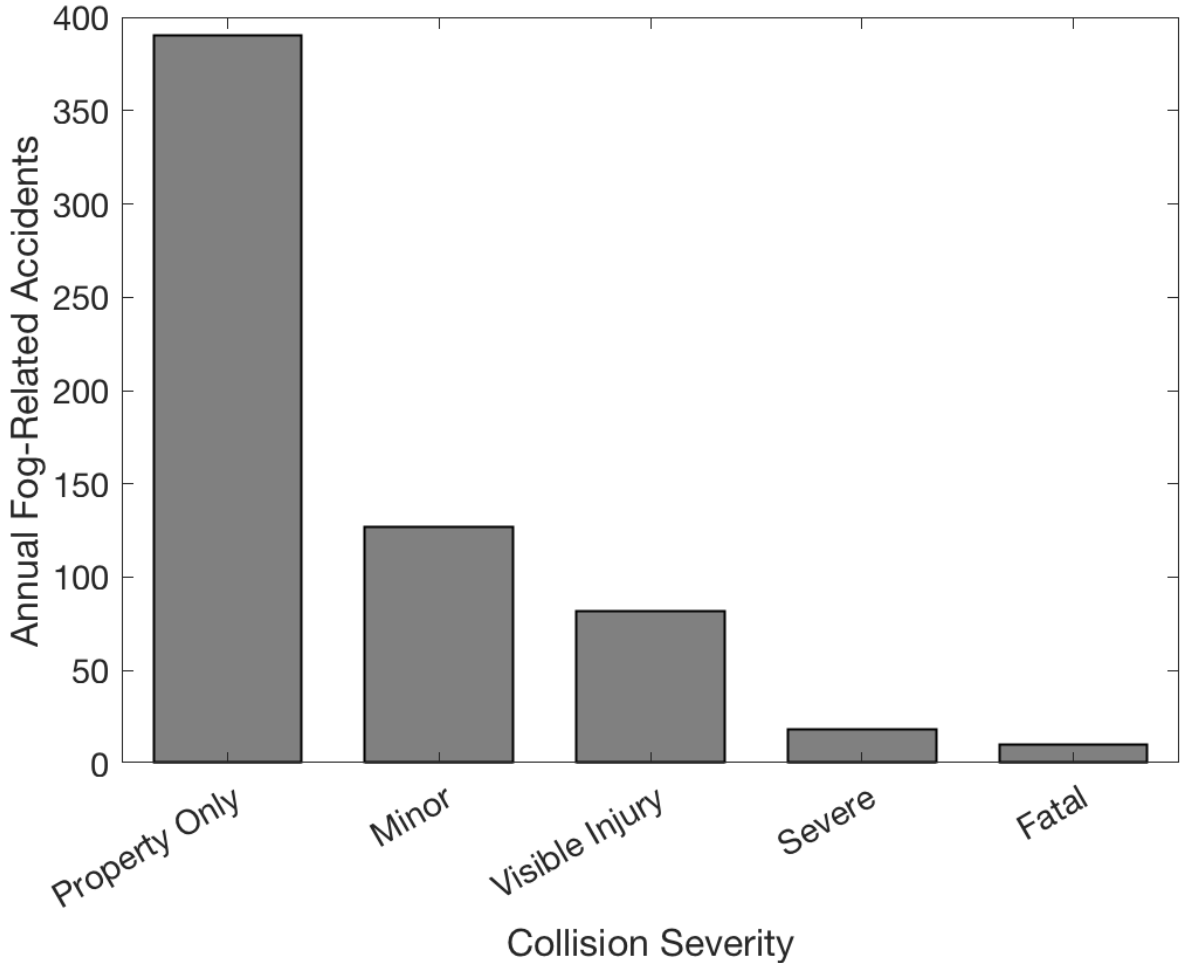

Figure 2. Bar plot of annually-averaged totals for wintertime, Nov-Mar (NDJFM), fog-related accident severity, as classified in police accident report. Data from California Highway Patrol Accident Investigation Unit Statewide Integrated Traffic Records System. Fog seasons of 2001-02 to 2005-06 not included due to erroneous reporting in data set.

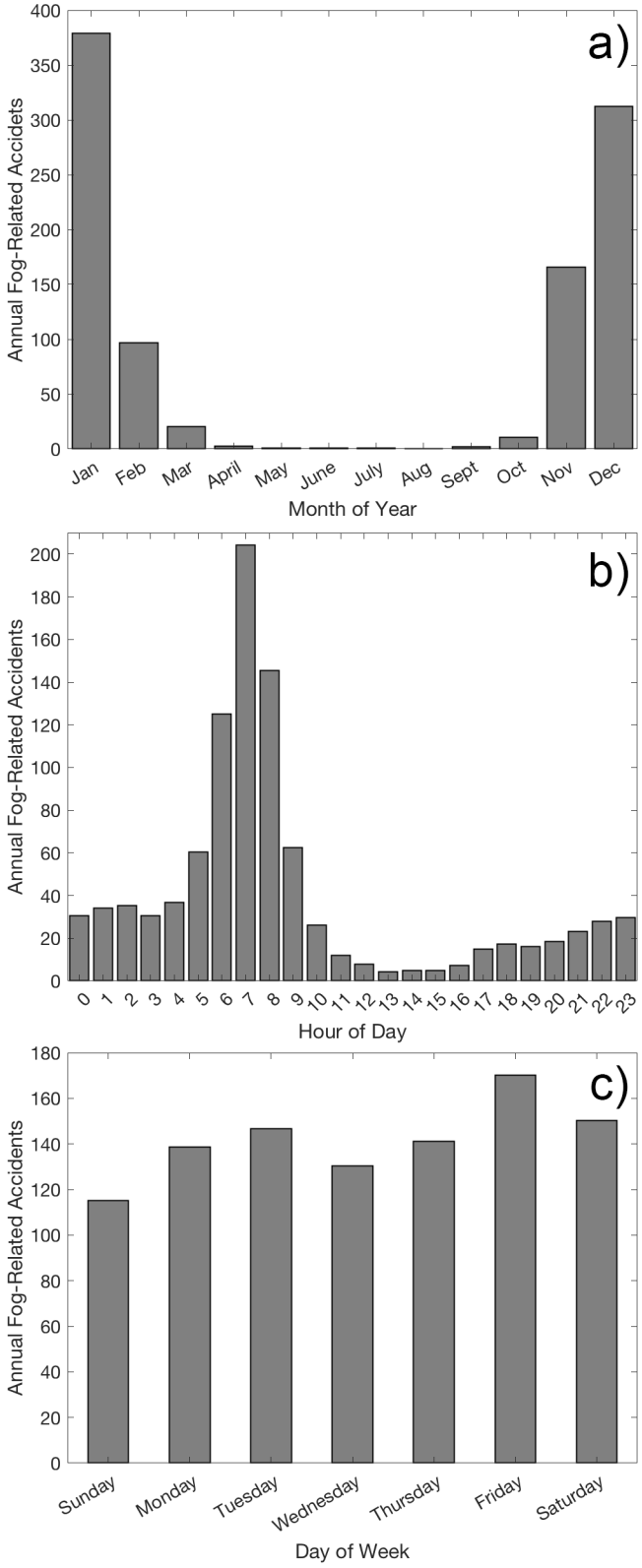

Figure 3. Panel of average fog-related accidents (1996-2016) by a) month of year, b) hour of day, and c) day of week for districts 3, 10, and 6 during Central Valley radiation fog season (NDJFM).

Table 2. Districts 3, 10, and 6 fog-related accidents per month, 1996-2016

Month	Fog-Related Accidents	%
January	7,582	38.2%
February	1,936	9.8%
March	413	2.1%
April	56	0.3%
May	21	0.1%
June	14	0.1%
July	12	0.1%
August	8	0.0%
September	41	0.2%
October	207	1.0%
November	3,318	16.7%
December	6,242	31.4%
Total	19,850	

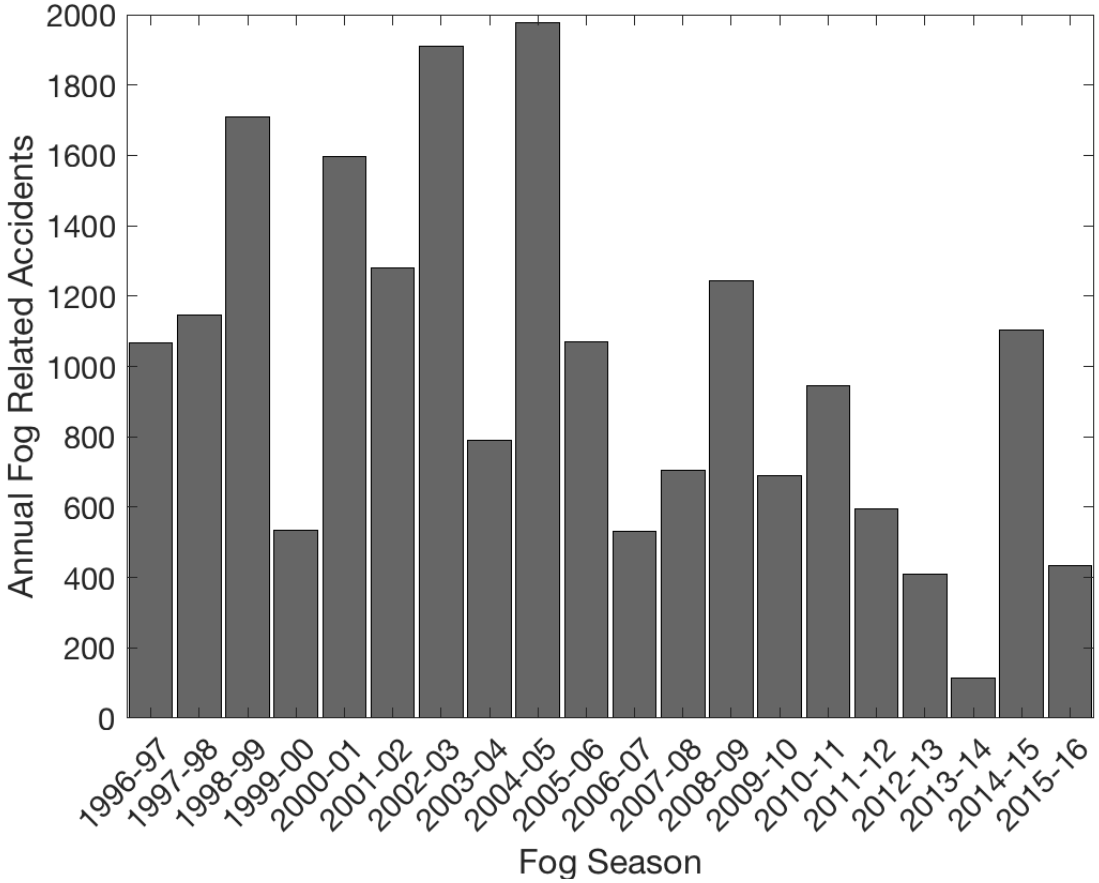

Figure 4. Sum of wintertime (NDJFM) fog-related accidents by year in districts 3, 10, and 6 from 1996-2016.

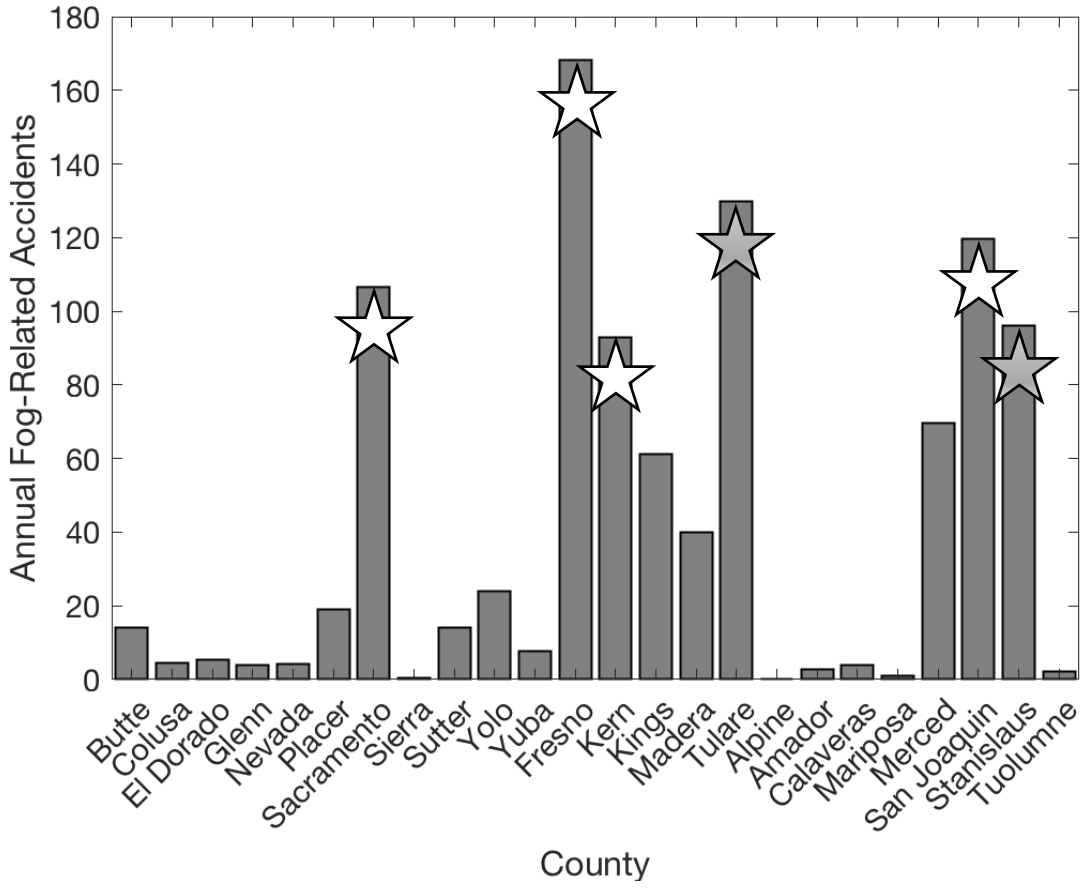

Figure 5. Annual average wintertime (NDJFM) fog-related accidents by county located in districts 3, 10, and 6 from 1996-2016. Counties with stars are focus of study: white stars indicate sites with corresponding visibility data from airport within boundaries; grey stars indicate sites included in some analysis, but lacking complete visibility records.

Table 3. Description of counties in primary study region

District Number	County	County Number	Local Airport	Lat (°)	Lon (°)	Population[a]	Size (km^2)	Population Density (pp/km^2)	VKT [b] Fog Season^{-1} (10^6)
3	Sacramento	34	Sacramento	38.51	-121.5	1,531,000	2,502	612	7,960
10	San Joaquin	39	Stockton	37.90	-121.3	752,000	3,623	206	4,318
6	Fresno	10	Fresno	36.78	-119.7	994,000	15,444	64	5,441
6	Kern	15	Bakersfield	35.43	-119.1	897,000	21,088	42	5,445

a – *2018 estimate*
b – *1996-2016 average for Jan, Feb, Mar, Nov, Dec*

Table 4. Fog season (NDJFM) trends in fog-related accidents, accidents per hour, and injuries, 1996-2016

County / Airport	Fog Accidents (%)	Accidents Fog Hour $^{-1}$ (%)[a]	Injuries (%)
Sacramento / Sacramento	-65	-46	-55
San Joaquin / Stockton	-68	-49	-60
Fresno / Fresno	-71	-	-78
Kern / Bakersfield	-72	-	-79
Total	-65[b]	-	-72[b]

only significant trends ($p < 0.05$) reported
[a]*fog hour defined as visibility < 650 m*
[b]*totals reported for district 3, 10, 6*

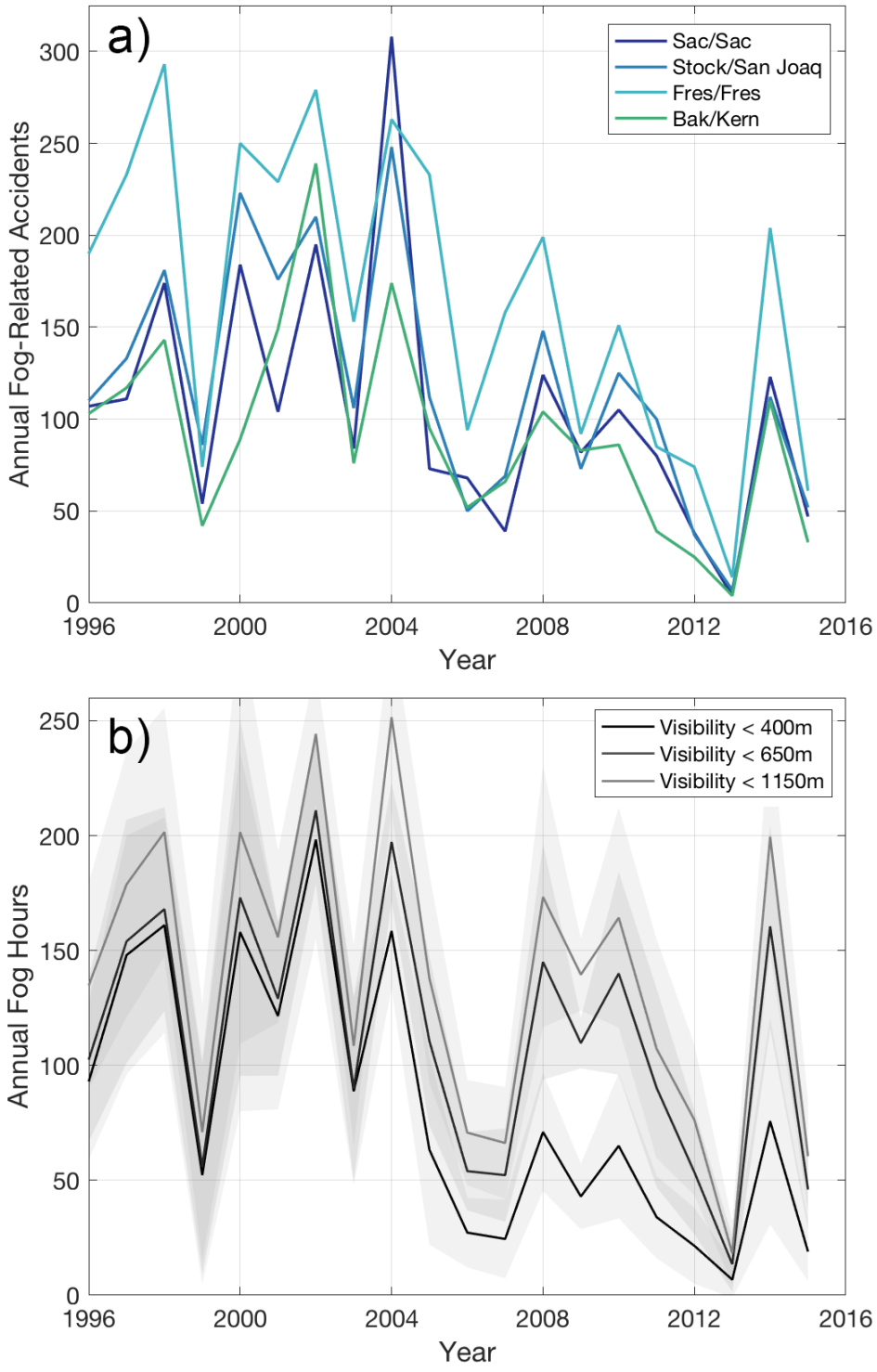

Figure 6. *Temporal trends in a) Annual fog-related accidents in four counties – Sacramento (navy), San Joaquin (blue), Fresno (teal), and Kern (green) – summed for each winter season beginning in 1996-7 and ending in 2015-6. b) Corresponding annual sums of fog hours, averaged from airports within each county. Fog hour defined in three visibility categories as any hour where visibility falls below 400, 650, or 1150 meters, respectively, at airport.*

Table 5. Description and trends of vehicle-kilometers traveled per fog season, averaged annually, Jan-Dec (JFMND), 2002-2016

County	2002 Fog Season Vehicle-Kilometers (10^9)	2016 Fog Season Vehicle-Kilometers (10^9)	Trend in Vehicle-Miles Fog Season^{-1} (%)	Average Vehicle-Kilometers Fog Season^{-1} (10^9)
Sacramento	7.2	8.7	15	7.9
Stockton	4.3	4.5	-	4.3
Fresno	5.2	5.9	7.5	5.4
Bakersfield	5.4	6.3	5.7	5.4
Total	22	25	7.9	23

only significant trends ($p < 0.05$) reported

[a]*totals reported for Sacramento, San Joaquin, Fresno, and Kern County only*

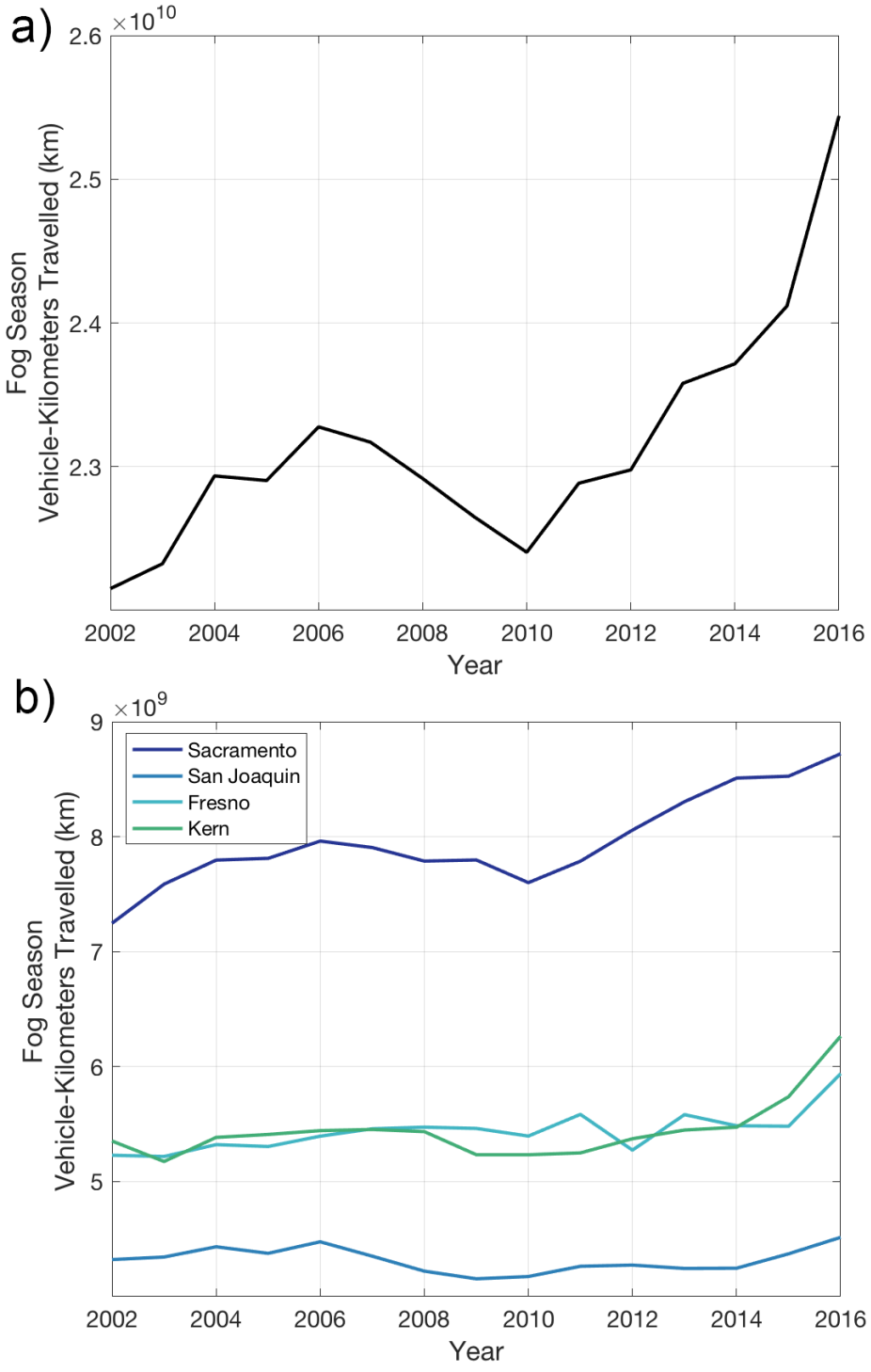

Figure 7. a) Temporal trend (2002-2016) in total vehicle-kilometers traveled in four counties – Sacramento (navy), San Joaquin (blue), Fresno (teal), and Kern (green) – during fog season months (JFMND). b) Annual Fog season vehicle-kilometers traveled by county.

Table 6. Fog season trends (JFMND) in fog-related accidents, vehicle-kilometers, and rate of accident/kilometer, 2002-2015

County	Fog Accidents (%)	Vehicle-Kilometers Season^{-1} (%)	Accidents Vehicle-Kilometers^{-1} Season^{-1} (%)
Sacramento	-63	12	-73
San Joaquin	-79	-	-79
Fresno	-82	5.4	-84
Kern	-87	2.4	-87
Total	-78[a]	5.4[a]	-80[a]

only significant trends ($p < 0.05$) reported

[a]*totals reported for Sacramento, San Joaquin, Fresno, and Kern County only*

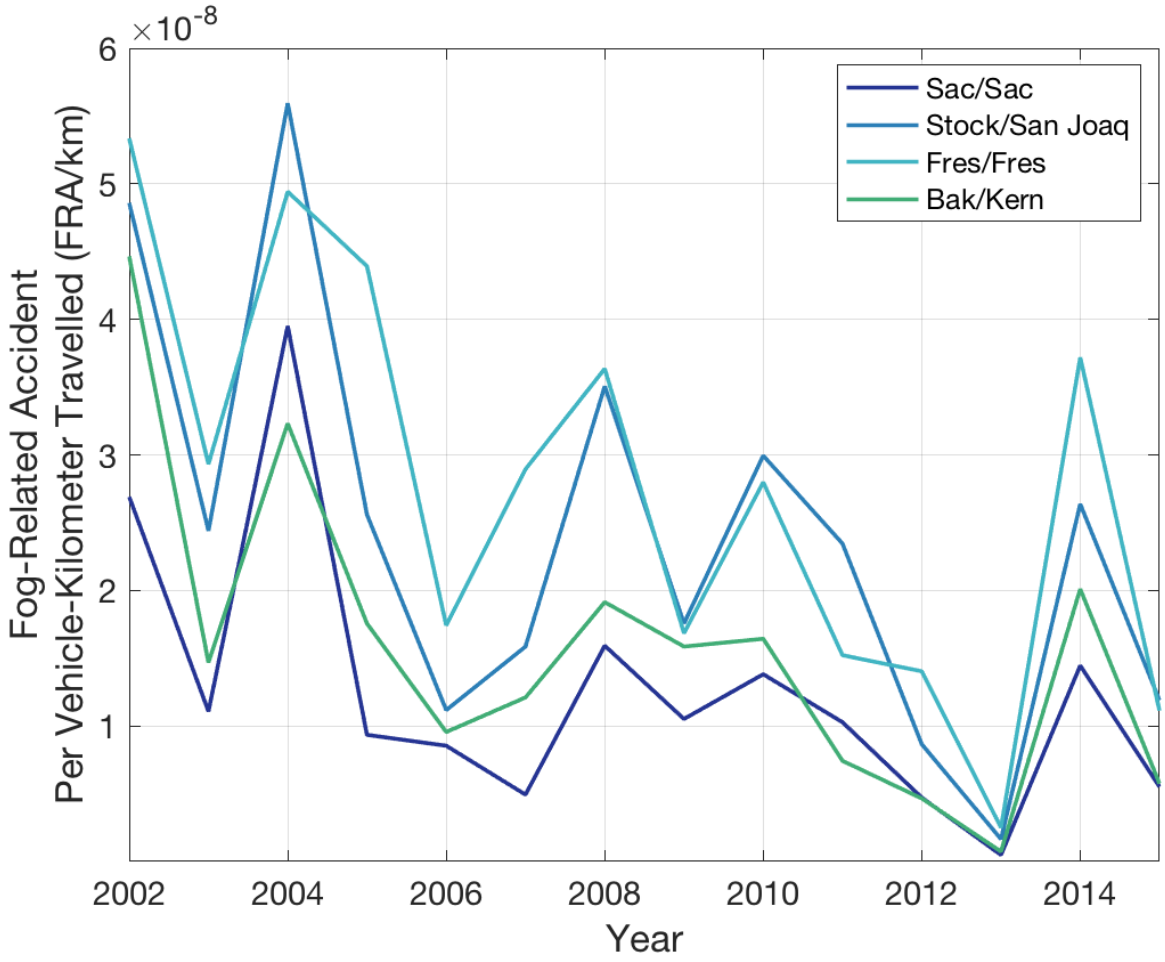

Figure 8. Temporal trend (2002-2015) in fog-related accidents per kilometer of vehicle travel for Sacramento (navy), San Joaquin (blue), Fresno (teal), and Kern (green) County. Calculated by dividing the number of accidents (totaled by calendar year rather than fog season) by the total vehicle-kilometer traveled for those months.

Table 7. Percentage of fog-related accident occurring when visibility below thresholds, 1996-2016

County / Airport	Visibility ≤ 400 m (%)	Visibility ≤ 650 m (%)	Visibility ≤ 1150 m (%)
Sacramento / Sacramento	38	55	62
San Joaquin / Stockton	47	59	65
Fresno / Fresno	44	48	54
Kern / Bakersfield	29	39	44

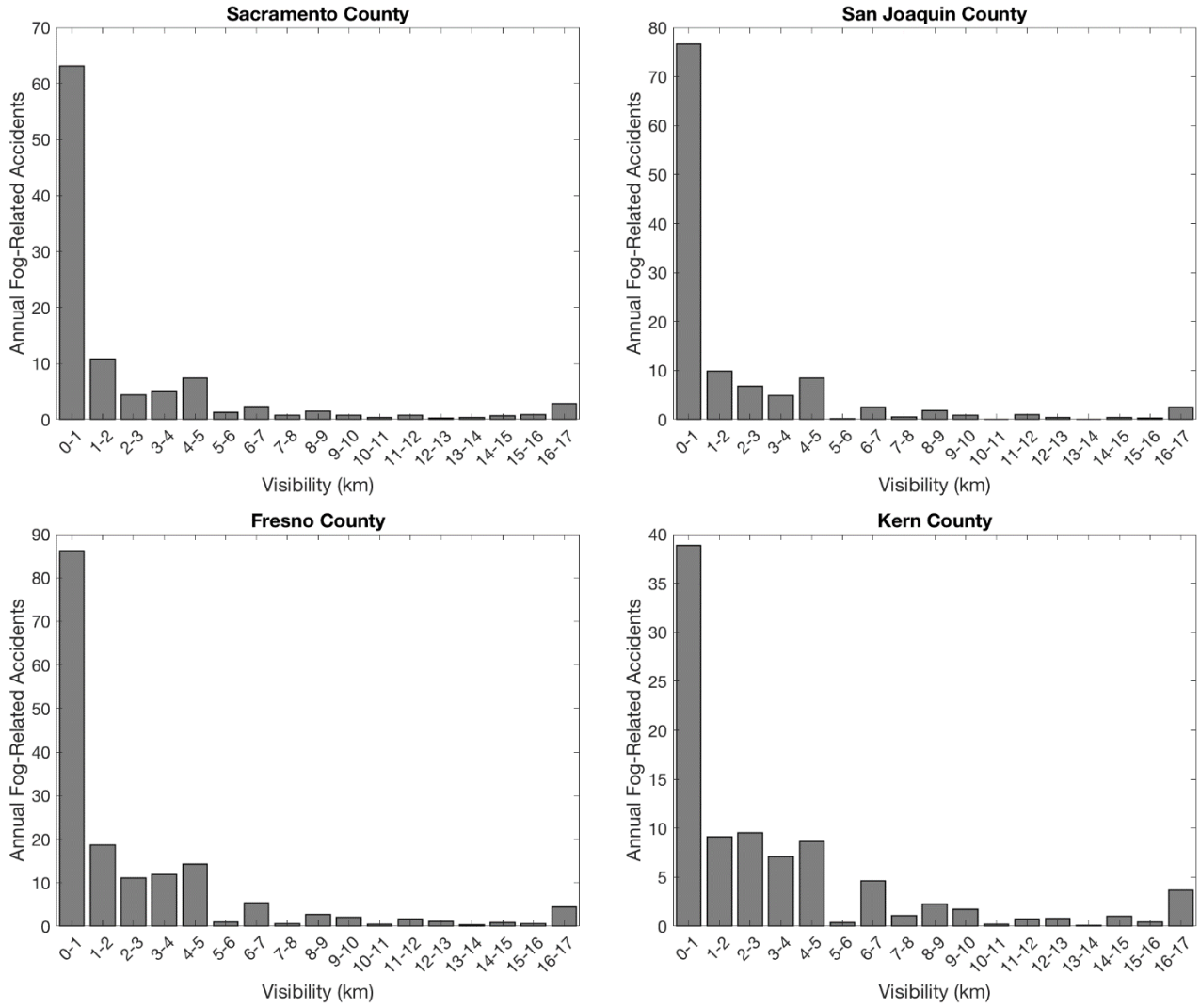

Figure 9. Annual average frequency of a fog-related accident occurring during each visibility range over the 20-year study by county. NCDC data for Sacramento Executive Airport, Stockton Metropolitan Airport, Fresno Yosemite International Airport, and Bakersfield Municipal Airport were used to determine visibility.

Table 8. Total fog-related accidents by visibility at adjacent airport, 1996-2016

	Sacramento / Sacramento		San Joaquin / Stockton		Fresno / Fresno		Kern / Bakersfield	
Visibility (km)	Accidents	%	Accidents	%	Accidents	%	Accidents	%
0-1	1262	61	1533	65	1723	53	777	43
1-2	216	10	198	8.4	374	11	183	10
2-3	87	4.2	137	5.8	222	6.8	191	11
3-4	103	5.0	99	4.2	238	7.3	142	7.8
4-5	148	7.1	170	7.2	286	8.8	173	10
5-6	26	1.3	4	0.2	19	0.6	8	0.4
6-7	47	2.3	51	2.2	109	3.3	93	5.1
7-8	16	0.8	11	0.5	13	0.4	22	1.2
8-9	31	1.5	36	1.5	54	1.7	46	2.5
9-10	16	0.8	18	0.8	40	1.2	35	1.9
10-11	8	0.4	0	0.0	9	0.3	4	0.2
11-12	15	0.7	19	0.8	33	1.0	15	0.8
12-13	6	0.3	9	0.4	23	0.7	16	0.9
13-14	8	0.4	0	0.0	7	0.2	2	0.1
14-15	14	0.7	8	0.3	16	0.5	21	1.2
15-16	18	0.9	6	0.3	11	0.3	9	0.5
16-17	57	2.7	51	2.2	89	2.7	74	4.1

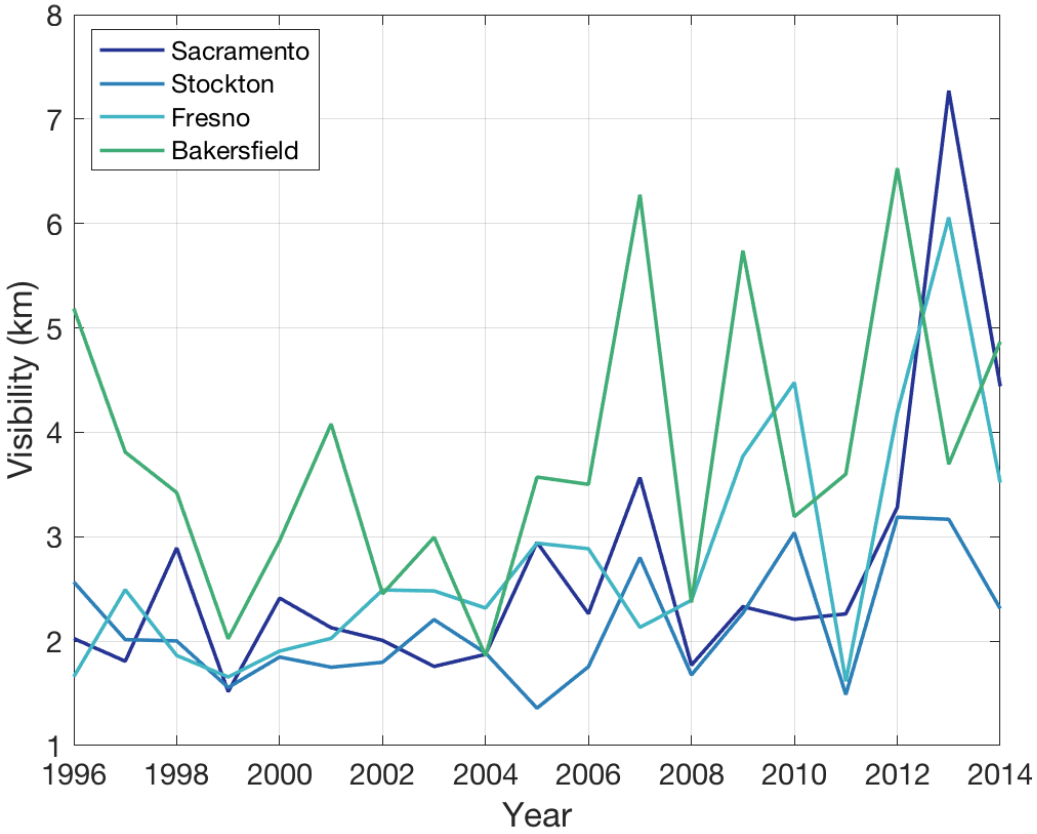

Figure 10. Temporal trends in average fog season (NDJFM) visibility during hour of fog-related accidents at adjacent airports. NCDC data for Sacramento Executive Airport (navy), Stockton Metropolitan Airport (blue), Fresno Yosemite International Airport (teal), and Bakersfield Municipal Airport (green) were used to determine visibility.

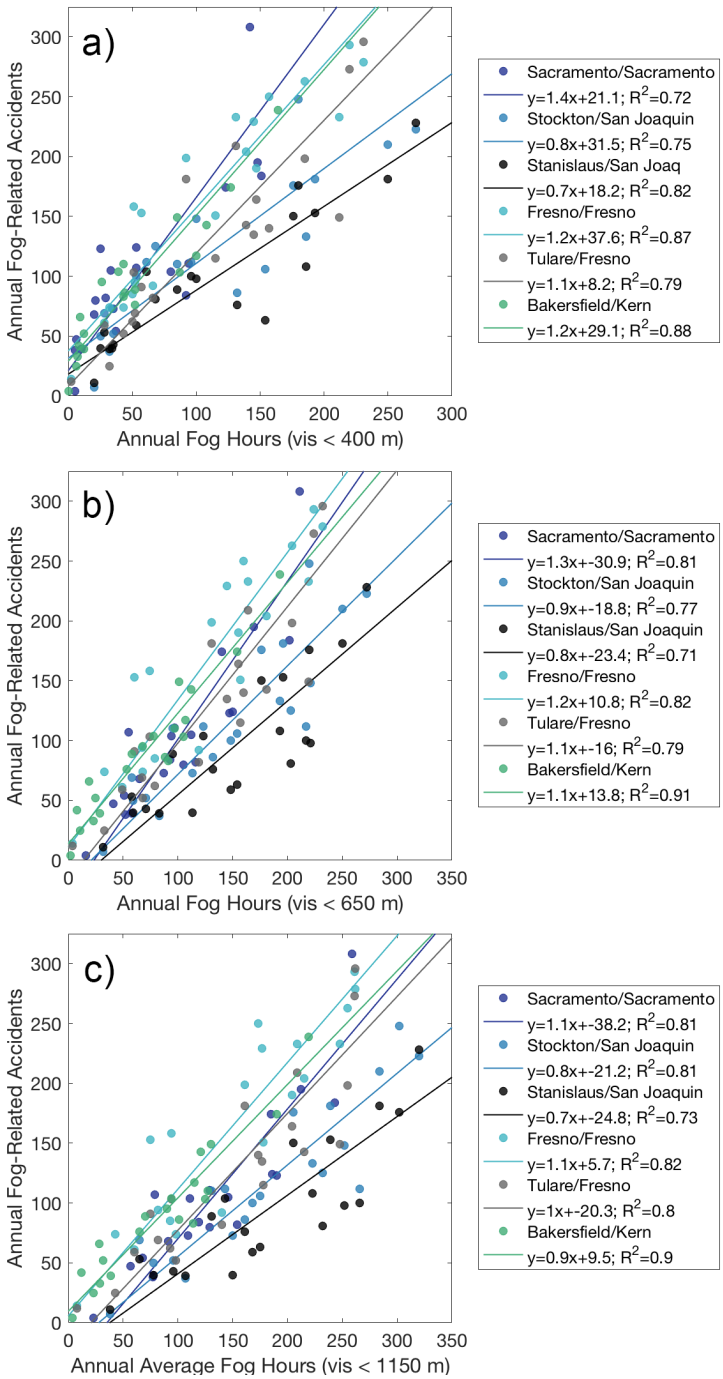

Figure 11. Correlation between annual (NDJFM) fog-related accidents per county and total fog hours at nearby airports. Sacramento Executive Airport (navy), Stockton Metropolitan Airport (cobalt), Fresno Yosemite International Airport (teal), and Bakersfield Municipal Airport (green) were used to determine the number of fog hours in Sacramento, San Joaquin, Fresno, and Kern Counties, respectively. Nearby counties of Tulare (grey) and Stanislaus (black) were correlated with adjoining county airports (Stockton and Fresno, respectively). Three visibility distances were investigated to identify fog: a) 400 m, b) 650 m, and c) 1150 m.

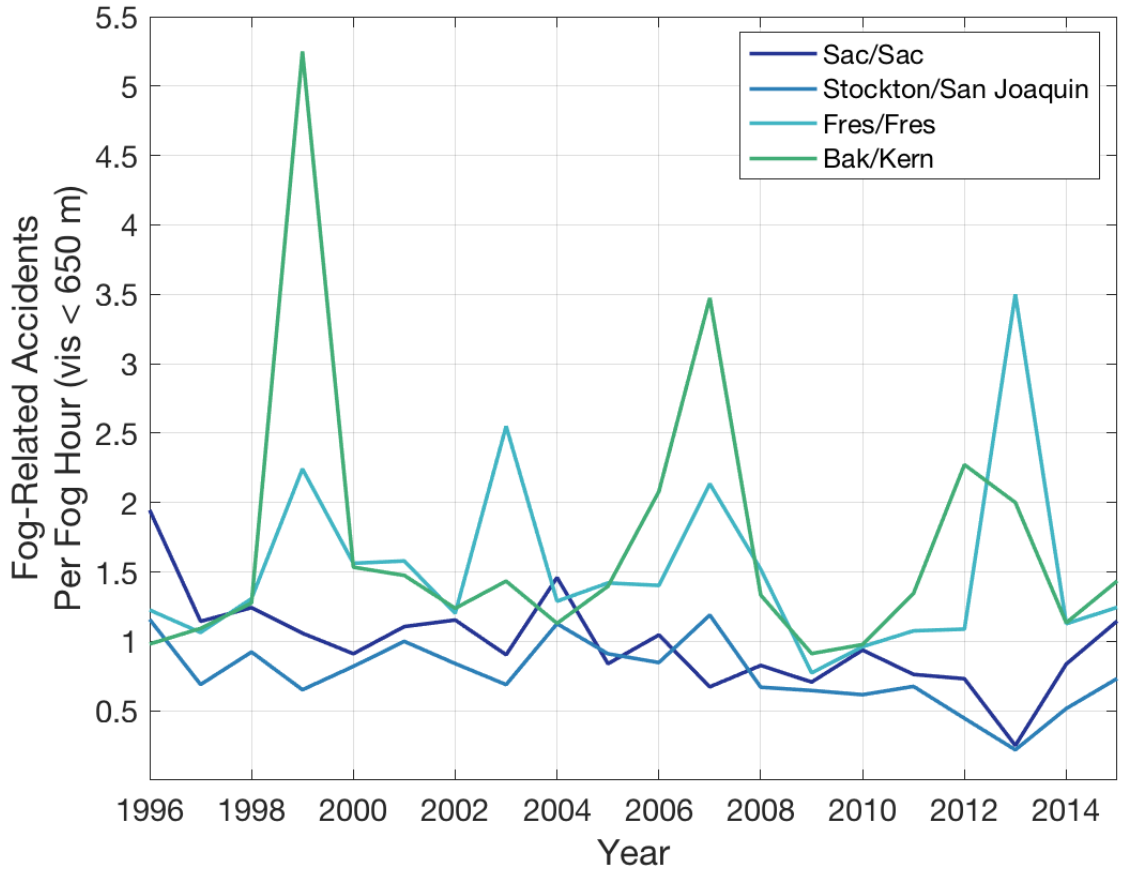

Figure 12. Wintertime temporal trend (1996-2016) in visibility at adjacent airports in four counties investigated. Each point found by averaging the visibility during a fog-related accident. NCDC data for Sacramento Executive Airport (navy), Stockton Metropolitan Airport (blue), Fresno Yosemite International Airport (teal), and Bakersfield Municipal Airport (green) were used to determine visibility.

Table 9. Total fog-related accidents, fog hours (visibility ≤ 650 m), rate of accidents per fog hour per fog season (NDJFM), 1996-2016

	Sacramento			Stockton			Fresno			Bakersfield		
Year	Accidents	Fog Hours	Rate	Accidents	Fog Hours	Rate	Accidents	Fog Hours	Rate	Accidents	Fog Hours	Rate
1996-97	107	55	1.95	110	95	1.16	190	155	1.23	103	105	0.98
1997-98	111	97	1.14	133	193	0.69	233	219	1.06	117	107	1.09
1998-99	174	140	1.24	181	196	0.92	293	224	1.31	143	112	1.28
1999-00	54	51	1.06	86	132	0.65	74	33	2.24	42	8	5.25
2000-01	184	202	0.91	223	272	0.82	250	160	1.56	89	58	1.53
2001-02	104	94	1.11	176	176	1.00	229	145	1.58	149	101	1.48
2002-03	195	169	1.15	210	250	0.84	279	232	1.20	239	193	1.24
2003-04	84	93	0.90	106	154	0.69	153	60	2.55	76	53	1.43
2004-05	308	211	1.46	248	220	1.13	263	204	1.29	174	154	1.13
2005-06	73	87	0.84	112	123	0.91	233	164	1.42	95	68	1.40
2006-07	68	65	1.05	50	59	0.85	94	67	1.40	52	25	2.08
2007-08	39	58	0.67	69	58	1.19	158	74	2.14	66	19	3.47
2008-09	124	150	0.83	148	221	0.67	199	131	1.52	104	78	1.33
2009-10	82	116	0.71	73	113	0.65	92	119	0.77	83	91	0.91
2010-11	105	112	0.94	125	203	0.62	151	157	0.96	86	88	0.98
2011-12	80	105	0.76	100	148	0.68	85	79	1.08	39	29	1.34
2012-13	38	52	0.73	37	83	0.45	74	68	1.09	25	11	2.27
2013-14	4	16	0.25	7	32	0.22	14	4	3.50	4	2	2.00
2014-15	123	147	0.84	112	217	0.52	204	181	1.13	110	97	1.13
2015-16	47	41	1.15	52	71	0.73	61	49	1.24	33	23	1.43
sum	2104	2061	-	2358	3016	-	3329	2525	-	1829	1422	-
mean	105	103	1.0	118	151	0.8	166	126	1.5	91	71	1.7

Table 10. Percentage of fog-related accident categorized by five severity levels, 1996-2016[a]

County	Property Damage Only (%)	Minor Injury (%)	Visible Injury (%)	Severe Injury (%)	Fatal (%)
Sacramento	57.1	25.1	13.1	3.4	1.3
San Joaquin	63.5	20.4	11.4	2.5	2.3
Fresno	58.2	23.3	13.2	3.3	2.0
Kern	63.6	18.7	14.1	2.1	1.6
Total	62.1	20.2	13.1	2.9	1.7

[a]*fog seasons of 2001-02 to 2005-6 not included*

[b]*totals reported for district 3, 10, 6*

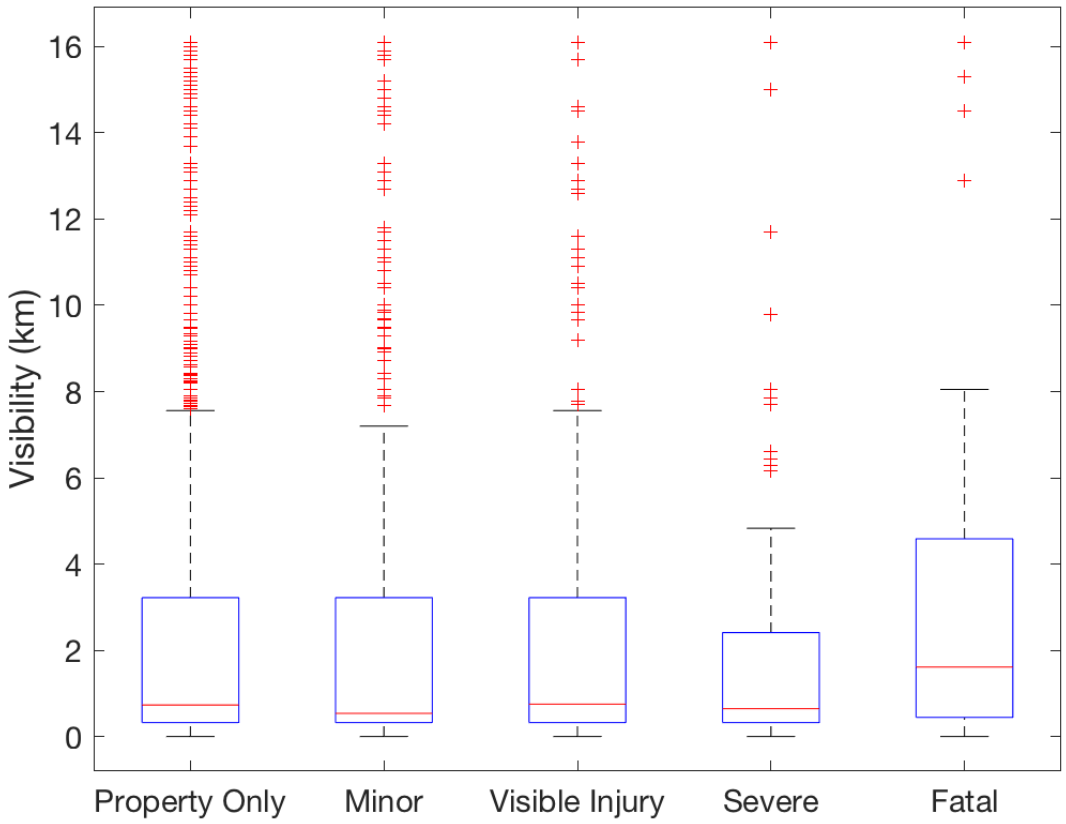

Figure 13. Hourly visibility during all fog-related accidents in Sacramento, San Joaquin, Fresno, and Kern County, distributed by the severity of the accident as defined by the police accident reports. Red line indicates the median. Bottom and top edges of box indicate the 25th and 75th percentiles. Black dotted line (whiskers) extend to the most extreme data points not considered outliers. Red + symbol indicates outliers if they are greater than $q_3 + w \times (q_3 - q_1)$ or less than $q_1 - w \times (q_3 - q_1)$, where w is the maximum whisker length, and q_1 and q_3 are the 25th and 75th percentiles of the sample data, respectively. NCDC data for Sacramento Executive Airport, Stockton Metropolitan Airport, Fresno Yosemite International Airport, and Bakersfield Municipal Airport were used to determine visibility.

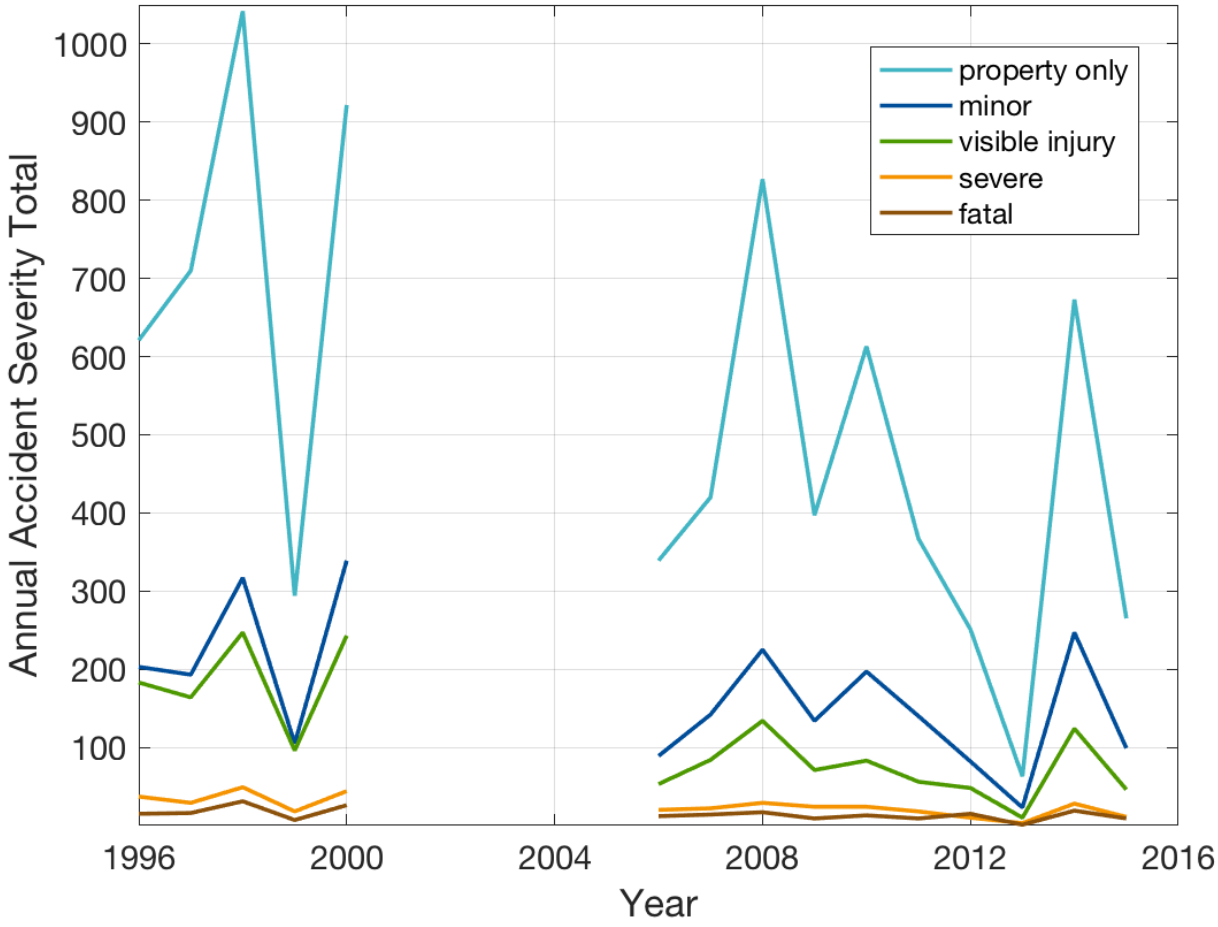

Figure 14. Temporal trends (1996-2016) in fog-related accident of different severities per fog season (NDJFM), as defined by police accident reports from the four primary counties: Sacramento, San Joaquin, Fresno, and Kern.

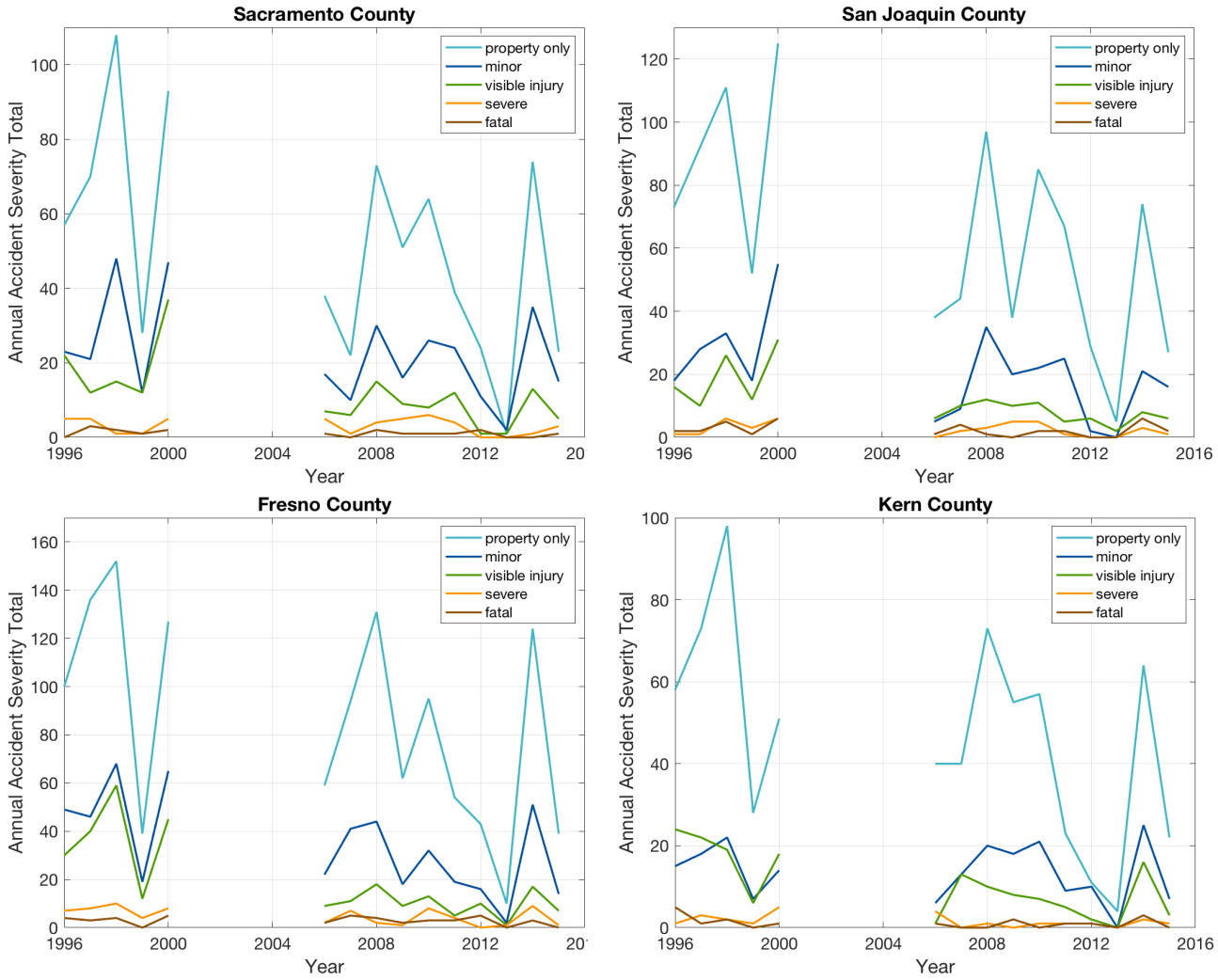

Figure 15. Temporal trend (1996-2016) in fog-related accident of different severities per fog season (NDJFM), as defined by police accident reports from the four primary counties: Sacramento, San Joaquin, Fresno, and Kern.

Table 11. Trends in county accident severity, 1996-2016

County	Sacramento (%)	San Joaquin (%)	Fresno (%)	Kern (%)	All Districts (%)
Property Only	-	-66	-64	-63	-61
Minor	-	-	-78	-	-
Visible Injury	-73	-65	-84	-93	-83
Severe	-	-	-78	-	-70
Fatal	-	-	-	-	-

only significant trends ($p < 0.05$) reported

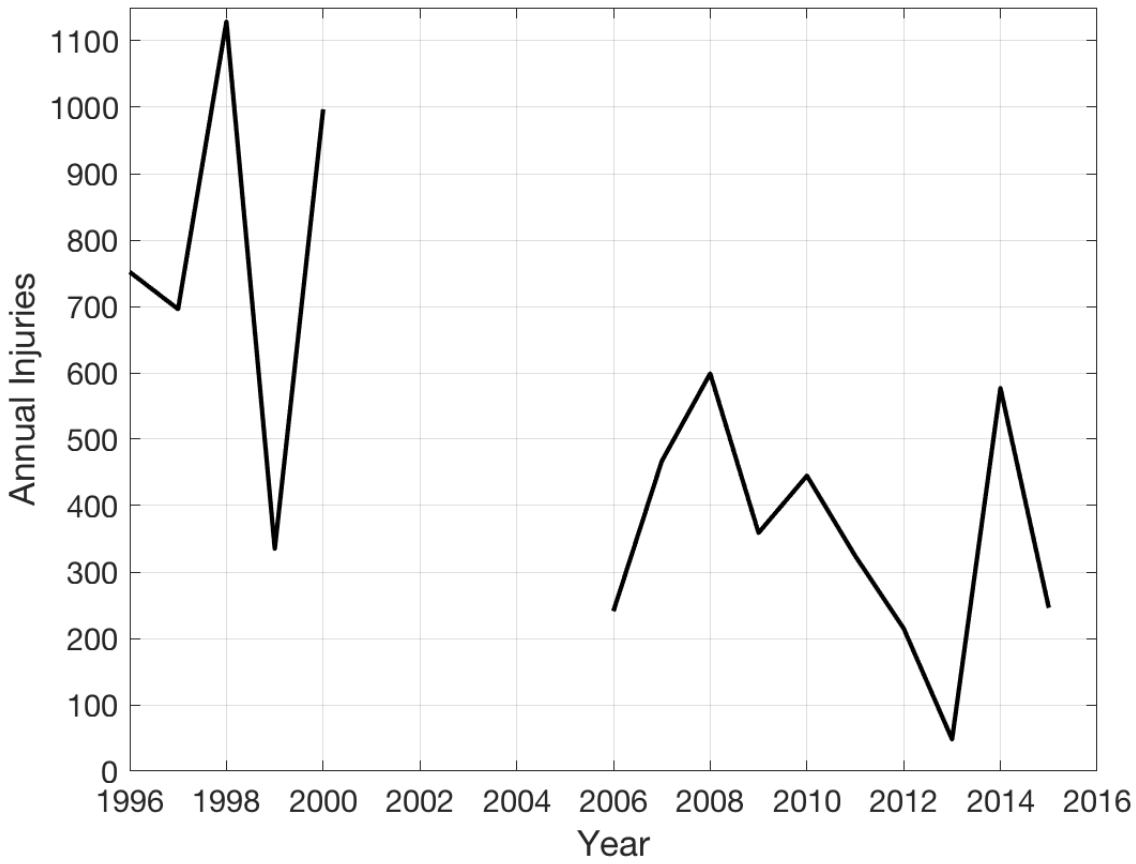

Figure 16. Temporal trend (1996-2016) in annual number of injuries from fog-related accidents, summed for the fog season of NDJFM, for the districts of 3, 10, 6. Fog seasons of 2001-2002 to 2005-2006 not included due to questionable reporting in police accident reports.

Table 12. Percent frequency of number of collisions per accident, 1996-2016

	1 collision (%)	2 collisions (%)	3 collisions (%)	4-6 collisions (%)	7-10 collisions (%)	11-15 collisions (%)	16-20 collisions (%)	21-30 collisions (%)	> 31 collisions (%)
1996	32.4	57.4	7.6	2.5	0.1	0.0	0.0	0.0	0.0
1997	35.3	56.1	6.6	1.5	0.4	0.2	0.0	0.0	0.0
1998	29.8	61.4	6.6	1.7	0.1	0.3	0.0	0.0	0.0
1999	30.2	59.2	8.1	2.3	0.2	0.0	0.0	0.0	0.0
2000	31.2	59.8	7.1	1.8	0.1	0.0	0.0	0.0	0.0
2001	-	-	-	-	-	-	-	-	-
2002	-	-	-	-	-	-	-	-	-
2003	-	-	-	-	-	-	-	-	-
2004	-	-	-	-	-	-	-	-	-
2005	-	-	-	-	-	-	-	-	-
2006	39.2	54.8	5.5	0.6	0.0	0.0	0.0	0.0	0.0
2007	31.1	59.5	6.7	2.3	0.0	0.1	0.0	0.0	0.1
2008	34.3	57.6	5.9	1.7	0.3	0.1	0.0	0.0	0.0
2009	38.1	55.1	5.4	1.1	0.2	0.2	0.0	0.0	0.0
2010	41.8	50.9	6.1	1.0	0.2	0.0	0.0	0.0	0.0
2011	35.8	56.4	6.4	1.2	0.2	0.0	0.0	0.0	0.0
2012	39.2	49.8	8.4	2.7	0.0	0.0	0.0	0.0	0.0
2013	40.0	48.0	7.0	4.0	1.0	0.0	0.0	0.0	0.0
2014	39.2	52.2	6.6	1.8	0.1	0.0	0.0	0.0	0.0
2015	32.8	57.7	8.1	1.4	0.0	0.0	0.0	0.0	0.0

Chapter 5

Conclusion

1. Summary

Fog frequency has been changing substantially in many places around the world over the past century. Understanding the drivers of changing fog trends has important health, safety, and ecological implications. In this dissertation, I presented a rigorous investigation of the drivers causing trends in Central Valley wintertime radiation fog frequency and duration. I compiled a 75-year fog climatology spanning 15 sites which includes data on visibility, fog frequency, fog duration, climate variables, and air pollution variables. Using linear regression to categorize trends and Fourier transformation to investigate the periodicity, I identified the drivers of short-term and long-term variability to elucidate the cause of increasing fog frequency from 1930-1970, followed by rapid decline after 1980. The spatial and temporal trends in NO_x concentration, as a proxy for ammonium nitrate aerosol, best explains the spatial and temporal trends in annual fog events, whereas meteorological variability correlate better with the interannual signals in the fog record. The novel conclusion that reductions in Central Valley fog frequency were mainly driven by legislated reductions in air pollution since the Clean Air Act of 1970 took effect was of tremendous scientific and public interest.

To further understand the climatic and pollution variables contributing to fog formation and their relative impact on daily timescales, I continued on a more detailed analysis of the Central Valley and contrasted the results with the Po Valley, which experienced a similar decline in fog frequency and air pollution since 1980. I found that a majority of the variance in low visibility, as an indicator of dense fog, is explained by low dew point depression, high NO_x concentration, low wind speed, and precipitation. While dew point depression is the strongest driver of daily variability, the large impact of NO_x concentration on the visibility response shows that rapid declines in both valleys (61-65%) has had a critical impact on the diminished fog season since 1980. This demonstrates an unexpected way that regulatory measures to mitigate pollution emissions had important impacts, not only on the health outcomes of those potentially exposed, but also through co-benefits in reducing fog frequency that was anthropogenically enhanced by air pollution.

To further understand the safety implications of reductions in air pollution and fog frequency, I analyzed a 20-year record of fog-related accidents in the Central Valley. The results show that over 80% of the variance in the fog-related accident record was determined by annual number of fog events. As fog frequency decreased, the valley experienced a 72% reduction in fog-related accident injuries, annually seeing an average of 550 fewer injuries in 2015-2016 than 1996-1997. The strong link between the historical number of Central Valley fog events and trends in pollution concentration provide a direct measure of how regulations that led to decreases in aerosol concentration, and thereby wintertime fog frequency, also resulted in a declining trend in fog-related accidents.

2. Future directions

2.1. Extend radiation fog analysis to regions of increasing air pollution

Valley radiation fog occurs throughout the world and varied trends in frequency have been observed depending on the location, with trends generally following changes in air pollution. Future analyses should focus on determining a more fundamental relationship between anthropogenic emissions and dense radiation fog trends by extending this work to regions of increasing pollution. For instance, regions with concurrent increases in pollution and fog frequency have been identified in India, Pakistan, Bangladesh, and throughout East-Central China (Fu et al., 2014; Mohan & Payra, 2009; Niu et al., 2010; Quan et al., 2011; Shi et al., 2008; Tiwari et al., 2011). Many studies focus on observations made over a limited period of time (weeks to months), making it challenging to determine long-term causes. Using the National Climate Data Center repository for hourly airport observations (http://www7.ncdc.noaa.gov/CDO/cdopoemain.cmd), future analyses can access meteorological data from airports in countries throughout the globe. Global guidelines for measuring visibility, which is the standard indicator of dense fog events, allow for standardized trends in regional fog frequency to be determined. Accessing local air pollution data poses a greater challenge, since many countries do not have publicly available data sources or have only recently begun implementing air quality monitoring programs. Instead, future analyses could use satellite retrievals to determine remotely sensed trends in air pollution observations. Hilboll (2013) presents a methodology for estimating the NO_2 column trend of a region by combining retrievals from GOME (Global Ozone Monitoring Experiment) and SCHIAMACHY (SCanning Imaging Absorption SpectroMeter for Atmospheric CHartographY), despite their differing spatial resolution, viewing geometry, and time of measurement. Together with climatology data from the National Climate Data Center, future analyses should investigate the temporal and spatial correlations of each region's fog trend to the possible predictor variables discussed in this dissertation. Relationships between predictor variables can then be contrasted with the results here, as well as compared with a pristine environment with little pollution trend and known radiation fog occurrence. The challenge will be finding a pristine location that also has sufficiently long-term airport visibility measurements. Another important requirement is to limit this work to radiation fog. Past reviews of fog trends frequently consider declining trends in radiation, advection, and radiation-advection fog altogether, without considering how differing mechanisms, such as advection fog's dependency on sea surface temperatures and synoptic-scale systems, impact the driving components of the trend.

2.2. Investigate the competing impact of urbanization and air pollution

While there exist regions of both increasing fog formation and increasing air pollution, there are also many examples of urbanization limiting fog by way of the urban heat island (UHI) effect (Sachweh and Koepke, 1995; Sachweh and Koepke, 1996; Underwood et al., 2008; Shi et al., 2008). Current literature regards the aerosol enhancement and UHI effect as contradictory hypotheses; however, future analyses should investigate an alternative approach whereby these effects instead coexist in competition. I hypothesize that there is some threshold whereby the increase in temperature due to urban heat storage overshadows the impact of a rapid growth in hygroscopic CCN for fog formation. The competition between temperature and composition has received recent attention in model analysis (Klemm et al., 2016), but would benefit from a robust

study of surface measurements. One place to begin would be to investigate this varied response by identifying rapidly developing regions, such as in the North China Plain, within which some cities experience the dominating UHI effect (decreasing fog), while others demonstrate a dominating aerosol effect (increasing fog). Comparing the temporal trends in meteorology and aerosol concentration may reveal key characteristics responsible for the UHI-dominating versus aerosol-dominating response.

Preliminary analysis of UHI in the Central Valley demonstrates that the response to urban temperatures is not well understood. While Underwood (2008) identified urban clear islands (UCI) in radiation fog from satellite observations, suggesting that dissipation rates in cities are markedly faster than rural environments, my own analysis in Sacramento shows urban airports had higher fog frequency than adjacent, more rural regions. This ongoing investigation requires more attention to the back-trajectory of pollution plumes, as the rural regions may have unforeseen higher concentrations of precursor emissions than estimated by its proximity to the city center. Additionally, information on changes in surface roughness, surface porosity, distance to water sources such as rivers, and microclimates within urban and suburban regions could be useful.

Shi (2008) investigated this sensitivity in the Anhui Province of China and proposed that the fog frequency declined in *older* cities due to the UHI effect, while the fog frequency increased in *newer* cities as a result of increasing aerosol concentration. New cities were defined as those with smaller, but growing populations whereas old cities were ones that once developed rapidly both in area and population, but have leveled out. This would support the idea that after a certain threshold of expansion, the temperature rise from UHI makes the atmospheric environment inhospitable to condensation despite increasing aerosol concentration.

Studies for other regions of China show conflicting rates of increase and decrease for fog frequency than that of Anhui Province, suggesting that its results may not be true of all areas. For instance, Fu (2010) found that in some sites, rapidly increasing urban expansion decreased wind speed within the urban footprint, thus promoting fog frequency. Ideally, a multivariate model that accounts for aerosol loading, climate, urban density, and land use is necessary to fully understand the sensitivity of this potential threshold. Understanding the competing role of UHI and aerosol concentration on fog formation would provide important insights into future fog trends, particularly in developing countries, many of which have experienced significant productivity and economic consequences from the frequency of dense fog in recent decades.

2.3. Expand understanding of water availability: role of precipitation, soil moisture, and boundary layer height

Future analyses could also examine conflicting literature for how moisture sources thermodynamically impact fog formation.

In this dissertation, the role of wintertime precipitation in the Central Valley – where the majority of annual rain events come in 9-10 large systems, between which conditions are calm and sunny – remains somewhat uncertain. In Chapter 2, annual sums in precipitation, as well as the signal of the El Nino Southern Oscillation index, were investigated for their correlation to fog trends. Chapter 3 also analyzed precipitation by investigating the impact that daily precipitation, as well

as 1- and 2-day lags after rain events, had on low visibility. Unexpectedly, the impact was minor, despite the known reliance of fog formation on supersaturated conditions from some local water source. Thus, additional exploration of the role that duration, intensity, and periodicity California's wintertime storm systems have on fog formation would likely yield interesting results. This would involve categorizing winters by number and severity of storms to investigate the correlation with annual number of fog days.

Precipitation ultimately impacts soil moisture, and yet the significance of soil moisture to radiation fog formation remains debated. Some suggest that it increases the nighttime heat conductivity of the soil, thus decreasing radiative cooling and decreasing diurnal temperature range (Bergot et al., 1994). Others argue that fog frequency is sharply enhanced by soil moisture, causing formation to begin directly from the surface due to the abundance of water (Sierbert et al. 1992). This relationship can be further explored by isolating the conditions most frequent for fog events, and then analyzing how changes in soil moisture impacted the rate of formation, similar to the analysis done in Chapter 2. Data for soil moisture can be found dating back to 1982 using the California Irrigation Management Information System (CIMIS).

Boundary layer height is also sensitive to changes in soil moisture, in which high soil moisture is associated with a lower PBL because greater energy flux is in latent rather than sensible heat, and thus not driving upward convection (Bianco et al., 2011). Changes in boundary layer height could have a significant impact on not only fog formation, but also CCN number concentration. Reanalysis tools, such as NASA's Modern Era-Retrospective Analysis for Research and Applications (MERRA), now offer the opportunity to determine mixing height through historical reprocessing of conventional data and satellite retrievals (Rienecker et al., 2011). Trends in mixing height can then be compared to the spatial and temporal signature of Central Valley fog frequency to identify its influence on formation. Reanalysis tools can also be used to further elucidate the impact of the Great Basin High, which is often cited as having controlling influence on inversion layer depth in the valley, though the literature provides little numerical support for this assertion.

2.4. Investigating impact of trends in aerosol speciation on the water activity coefficient

This dissertation focused primarily on the precursors to aerosol formation due the longer length of record. However, since the mid-2000s, the California Air Resource Board has data on the chemical speciation of aerosols. Future analyses could look at how changes in aerosol speciation impact fog formation using the Extended Aerosol Thermodynamics Model (E-AIM) http://www.aim.env.uea.ac.uk/aim/aim.php). This simple, publicly-available model, when inputted with the humidity and temperature of a known Central Valley winter event, determines aerosol water uptake. Adjustments can then be made to NO_3^-, NH_4^+, and organic species over varying concentrations as seen in the record to model changes in the water activity coefficient. Model results would allow researchers to determine the response of Central Valley conditions to aerosol hygroscopicity, temperature, and relative humidity trends. Another important outcome would be to further investigate how trends in biomass burning impacted fog formation, as there remains uncertainty in the literature about how this mix of inorganic and organic emissions would impact fog CCN and aerosol activation. For example, wintertime rice burning was a common occurrence until state legislation in 1990 and 2000 forced a change in methods, resulting in significant decreases in NO_x, volatile organic compounds, and particulate matter (Blank et al.,

1993). The results of these changes on fog formation have yet to be addressed in the literature and could be used to support air quality legislation.

References:

Abdel-Aty, M., Ekram, A., Huang, H., & Choi, K. (2011). A study of visibility obstruction related crashes due to fog and smoke. *Accident Anal. Prev.*, *43*, 1730–1737. Retrieved from http://www.wctrs-society.com/wp-content/uploads/abstracts/lisbon/selected/01034.pdf

Agarwal, M., Maze, T.H., & Souleyrette, R. (2005). *Impact of Weather on Urban Freeway Traffic Flow Characteristics and Facility Capacity*. Retrieved August 7, 2019, from the Center for Transportation Research and Education: https://trid.trb.org/view/772850

Akaike, H. (1974). A new look at the statistical model identification. *IEEE Transactions on Automatic Control*, (AC-19), 716–723. http://dx.doi.org/10.1109/TAC.1974.1100705

American Lung Association (2016). *State of the Air 2016*. (Vol. 56). Chicago, IL. https://doi.org/10.1017/CBO9781107415324.004

Andreae, M. O., & Rosenfeld, D. (2008). Aerosol-cloud-precipitation interactions. Part 1. The nature and sources of cloud-active aerosols. *Earth-Science Reviews*, *89*(1-2), 13–41. http://doi.org/10.1016/j.earscirev.2008.03.001

Appleton, A. (2018, December 6). When do schools call a foggy day? It's rare, but here's what to do when it happens. *The Fresno Bee*. Retrieved July 31, 2019, from https://www.fresnobee.com/news/local/education/article222210795.html

ARPA, Emilia-Romagna. (2013). *Piano regionale integrato per la qualità dell'aria dell'Emilia-Romagna: quadro conoscitivo.* Centro Tematico Regionale Qualità dell'Aria Rapporto finale, Giugno 2013.

Ashley, W. S., Strader, S., Dziubla, D. C., & Haberlie, A. (2015). Driving Blind: Weather-Related Vision Hazards and Fatal Motor Vehicle Crashes. *Bulletin of the American Meteorological Society*, *96*(May), 755–778. https://doi.org/10.1175/bams-d-14-00026.1

Baldocchi, D., & Waller, E. (2014). Winter fog is decreasing in the fruit growing region of the Central Valley of California. *Geophysical Research Letters*, *41*, 799–804. https://doi.org/10.1002/2014GL060018

Baldocchi, D., & Wong, S. (2008). Accumulated winter chill is decreasing in the fruit growing regions of California. *Climatic Change*, *87,* 153-166. https://doi.org/10.1007/s10584-007-9367-8

Barmpadimos, I., Hueglin, C., Keller, J., Henne, S., & Prevot, A. S. H. (2011). Influence of meteorology on PM10 trends and variability in Switzerland from 1991-2008. *Atmospheric Chemistry and Physics*, *11*, 1813-1835. https://doi.org/10.5194/acp-11-1813-2011

Battye, W., Aneja, V. P., & Roelle, P. A. (2003). Evaluation and improvement of ammonia emissions inventories. *Atmospheric Environment*, *37*(27), 3873–3883. https://doi.org/10.1016/S1352-2310(03)00343-1

Belorid, M., Lee, C.B., & Kim, J.C. (2015). Distribution and long-term trends in various fog types over South Korea. *Theoretical Applied Climatology*, *122*(3-4), 699-710. http://doi.org/10.1007/s00704-014-1321-x

Bendix, J. (1994) Fog Climatology of the Po Valley. *Rivista di Meteorologia Aeronautica*, (3-4), 25-35.

Bergot, T., & Guedalia, D. (1994). Numerical Forecasting of Radiation Fog. Part I: Numerical Model and Sensitivity Tests. *Monthly Weather Review, 122*(6), 1218–1230. https://doi.org/10.1175/1520-0493(1994)122<1218:NFORFP>2.0.CO;2

Bianco, L., I. V. Djalalova, C. W. King, and J. M. Wilczak. (2011). Diurnal evolution and annual variability of boundary-layer height and its correlation to other meteorological variables in California's Central Valley. *Boundary-Layer Meteorology, 140* (3), 491-511. https://doi.org/10.1007/s10546-011-9622-4

Bigi, A. and Ghermandi, G. (2016). Trends and variability of atmospheric PM2.5 and PM10-2.5 concentrations in the Po Valley, Italy. *Atmospheric Chemistry & Physics, 16*(24), 1-19. https://doi.org/10.5194/acp-16-15777-2016

Black, A.W. & Ashley, W.S. (2010). Nontornadic convective wind fatalities in the United States. *National Hazards, 54*, 355–366. https://10.1007/s11069-009-9472-2

Blincoe, L., Seay, A., Zaloshnja, E., Miller, T., Romano, E., Luchter, S., & Spicer, R. (2002). NHTSA Technical Report: The Economic Impact of Motor Vehicle Crashes, 2000. Retrieved August 7, 2019, from the United States Department of Transportation National Highway Traffic Safety Administration: https://rosap.ntl.bts.gov/view/dot/15504

Bonfils, C., & Lobell, D. (2007). Empirical evidence for a recent slowdown in irrigation-induced cooling. *Proceedings of the National Academy of Sciences of the United States of America, 104*(34), 13582–13587. http://doi.org/10.1073/pnas.0700144104

Brimblecombe, P. (1977). London air pollution, 1500-1900. *Atmospheric Environment*, *11*(12), 1157–1162. https://doi.org/10.1016/0004-6981(77)90091-9

Brook, J.R., Dann, T. F., & Burnett, R. T. (1997). The Relationship Among TSP, PM10, PM2.5, and Inorganic Constituents of Atmospheric Participate Matter at Multiple Canadian Locations. *Journal of the Air & Waste Management Association, 47*(1), 2-19. https://doi.org/10.1080/10473289.1997.10464407

Brooks, J.l, Crisler, M., Klein, N., Goodenough, R., Becco, R., Giurl, C., Tyler, P., Hilpert, A., Miller, Y., Grygier, J., Burroughs, B., Martin, A., Ray, R., Palmer, C. & Beck, C. (2011)

Speed choice and driving performance in simulated foggy conditions. *Accident Analysis and Prevention, 43,* 698 – 705. https://doi.org/10.1016/j.aap.2010.10.014

Buchner, A., Brandt, M., Bell, R., and Weise, J. (2006). Car Backlight Position and Fog Density Bias Observer-Car Distance Estimates and Time-to-Collision Judgments. *Human Factors, 48*, 300-317. https://journals.sagepub.com/doi/10.1518/001872006777724363

Burkey, Jeff. (2006). A non-parametric monotonic trend test computing Mann-Kendall Tau, Tau-b, and Sens Slope written in Mathworks-MATLAB implemented using matrix rotations. King County, Department of Natural Resources and Parks, Science and Technical Services section. Seattle, Washington. USA. http://www.mathworks.com/matlabcentral/fileexchange/authors/23983

California Air Resources Board (2009). CEPAM: 2009 Almanac - Standard Emissions Tool, California Air Resources Board: Sacramento, CA. https://www.arb.ca.gov/app/emsinv/fcemssumcat2009.php

California Air Resources Board (2012). Key Events in the History of Air Quality in California. Retrieved from http://www.retailcrc.org/RegGuidance/Lists/RNGList/Attachments/659016/GCA00046.pdf

California Department of Food and Agriculture. (2018). *California County Agricultural Commissioners' Reports: Crop Year 2016-2017.* Sacramento, CA. Retrieved from https://www.nass.usda.gov/Statistics_by_State/California/Publications/AgComm/2014/2014cropyearcactb00.pdf

Caserini, S., Giani, P., Cacciamani, C., Ozgen, S., and Lonati, G. (2016). Influence of climate change on the frequency of daytime temperature inversions and stagnation events in the Po Valley: historical trend and future projections. *Atmospheric Research*, *184*, 15-23. http://dx.doi.org/10.1016/j.atmosres.2016.09.018

Charlson, R. J., Seinfeld, J. H., Nenes, A., Kulmala, M., Laaksonen, A., & Facchini, M. C. (2001). Reshaping the Theory of Cloud Formation. *Science*, *292*(5524), 2025 LP-2026. https://doi.org/10.1126/science.1060096

Chow, J. C., Chen, L.-W. A., Watson, J. G, Lowenthal, D. H., Magliano, K. A., Turkiewicz, K., and Lehrman, D. E. (2006). PM2.5chemical composition and spatiotemporal variability during the California Regional PM10/PM2.5Air Quality Study (CRPAQS). *J. Geophys. Res., 111*, D10S04. https://doi.org/10.1029/2005JD006457

Christy, J. (2004). Irrigation-Induced Warming in Central California? Fourteenth Conference on *Applied Climatology*, *53*(9), 1689–1699. http://doi.org/10.1017/CBO9781107415324.004

Christy, J. R., Norris, W. B., Redmond, K., & Gallo, K. P. (2006). Methodology and results of calculating central California surface temperature trends: Evidence of human-induced climate change? *Journal of Climate, 19*(4), 548–563. http://doi.org/10.1175/JCLI3627.1

Collett, J.L., Bator, A., Sherman, D.E., Moore, K.F., Hoag, K.J., Demoz, B.B., Rao, X., and Reilly, J.E. (2002). The chemical composition of fogs and intercepted clouds in the United States. *Atmospheric Research, 64*(1-4), 29-40. http://doi.org/10.1016/S0169-8095(02)00077-7

Congressional Research Service. (2005). *CRS Report for Congress: California's San Joaquin Valley: A Region in Transition.* Retrieved on August 16, 2019 from the California Department of Food and Agriculture: https://www.cdfa.ca.gov/agvision/files/California/California_CRSReportforCongressSanJoaquinValley-ARegioninTransition.pdf

Cordero, E.C., Kessomkiat, W., Abatzoglou, J., & Mauget, S.A. (2010). The identification of distinct patterns in California temperature trends. *Climatic Change, 108*, 357-382. http://doi.org/10.1007/s10584-011-0023-y

Cusack, M., Alastuey, A., Perez, N., Pey, J., & Querol, X. (2012) Trends in particulate matter (PM2.5) and chemical composition at a regional background site in the Western Mediterranean over the last nine years (2002-2010). *Atmospheric Chemistry & Physics, 12*, 8341-8357. https://doi.org/10.5194/acp-12-8341-2012

Dai, A., Trenberth, K. E., & Karl, T. R. (1999). Effects of clouds, soil moisture, precipitation, and water vapor on diurnal temperature range. *Journal of Climate, 12*(8 PART 2), 2451–2473. http://doi.org/10.1175/1520-0442(1999)012<2451:EOCSMP>2.0.CO;2

Dusek, U., Frank, G. P., Hildebrandt, L., Curtius, J., Schneider, J., Walter, S., … Andreae, M. O. (2006). Size Matters More Than Chemistry Aerosol Particles. *Science, 312*(5778), 1375–1378. http://doi.org/10.1126/science.1

Eeftens, M., Tsai, M.Y., Ampe, C., Anwander, B., Beelen, R., Bellander, T., et al. (2012). Spatial variation of PM2.5, PM10, PM2.5 absorbance, and PMcoarse concentrations between and within 20 European study areas and the relationship with NO2 – Results of the ESCAPE project. *Atmospheric Environment, 62*, 303-317. http://dx.doi.org/10.1016/j.atmosenv.2012.08.038

Elridge, R. G. (1966). Haze and fog aerosol distributions. *Journal of the Atmospheric Sciences, 23*, 605-613. http://doi.org/1520-0469(1966)023<0605:HAFAD>2.0.CO;2

Energy Information Administration (2017). *State Energy Data System (SEDS): 1960-2016.* Washington, DC, Energy Information Administration, U.S. Department of Energy. https://www.eia.gov/state/seds/

Environmental Protection Agency (EPA) (2000). *National Air Pollutant Emission Trends, 1900-1998*. Durham, North Carolina. https://nepis.epa.gov/Exe/ZyPURL.cgi?Dockey=2000ETJA.TXT

European Environment Agency (EEA) (2014) *Air quality in Europe – 2014 report*. Retrieved April 12, 2016 from the European Environmental Agency: https://www.eea.europa.eu/publications/air-quality-in-europe-2014

Fischer, D. T., Still, C. J., & Williams, A. P. (2009). Significance of summer fog and overcast for drought stress and ecological functioning of coastal California endemic plant species. *Journal of Biogeography*, 36(4), 783–799. https://doi.org/10.1111/j.1365-2699.2008.02025-x

Frank, G. (1998). Droplet Formation and Growth in Polluted Fogs. *Contr. Atmospheric Physics, 71*(1), 65-85. http://doi.org/0005-8173/98010065-21

Freund, R. J. and Wilson, W. J. (1998). *Regression Analysis: Statistical modeling of a response variable*, Academic Press, San Diego and London, 192 pp.

Frost, G. J., McKeen, S.A., Trainer, M., Ryerson, T. B., Neuman, J. A., Roberts, J. M., et al. (2006). Effects of changing power plant NOx emissions on ozone in the eastern United States: Proof of concept. *Journal of Geophysical Research-Atmospheres, 111*(D12): 1-19. https://doi.org/10.1029/2005JD006354

Fu, G. Q., Xu, W. Y., Yang, R. F., Li, J. B., & Zhao, C. S. (2014). The distribution and trends of fog and haze in the North China Plain over the past 30 years. *Atmospheric Chemistry and Physics, 14*(21), 11949-11958. http://www.doi.org/10.5194/acp-14-11949-2014

Gilardoni, S., Massoli, P., Giulianelli, L., Rinaldi, M., Paglione, M., Pollini, F., … Fuzzi, S. (2014). Fog scavenging of organic and inorganic aerosol in the po valley. *Atmospheric Chemistry and Physics, 14*(13), 6967–6981. https://doi.org/10.5194/acp-14-6967-2014

Giulianelli, L., Gilardoni, S., Tarozzi, L., Rinaldi, M., Decesari, S., Carbone, C., … Fuzzi, S. (2014). Fog occurrence and chemical composition in the Po valley over the last twenty years. *Atmospheric Environmen*t, 98, 394–401. http://doi.org/10.1016/j.atmosenv.2014.08.080

Gray, E., Gilardoni, S., Baldocchi, D., McDonald, B.C., Facchini, M.C., & Goldstein, A.H. (2019). Impact of Air Pollution Controls on Radiation Fog Frequency in the Central Valley of California. *Journal of Geophysical Research: Atmospheres*, 124(11), 5889-5905. https://doi.org/10.1029/2018JD029419

Gregor, H. (1963). Spatial Disharmonies in California Population Growth. *Geographical Review, 53*(1), 100-122. https://doi.org/10.2307/212811

Gultepe, I., Tardif, R., Michaelides, S. C., Cermak, J., Bott, a., Bendix, J., et al. (2007). Fog Research: A Review of Past Achievements and Future Perspectives. *Pure and Applied Geophysics*, *164*(6–7), 1121–1159. https://doi.org/10.1007/s00024-007-0211-x

Hamilton, B.T., Arnold, L., & Grabowski, J. (2014). L. Arnold and J Grabowski (2014) *Hidden highways: fog and traffic crashes on America's roads.* Retrieved August 6, 2019 from the AAA Foundation for Traffic Safety Report: https://aaafoundation.org/wp-content/uploads/2017/12/FogAndCrashesReport.pdf

Harrison, R.M., Deacon, A.R., & Jones, M.R. (1997). Sources and processes affecting concentrations of PM10 and PM2.5 particulate matter in Birmingham (U.K.). *Atmospheric Environment*, 31(24), 4103-4117. https://doi.org/10.1016/S1352-2310(97)00296-3

Hassler, B., et al. (2016). Analysis of long-term observations of NOx and CO in megacities and application to constraining emissions inventories. *Geophysical Research Letters*, 43(18), 9920-9930. https://doi.org/10.1002/2016GL069894

Hastie, T.J. and Tibshirani, R.J. (1990) *Generalized Additive Models.* CRC Press. https://doi.org/10.1002/9781118445112.stat03141

Herckes, P., Marcotte, a. R., Wang, Y., & Collett, J. L. (2015). Fog composition in the Central Valley of California over three decades. *Atmospheric Research*, 151, 20–30. https://doi.org/10.1016/j.atmosres.2014.01.025

Hilboll, A., Richter, A., & Burrows, J. P. (2013). Long-term changes of tropospheric NO2 over megacities derived from multiple satellite instruments. *Atmospheric Chemistry and Physics, 13*(8), 4145–4169. http://doi.org/10.5194/acp-13-4145-2013

Hudson, J. G. (1980). Relationship Between Fog Condensation Nuclei and Fog Microstructure. *Journal of the Atmospheric Sciences.* http://doi.org/10.1175/1520-0469(1980)037<1854:RBFCNA>2.0.CO;2

Jackson, L. S., Carslaw, N., Carslaw, D. C., and Emmerson, K.M. (2009). Modelling trends in OH radical concentrations using generalized additive models, *Atmospheric Chemistry & Physics*, 9, 2021–2033. http://doi.org10.5194/acp-9-2021-2009

Jacob, D.J., Shair, Shair, F.H., Waldman, J.M., Munger, J.W., & Hoffman, M. (1986). Transport and Oxidation of SO2 in a Stagnant Foggy Valley. *Atmospheric Environment*, 21(6), 1305–1314. http://doi.org/10.1016/0004-6981(67)90077-7

Jacob, D.J., Waldman, J.M., Munger, J.W., & Hoffmann, M. (1984). A field investigation of physical and chemical mechanisms affecting pollutant concentrations in fog droplets. *Tellus*, B, 36. 10.3402/tellusb.v36i4.14909

Kendall, M. G. (1955). *Rank correlation methods (2nd ed.)*. Oxford, England: Hafner Publishing Co. https://doi.org/10.1111/j.2044-8317.1956.tb00172.x

Killam, D., Bui, A., LaDochy, S., Ramirez, P., Willis, J., & Patzert, W. (2014). California getting wetter to the north, drier to the south: natural variability or climate change? *Climate, 2*(3), 168–180. https://doi.org/10.3390/cli2030168

Killam, D., Bui, A., LaDochy, S., Ramirez, P., Willis, J., and Patzert, W. (2014). California getting wetter to the north, drier to the south: natural variability or climate change? *Climate, 2*, 168-80. https://doi.org/10.3390/cli2030168

Kirchstetter, T. W., Preble, C. V., Hadley, O. L., Bond, T. C., & Apte, J. S. (2017). Large reductions in urban black carbon concentrations in the United States between 1965 and 2000. *Atmospheric Environment, 151*, 17–23. https://doi.org/10.1016/j.atmosenv.2016.11.001

Klemm, O., & Lin, N. H. (2016). What causes observed fog trends: Air quality or climate change? *Aerosol and Air Quality Research, 16*(5), 1131–1142. https://doi.org/10.4209/aaqr.2015.05.0353

Köhler, H. (1936). The nucleus in and the growth of hygroscopic droplets. *Transactions of the Faraday Society, 32*(1152), 1152. http://doi.org/10.1039/tf9363201152

Kokkola, H., Romakkaniemi, S., & Laaksonen, A. (2002). On the formation of radiation fogs under heavily polluted conditions. *Atmospheric Chemistry and Physics Discussions, 3*(1), 389–411. http://doi.org/10.5194/acpd-3-389-2003

Kulmala, M., Korhonen, P., Laaksonen, A., & Vesala, T. (1995). Changes in Cloud Properties Due to NOx Emissions. *Geophysical Research Letters, 22*(3), 239–242. https://doi.org/10.1029/94GL02691

Kulmala, M., Laaksonen, A., Charlson, R. J., & Korhonen, P. (1997). Clouds without supersaturation. *Nature, 388*(July), 336–337. http://doi.org/10.1038/41000

Kulmala, M., Toivonen, A., Mattila, T., and Korhonen, P. (1998). Variations of cloud droplet concentrations and the optical properties of clouds due to changing hygroscopicity: A model study, *J. Geophys. Res., 103*(D13), 16183–16195, http://doi.org/10.1029/98JD00880

Laaksonen, A., Korhonen, P., Kulmala, M., & Charlson, R. J. (1998). Modification of the Köhler Equation to Include Soluble Trace Gases and Slightly Soluble Substances. *Journal of the Atmospheric Sciences, 55*(1), 853–862. http://doi.org/10.1175/1520-0469(1998)055

LaDochy, S., Medina, R., & Patzert, W. (2007). Recent Calfornia climate variability: spatial and temporal patterns in temperature trends. *Climate Research, 33*, 159–169. http://doi.org/10.3354/cr033159

Lavelle, M. (2014). California's Fog is Fading Away, Crops Could Suffer. Climate Central. Retrieved August 7, 2019, from https://www.climatecentral.org/news/california-winter-fog-disappear-17526

Lee, Thomas F. (1987). Urban clear islands in California central valley fog. *Monthly Weather Review*, 115.8, 1794-1796. https://doi.org/10.1175/1520-0493(1987)115<1794:UCIICC>2.0.CO;2

Lin, R.G. & Weiss, K.R. (2007, November 4). 2 killed in huge pileup in the tule fog on California 99. *The Los Angeles Times*. Retrieved August 6, 2019, from https://www.latimes.com/archives/la-xpm-2007-nov-04-me-pileup4-story.html

Ling, L., Zhang, T., Kleinman, L., & Zhu, W. (2007). Ordinary least square regression, orthogonal regression, geometric mean regression and their applications in aerosol science. *Journal of Physics: Conference Series*, *78*, 012084. https://doi.org/10.1088/1742-6596/78/1/012084

Lomb, Nicholas R. (1976). Least-Squares Frequency Analysis of Unequally Spaced Data. *Astrophysics and Space Science. 39*, 447–462. https://doi.org/10.1007/BF00648343

Luedeling, E., Zhang, M., Luedeling, V., & Girvetz, E. H. (2009). Sensitivity of winter chill models for fruit and nut trees to climatic changes expected in California's Central Valley. *Agriculture, Ecosystems, and Environment, 133*(1–2), 23–31. https://doi.org/10.1016/j.agee.2009.04.016

MacCarley, Art. (1999). Evaluation of Caltrans District 10 Automated Warning System: Year Two Progress Report. Retrieved on August 19, 2019, from the U.S. Department of Transportation: https://ops.fhwa.dot.gov/weather/best_practices/1024x768/transform_param2.asp?xslname=pub.xsl&xmlname=publications.xml&keyname=338

Manara, V., Brunetti, M., Gilardoni, S., Landi, T.C., and Maugeri, M. (2019). 1951-2017 changes in the frequency of days with visibility higher than 10 km and 20 km in Italy. *Atmospheric Environment*, 214, 116861. https://doi.org/10.1016/j.atmosenv.2019.116861

Mann, H. (1945). Nonparametric Tests Against Trend. Econometrica, *13*(3), 245-259. http://doi.org/10.2307/1907187

Marcazzan, G., Vaccaro, S., Valli, G., & Vecchi, R. (2001). Characterisation of PM10 and PM2.5 particulate matter in the ambient air of Milan (Italy). *Atmospheric Environment, 35*, 4639-4650. https://doi.org/10.1016/S1352-2310(01)00124-8

Mariani, L. (2009). Fog in the Po Valley: Some meteo-climatic aspects. *Italian Journal of Agrometeorology, 3,* 35-44. https://doi.org/10.1.1.626.3349

McDonald, B. C., Dallmann, T. R., Martin, E. W., & Harley, R. a. (2012). Long-term trends in nitrogen oxide emissions from motor vehicles at national, state, and air basin scales. *Journal of Geophysical Research: Atmospheres, 117*(17), 1–11. https://doi.org/10.1029/2012JD018304

Mehler, B., Reimer, B., Lavalliere, M., Dobres, J., Coughlin, J.F. (2014) Evaluating Technologies Relevant to the Enhancement of Driver Safety. Retrieved August 7, 2019, from the AAA Foundation for Traffic Safety: https://newsroom.aaa.com/tag/evaluating-technologies-relevant-to-the-enhancement-of-driver-safety/

Mohan, M., & Payra, S. (2009). Influence of aerosol spectrum and air pollutants on fog formation in urban environment of megacity Delhi, India. *Environmental Monitoring and Assessment, 151*(1-4), 265–277. http://doi.org/10.1007/s10661-008-0268-8

Montgomery, D. C. and Peck, E. A. Introduction to Linear Regression Analysis, 4th edn.,WileyBlackwell, New York, USA, 2006. https://doi.org/10.1111/insr.12020_10

Morss, R.E., Demuth, J.L., & Lazo, J.K. (2008). Communicating Uncertainty in Weather Forecasts: A Survey of the U.S. Public. *Weather and Forecasting, 23*, 974-99. https://doi.org/10.1175/2008WAF2007088.1

National Highway Traffic Safety Administration's National Center for Statistics and Analysis. (2013). How Vehicle Age and Model Year Relate to Driver Injury Severity in Fatal Crashes. Retrieved August 6, 2019 from the National Center for Statistics and Analysis: https://crashstats.nhtsa.dot.gov/Api/Public/ViewPublication/811825

National Weather Service, San Joaquin Valley Weather Forecasting Office. HNX Experimental Fog Severity Index. National Weather Service – National Oceanic and Atmospheric Administration. Retrieved August 5, 2019 from https://www.weather.gov/hnx/HNXFogSI.html

National Weather Service. (2019). Weather Related Fatality and Injury Statistics. National Weather Service – National Oceanic and Atmospheric Administration. Retrieved August 6, 2019 from https://www.weather.gov/hazstat/

Neiburger, M. & Wurtele, M.G. (1949), On the nature and size of particles in haze, fog, and stratus of the Los Angeles region. *Chemical Reviews*, 44, 321–335.

Niu, S., Lu, C., Yu, H., Zhao, L., & Lü, J. (2010). Fog research in China: An overview. *Advances in Atmospheric Sciences, 27*(3), 639–662. http://doi.org/10.1007/s00376-009-8174-8

Oke, T. R. (1973). City size and the urban heat island. Atmospheric Environment, 7, 769–779. http://doi.org/10.1016/0004-6981(73)90140-6

Petters, M. D., & Kreidenweis, S. M. (2007). A single parameter representation of hygroscopic growth and cloud condensation nucleus activity-Part 3: Including surfactant partitioning.

Atmospheric Chemistry and Physics, 13(2), 1961–1971. https://doi.org/10.5194/acp-13-1081-2013

Pisano, P. A., & Goodwin, L.C. (2002). Surface transportation weather applications. Retrieved August 6, 2019 from the Federal Highway Administration/Mitretek Systems, Inc. https://trid.trb.org/view/732438

Pisano, P. A., Goodwin, L. C., and Rossetti, M. A. (2008). USDOT Research and Innovative Technology Administration Title: US Highway Crashes in Adverse Road Weather Conditions. Retrieved from August 6, 2019, from American Meteorological Society Conference: https://ams.confex.com/ams/88Annual/techprogram/paper_133554.htm

Preble, C. V., Dallmann, T. R., Kreisberg, N. M., Hering, S. V., Harley, R. A., & Kirchstetter, T. W. (2015). Effects of Particle Filters and Selective Catalytic Reduction on Heavy-Duty Diesel Drayage Truck Emissions at the Port of Oakland. *Environmental Science and Technology, 49*(14), 8864–8871. https://doi.org/10.1021/acs.est.5b01117

Pusede, S. E. & Cohen, R. C. (2012). On the observed response of ozone to NOx and VOC reactivity reductions in San Joaquin Valley California 1995-present. *Atmospheric Chemistry and Physics, 12*, 8323-8339, https://doi.org/10.5194/acp-12-8323-2012

Pusede, S. E., Duffey, K. C., Shusterman, A. A., Saleh, A., Laughner, J. L., Wooldridge, P. J., et al. (2016). On the effectiveness of nitrogen oxide reductions as a control over ammonium nitrate aerosol. *Atmospheric Chemistry and Physics, 16*(4), 2575–2596. https://doi.org/10.5194/acp-16-2575-2016

Putaud, J. P., Cavalli, F., Martins dos Santos, S., and Dell'Acqua, A. (2014). Long-term trends in aerosol optical characteristics in the Po Valley, Italy. *Atmospheric Chemistry & Physics, 14*, 9129-9136. https://doi.org/10.5194/acp-14-9129-2014

Quan, J., Zhang, Q., He, H., Liu, J., Huang, M., & Jin, H. (2011). Analysis of the formation of fog and haze in North China Plain (NCP). *Atmospheric Chemistry and Physics, 11*(15), 8205–8214. http://doi.org/10.5194/acp-11-8205-2011

Rienecker, M. (2011). MERRA: NASA's Modern-Era Retrospective Analysis for Research and Applications. *Journal of Climate, 32*(19), 3624–3648. http://doi.org/10.1175/JCLI-D-11-00015.1

Roach, W. T., Brown, R., Caughey, S. J., Garland, J. A., & Readings, C. J. (1976). The physics of radiation fog: I – a field study. *Quarterly Journal of the Royal Meteorological Society, 102*(432), 313–333. https://doi.org/10.1002/qj.49710243204

Rosey, F., Aillerie, I., Espié, and Vienne, F. (2017). Driver behavior in fog is not only a question of degraded visibility – A simulator study. *Safety Science, 95*(June), 50-61. https://doi.org/10.1016/j.ssci.2017.02.004

Russell, A. R., Valin, L. C., & Cohen, R. C. (2012). Trends in OMI NO2 observations over the United States: Effects of emission control technology and the economic recession. *Atmospheric Chemistry and Physics, 12*(24), 12197–12209. https://doi.org/10.5194/acp-12-12197-2012

Sachweh, M., & Koepke, P. (1995). Radiation fog and urban climate. *Geophysical Research Letters, 22*(9), 1073. http://doi.org/10.1029/95GL00907

Sachweh, M., & Koepke, P. (1996). Fog dynamics in an urbanized area. *Theoretical and Applied Climatology, 58*(1-2), 87–93. http://doi.org/10.1007/BF00867435

Salas, W., Green, P., Frolking, S., Li, C., & Boles, S. (2006). *Estimating irrigation water use for California agriculture: 1950s to present.* Retrieved from the California Energy Commission: http://www.energy.ca.gov/2006publications/CEC-500-2006-057/CEC-500-2006-057.PDF

Sartini, C., Sajani, S.Z., Ricciardelli, I., Delgado-Saborit, J., Scott, F., Trentini, A., Ferrari, S., & Poluzzi, V. (2013) Ultrafine particle concentrations in the surrounds of an urban area: comparing downwind to upwind conditions using Generalized Additive Models (GAMs). *Environmental Science Processes Impacts, 15,* 2087. https://doi.org/10.1039/c3em00228d

Scargle, J.D. (1982). Studies in Astronomical Time Series Analysis. II. Statistical Aspects of Spectral Analysis of Unevenly Spaced Data. *Astrophysical Journal*. *263*, 835–853. https://doi.org/10.1086/160554

Schiferl, L. D., Heald, C. L., Nowak, J. B., Holloway, J. S., Neuman, J. A., Bahreini, R., et al. (2014). An investigation of ammonia and inorganic particulate matter in California during the CalNex campaign. *Journal of Geophysical Research: Atmospheres, 119*(4), 1883–1902. https://doi.org/10.1002/2013JD020765

Sen, P. K. (1968). Robustness of some nonparametric procedures in linear models. *The Annals of Mathematical Statistics, 39*(6), 1913–1922. https://doi.org/10.2307/2239290

Sen, P.K. (1968). Estimates of the regression coefficient based on Kendall's tau. *Journal of the American Statistical Association. 63*, 1379–89. http://dx.**doi**.org/10.1080/01621459.1968.10480934

Senn, C.L. (1948). General atmospheric pollution: Los Angeles "smog." *Am. J. Public Health Nations Health, 38*, 962-965. https://doi.org/10.2105/AJPH.38.7.962

Shi, C., Roth, M., Zhang, H., & Li, Z. (2008). Impacts of urbanization on long-term fog variation in Anhui Province, China. *Atmospheric Environment, 42*(36), 8484–8492. http://doi.org/10.1016/j.atmosenv.2008.08.002

Sierbert, J., Bott, A., & Zdunkowski, W. (1992). Influence of a Vegetation-Soil Model on the Simulation of Radiation Fog. *Contributions to Atmospheric Physics, 65*(2), 93–106.

Stockwell, W. R., Watson, J. G., Robinson, N. F., Steiner, W., & Sylte, W. W. (2000). The ammonium nitrate particle equivalent of NO emissions for wintertime conditions in Central California's San Joaquin Valley. *Journal of Geophysical Research, 34*(V), 4711–4717. http://doi.org/10.1016/S1352-2310(00)00148-5

Struglia, R., Winter, P.I., and Meyer, A. (2003). Southern California Socioeconomic Assessment: Sociodemographic Conditions, Projections, and Quality of Life Indices. Gen. Tech. Rep. PSW-GTR-187. Retrieved on August 16, 2019 from the United States Department of Agriculture: https://www.fs.usda.gov/treesearch/pubs/7299

Suckling, P.W., & Mitchell, M.D. (1988). Fog climatology of the Sacramento urban area. *The Professional Geographer. 40*, 186 - 194. https//doi.org/10.1111/j.0033-0124.1988.00186.x

Syed, F.S. (2012). On the fog variability over south Asia. Climate Dynamics, 39(12), 2993-3005. http://doi.org/10.1007/s00382-012-1414-0

Theil, H. (1950). A rank-invariant method of linear and polynomial regression analysis I. *Nederlandse Akademie Wetenchappen, 53*(Series A), 386–392. https://doi.org/10.1007/978-94-011-2546-8

Theil, H. (1992). *A rank-invariant method of linear and polynomial regression analysis. In Henri Theil's Contributions to Economics and Econometrics* (Advanced Studied in Theoretical and Applied Econometrics Volume 23, pp 345-81). Springer Netherlands. Retrieved from: https://link.springer.com/chapter/10.1007%2F978-94-011-2546-8_20

Tiwari, S., Payra, S., Mohan, M., Verma, S., & Bisht, D. S. (2011). Visibility degradation during foggy period due to anthropogenic urban aerosol at Delhi, India. *Atmospheric Pollution Research, 2*(July), 116–120. http://doi.org/10.5094/apr.2011.014

Underwood, S. J. and Hansen, C. (2008). Investigating urban clear islands in fog and low stratus clouds in the San Joaquin Valley of California. Physical Geography, 29(5), 442-454. https://doi.org/10.2747/0272-3646.29.5.442

Underwood, S. J., Ellrod, G. P., & Kuhnert, A. L. (2004). A multiple-case analysis of nocturnal radiation-fog development in the Central Valley of California utilizing the GOES nighttime fog product. Journal of Applied Meteorology, 43(2), 297–311. https://doi.org/10.1175/1520-0450(2004)043<0297:AMAONR>2.0.CO;2

United States Census Bureau (2011). *Historical US Census Populations of Places, Towns, and Cities in California 1850-1990*. Retrieved from http://www.dof.ca.gov/Reports/Demographic_Reports/documents/2010-1850_STCO_IncCities-FINAL.xls.

United States Department of Commerce, National Oceanographic and Atmospheric Administration (2005). *Federal Meteorological Handbook No. 1: Surface Weather Observations and Reports*. Retrieved August 7, 2019, from the Office of Federal Coordinator for Meteorological Services and Supporting Research: https://www.ofcm.gov/publications/fmh/FMH1/FMH1_2017.pdf

United States Department of Transportation (2017). *Best Practices for Road Weather Management: California DOT Fog Detection and Warning System*. Retrieved July 2, 2019, from the Federal Highway Administration: https://ops.fhwa.dot.gov/publications/fhwahop12046/rwm05_california1.htm

United States Department of Transportation (2019). *How Do Weather Events Impact Roads?* Federal Highway Administration. Retrieved July 2, 2019, from the Federal Highway Administration: https://ops.fhwa.dot.gov/weather/q1_roadimpact.htm

van Oldenborgh, G. J., Yiou, P., & Vautard, R. (2010). On the roles of circulation and aerosols in the decline of mist and dense fog in Europe over the last 30 years. *Atmospheric Chemistry and Physics, 10*(10), 4597–4609. http://doi.org/10.5194/acp-10-4597-2010

Vautard, R., Cattiaux, J., Yiou, P., Thépaut, J.-N., & Ciais, P. (2010). Northern Hemisphere atmospheric stilling partly attributed to an increase in surface roughness. *Nature Geoscience, 3*(11), 756–761. https://doi.org/10.1038/ngeo979

Wilkins, E. T. (1954). Air pollution aspects of the London fog of December 1952. *Quarterly Journal of the Royal Meteorological Society, 80*(344), 267–271. https://doi.org/10.1002/qj.49708034420

Williams, A. P., Gentine, P., Moritz, M. A., Roberts, D. A., & Abatzoglou, J. T. (2018). Effect of reduced summer cloud shading on evaporative demand and wildfire in coastal Southern California. *Geophysical Research Letters, 45*, 5653–5662. https://doi.org/10.1029/2018GL077319

Wood, S. N. (2008). Fast stable direct fitting and smoothness selection for generalized additive models. *Journal of the Royal Statistical Society: Series B (Statistical Methodology), 3*(70), 495-518. https://doi.org/10.1111/j.1467-9868.2007.00646.x